



Search for pair-produced vector-like T -quarks decaying into Ht final states in the lepton-plus-jets channel in pp collisions at $\sqrt{s} = 13$ TeV with the ATLAS detector

The ATLAS Collaboration

A search for pair-produced vector-like T -quarks in 139 fb^{-1} of pp collisions recorded by the ATLAS detector at a centre-of-mass energy $\sqrt{s} = 13$ TeV is presented. The search targets signal events where at least one T -quark decays into a Higgs boson and a top quark, $T \rightarrow Ht$, with subsequent decays of the Higgs boson into a bottom quark–antiquark pair, $H \rightarrow b\bar{b}$, and the top quark into a light charged lepton, a neutrino and a bottom quark, $t \rightarrow \ell^+ \nu_\ell b$, where $\ell = e/\mu$. The decay products of boosted heavy resonances are reconstructed using variable-radius, reclustered jets, and a neural network is employed to discriminate signal from Standard Model background processes. A profile-likelihood fit to the effective mass distribution is performed, and no excess above the Standard Model prediction is observed. Exclusion limits at 95% confidence level are set on the T -quark pair-production cross-section, corresponding to lower mass limits of 1.40 TeV in the SU(2) singlet representation, 1.56 TeV in the SU(2) doublet representation, and 1.66 TeV assuming the branching fraction of T -quarks to Ht to be 100%.

Contents

1	Introduction	2
2	ATLAS detector	4
3	Data and simulated event samples	4
3.1	Simulated signal samples	5
3.2	Simulated background samples	7
4	Object reconstruction	8
5	Analysis strategy	11
5.1	Preselection	11
5.2	Data-driven background reweighting	12
5.3	Multivariate signal classifier	12
5.4	Event categorisation	15
6	Systematic uncertainties	16
6.1	Experimental uncertainties	16
6.2	Theoretical modelling uncertainties	17
7	Statistical analysis	18
8	Results	20
8.1	Likelihood fit	20
8.2	Exclusion limits on pair-production of vector-like quarks	22
9	Conclusion	24
	Appendix	26
A	Complete list of neural network input variables	26
B	Complete set of data and predicted yields in analysis regions	27

1 Introduction

One of the unsolved questions of particle physics is the large hierarchy between the electroweak mass scale and the Planck scale. A possible way to alleviate the associated fine-tuning is to extend the Standard Model (SM) by introducing new, vector-like quarks (VLQs) [1–7], which can counterbalance the quadratically divergent radiative corrections to the Higgs boson mass. VLQs are defined as colour-triplet spin- $1/2$ fermions whose left- and right-handed chiral components have the same transformation properties under the weak-isospin SU(2) gauge group [8, 9]. The vector-like quarks in many of these models are expected to couple preferentially to third-generation SM quarks because of the large quark mass hierarchy in the SM [8, 10]. Several multiplet representations of vector-like quarks are possible, e.g. SU(2) singlets ($T^{2/3}$)

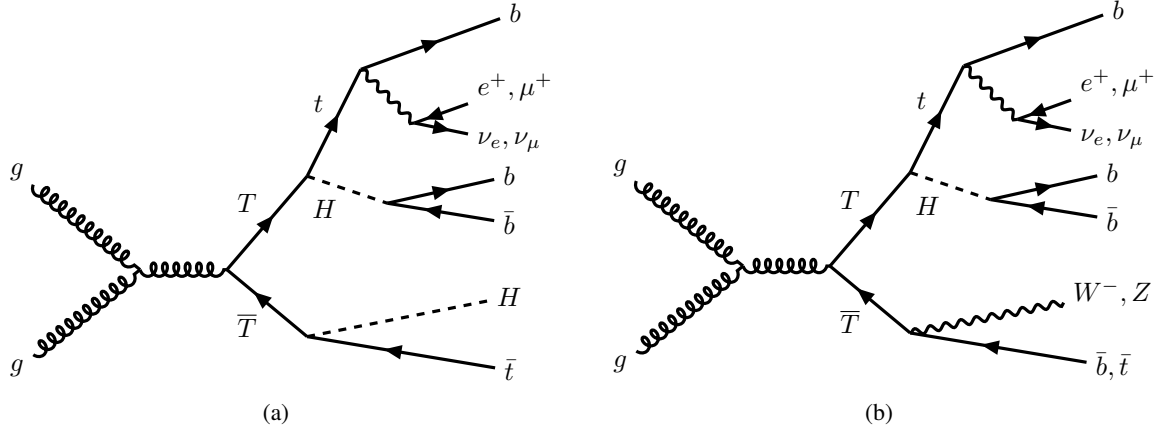


Figure 1: Leading-order Feynman diagrams of the processes targeted by the search: a pair-production of vector-like T -quarks, with at least one decaying through the $T \rightarrow Ht$ channel with subsequent decays $H \rightarrow b\bar{b}$ and $t \rightarrow \ell^+ \nu_\ell b$, $\ell = e/\mu$. The other T -quark can either (a) decay as $T \rightarrow Ht$ (leading to final state $HtH\bar{t}$) or (b) decay as $T \rightarrow Wb$ ($HtW\bar{b}$) or $T \rightarrow Zt$ ($HtZ\bar{t}$), with subsequent hadronic decays of the bosons and top quark(s).

or SU(2) doublets ($X^{5/3}, T^{2/3}$), where the superscript indicates the electric charge, which is omitted in the following. The up-type T -quarks are the focus of the search presented in this paper. They can decay into a W boson and a bottom quark (Wb), a Higgs boson and a top quark (Ht), or a Z boson and a top quark (Zt). The decay branching fractions are determined by the gauge representations of the vector-like quarks. In the asymptotic limit of very large VLQ mass, these branching fractions converge to 50% : 25% : 25% for $T \rightarrow Wb : Ht : Zt$ in the SU(2) singlet case, and 0 : 50% : 50% in the SU(2) doublet case [10, 11], which are the values used in this analysis.

This paper presents a search for pair-produced T -quarks in proton–proton collisions recorded at a centre-of-mass energy of $\sqrt{s} = 13$ TeV with the ATLAS detector [12] at the Large Hadron Collider (LHC), using the full Run 2 data corresponding to an integrated luminosity of 139 fb^{-1} . The search targets events where at least one T -quark decays into a Higgs boson and a top quark, $T \rightarrow Ht$, with a subsequent decay of the Higgs boson into a bottom quark–antiquark pair, $H \rightarrow b\bar{b}$, and a top quark into a light lepton, a neutrino and a bottom quark, $t \rightarrow \ell^+ \nu_\ell b$, as depicted in Figure 1. The second T -quark is allowed to decay via any of the three decay modes ($T \rightarrow Ht, Zt, Wb$), followed by fully hadronic decay of these particles. Only light leptons, i.e. electrons and muons, are targeted in this analysis. The signal topology selected by this search is therefore characterised by the presence of exactly one electron or muon, moderate missing transverse momentum from neutrinos, and multiple boosted hadronic objects from the quarks or hadronically decaying bosons. Explicit reconstruction of the signal decay products is combined with a neural network classifier to discriminate signal from background. The search is performed in the SU(2) singlet and doublet gauge representations as well as a scenario where the branching fraction of T -quarks to Ht is set to 100% ($\mathcal{B}(T \rightarrow Ht) = 100\%$). The results are interpreted as upper limits on the vector-like T -quark pair-production ($T\bar{T}$) cross-section as a function of T -quark mass.

The pair-production of T -quarks was previously searched for by the ATLAS Collaboration using 36 fb^{-1} of Run 2 data, both in the $T \rightarrow Ht$ channel [13] and in a combination of several decay channels [14]. More recently, several searches for the pair-production of T -quarks using the full Run 2 data were performed by the ATLAS Collaboration [15–18] and CMS Collaboration [19] in different decay channels. To date, the most stringent limits exclude masses below 1.48 TeV in the SU(2) singlet scenario, below 1.49 TeV in

the SU(2) doublet scenario, and below 1.50 TeV in the $\mathcal{B}(T \rightarrow Ht) = 100\%$ scenario, all set by the CMS search in Ref. [19].

The search presented here improves upon the previous ATLAS search in the $T \rightarrow Ht$ channel [13] in several key aspects. The modelling of the dominant $t\bar{t}$ and vector-boson backgrounds is improved through a data-driven reweighting technique. Explicit reconstruction of leptonic top-quark and W -boson candidates is performed, and the back-to-back topology characteristic of pair-produced heavy particles is exploited, providing additional handles for the separation of signal from background processes. Finally, a neural network is employed for signal-to-background discrimination, capitalising on the almost four-fold increase in integrated luminosity and enabling a more effective exploitation of the data.

2 ATLAS detector

The ATLAS experiment [12] at the LHC is a multipurpose particle detector with a forward–backward symmetric cylindrical geometry and a near 4π coverage in solid angle.¹ It consists of an inner tracking detector surrounded by a thin superconducting solenoid providing a 2 T axial magnetic field, electromagnetic and hadronic calorimeters, and a muon spectrometer. The inner tracking detector covers the pseudorapidity range $|\eta| < 2.5$. It consists of silicon pixel, silicon microstrip, and transition radiation tracking detectors. Lead/liquid-argon (LAr) sampling calorimeters provide electromagnetic (EM) energy measurements with high granularity within the region $|\eta| < 3.2$. A steel/scintillator-tile hadronic calorimeter covers the central pseudorapidity range ($|\eta| < 1.7$). The endcap and forward regions are instrumented with LAr calorimeters for EM and hadronic energy measurements up to $|\eta| = 4.9$. The muon spectrometer surrounds the calorimeters and is based on three large superconducting air-core toroidal magnets with eight coils each. The field integral of the toroids ranges between 2.0 and 6.0 T m across most of the detector. The muon spectrometer includes a system of precision tracking chambers up to $|\eta| = 2.7$ and fast detectors for triggering up to $|\eta| = 2.4$. The luminosity is measured mainly by the LUCID-2 [20] detector, which is located close to the beampipe. A two-level trigger system is used to select events [21]. The first-level trigger is implemented in hardware and uses a subset of the detector information to accept events at a rate close to 100 kHz. This is followed by a software-based trigger that reduces the accepted rate of complete events to 1.25 kHz on average depending on the data-taking conditions. A software suite [22] is used in data simulation, in the reconstruction and analysis of real and simulated data, in detector operations, and in the trigger and data acquisition systems of the experiment.

3 Data and simulated event samples

This search uses pp collision data at $\sqrt{s} = 13$ TeV collected by the ATLAS experiment in 2015–2018 and corresponding to an integrated luminosity of 139 fb^{-1} [20, 23, 24]. Events are only considered if they were recorded with a trigger selecting a single electron, a single muon, or based on the missing transverse

¹ ATLAS uses a right-handed coordinate system with its origin at the nominal interaction point (IP) in the centre of the detector and the z -axis along the beam pipe. The x -axis points from the IP to the centre of the LHC ring, and the y -axis points upwards. Polar coordinates (r, ϕ) are used in the transverse plane, ϕ being the azimuthal angle around the z -axis. The pseudorapidity is defined in terms of the polar angle θ as $\eta = -\ln \tan(\theta/2)$ and is equal to the rapidity $y = \frac{1}{2} \ln \left(\frac{E+p_z}{E-p_z} \right)$ in the relativistic limit. Angular distance is measured in units of $\Delta R \equiv \sqrt{(\Delta y)^2 + (\Delta \phi)^2}$.

momentum \vec{p}_T^{miss} (with magnitude E_T^{miss}), under stable beam conditions when all detector subsystems were known to be in a good operating condition [25].

Single-lepton triggers [26, 27] requiring the lepton to be isolated in the tracking system and the calorimeter are combined in a logical OR with triggers with a higher transverse momentum (p_T) threshold without isolation requirements to achieve maximum efficiency. Single-muon triggers with a p_T threshold of (20) 26 GeV in (2015) 2016–2018 and isolation requirements, are combined with triggers with a 50 GeV threshold with no isolation requirement. A trigger with a 60 GeV threshold but only relying on the barrel muon spectrometer was added for the 2017–2018 data-taking period. The lowest p_T threshold for single-electron triggers was (24) 26 GeV in (2015) 2016–2018. The E_T^{miss} trigger [28] used an E_T^{miss} threshold of 70 GeV in 2015 and a run-period-dependent E_T^{miss} threshold varying between 90 GeV and 110 GeV in other years.

The expected signal and background contributions are modelled by Monte Carlo (MC) simulated samples, with generators and configurations summarised in Table 1. The simulated events were processed through a simulation [29] of the ATLAS detector geometry and response using GEANT4 [30], and reconstructed with the same software as the collision data. All simulated samples, except those produced with SHERPA [31], used EVTGEN 1.2.0 [32] to model the heavy-flavour hadron decays. The effect of multiple interactions in the same and neighbouring bunch crossings (pile-up) was modelled by overlaying minimum-bias interactions simulated with PYTHIA 8.186 [33] using the A3 tune [34] onto the hard-scatter events according to the luminosity profile of the recorded data. Corrections were applied to simulated events to ensure that lepton and jet selection efficiencies, energy scales, and energy resolutions match those measured in data. The simulated samples were normalised to their respective cross-sections, calculated to the highest order available in perturbation theory. The top-quark and Higgs-boson masses were set to 172.5 GeV and 125 GeV, respectively, in all simulated samples. Although the search directly targets only light leptons, τ -lepton production and decay, in particular to electrons or muons, are included in all simulations.

3.1 Simulated signal samples

Vector-like T -quark pair-production signal samples were simulated at leading-order (LO) with PROTONS 2.2 [37] using the NNPDF2.3LO [38] parton distribution function (PDF) set, interfaced to PYTHIA 8.186 for parton showering and fragmentation with the A14 tune [39]. The theoretical $T\bar{T}$ cross-section was computed at approximate next-to-next-to-leading-order (NNLO) in quantum chromodynamics (QCD) with next-to-next-to-leading logarithmic (NNLL) soft-gluon resummation using TOP++ 2.0 [51–56] and the MSTW2008 NNLO [57, 58] PDF set. The vector-like quarks were forced to decay with equal branching fractions of $1/3$ to each of the three decay modes (Wb , Zt , Ht), and other sets of branching fractions consistent with the three benchmark scenarios (SU(2) singlet, SU(2) doublet, $\mathcal{B}(T \rightarrow Ht) = 100\%$) were obtained by reweighting. Samples were simulated assuming SU(2) singlet couplings for T -quark masses between 0.8 TeV and 2.0 TeV, with 0.1 TeV intervals between 1.0 TeV and 1.8 TeV, corresponding to theoretical cross-sections between (0.195 ± 0.020) pb at 0.8 TeV and (0.132 ± 0.024) fb at 2.0 TeV. Kinematic differences arising from the different chirality of SU(2) doublet and singlet couplings are found to be negligible, rendering the simulation of dedicated samples for the doublet scenario unnecessary.

Table 1: Summary of Monte Carlo samples used for event generation of signal and background processes. The samples used to estimate the systematic uncertainties are indicated in parentheses. V denotes the production of an electroweak boson (W or Z). The column labelled “Parton shower” refers to the generator used for the parton shower (PS), hadronisation and the underlying event. The parton distribution function (PDF) used for the matrix element (ME) is shown. “Tune” refers to the underlying set of tuned parameters for the PS generator. MG5_AMC refers to MADGRAPH5_AMC@NLO 2.2, 2.3 or 2.6 [35]. All samples include leading-logarithm photon emission, either modelled by the PS generator or by PHOTOS [36].

Process	Generator	ME order	Parton shower	PDF	Tune
<i>Signal</i>					
$T\bar{T}$	PROTOS 2.2 [37]	LO	PYTHIA 8.1 [33]	NNPDF2.3LO [38]	A14 [39]
<i>Top-quark pairs</i>					
$t\bar{t}$	POWHEG BOX [40–42]	NLO	PYTHIA 8.2 [43]	NNPDF3.0NLO [44]	A14
	(MG5_AMC [35])	(NLO)	(PYTHIA 8.2)	(NNPDF3.0NLO)	(A14)
	(POWHEG BOX)	(NLO)	(HERWIG 7.1.3 [45])	(NNPDF3.0NLO)	(HERWIG default)
$(t\bar{t}b\bar{b})$	(POWHEG BOX RES [46, 47])	(NLO)	(PYTHIA 8.3 [48])	(NNPDF3.1NNLO [49])	(A14)
<i>Other top</i>					
Single-top	POWHEG BOX	NLO	PYTHIA 8.2	NNPDF3.0NLO	A14
	(POWHEG BOX)	(NLO)	(PYTHIA 8.2)	(NNPDF3.0NLO)	(A14)
	(MG5_AMC)	(NLO)	(PYTHIA 8.2)	(NNPDF3.0NLO)	(A14)
	(POWHEG BOX)	(NLO)	(HERWIG 7.0.4)	(NNPDF3.0NLO)	(HERWIG default)
$t\bar{t}W, t\bar{t}Z/\gamma^*$	MG5_AMC	NLO	PYTHIA 8.2	NNPDF3.0NLO	A14
$t\bar{t}H$	POWHEG BOX	NLO	PYTHIA 8.2	NNPDF3.0NLO	A14
tZ	MG5_AMC	LO	PYTHIA 8.1	NNPDF2.3LO	A14
tH	MG5_AMC	NLO	PYTHIA 8.2	NNPDF3.0NLO	A14
$t\bar{t}t$	MG5_AMC	LO	PYTHIA 8.1	NNPDF2.3LO	A14
<i>Non-top</i>					
V +jets	SHERPA 2.2.11 [31]	NLO/LO	SHERPA 2.2.11 [50]	NNPDF3.0NNLO	SHERPA default
VV	SHERPA 2.2.1/2.2.2	NLO/LO	SHERPA 2.2.1/2.2.2	NNPDF3.0NNLO	SHERPA default
Multijet	PYTHIA 8.2	LO	PYTHIA 8.2	NNPDF2.3LO	A14

3.2 Simulated background samples

To suppress QCD and electroweak background processes that do not resemble the targeted signal topology, a series of preselection requirements are applied (see Section 5 for details). After preselection, the main source of background is the production of top quark–antiquark pairs ($t\bar{t}$), either alone or in association with jets. Moreover, the production of a single top quark in association with a W boson (Wt) contributes significantly in regimes of high transverse momentum. It is grouped into the “Other top” category when not shown separately. This category also includes subdominant background processes involving top quarks produced in association with bosons or additional top quarks, namely $t\bar{t}W$, $t\bar{t}Z/\gamma^*$, $t\bar{t}H$, tH , tZ , and four-top events. The remaining contributions originate mostly from W +jets, Z +jets and QCD multijet production processes, which are grouped into the “Non-top” category when not shown separately.

Standard Model $t\bar{t}$ events were produced in the five-flavour scheme at next-to-leading-order (NLO) with POWHEG BOX v2 [40–42, 59] using the NNPDF3.0_{NLO} [44] PDF set. Parton showering, hadronisation and the underlying event were simulated using PYTHIA 8.230 [43] with the NNPDF2.3_{LO} PDF set and the A14 tune. This sample was normalised to the integrated cross-section calculated by TOP++ 2.0 at NNLO in QCD, including resummation of NNLL soft-gluon terms. The h_{damp} parameter in POWHEG BOX, which controls the matching of the matrix element to the parton shower and effectively regulates the degree of high- p_T radiation, was set to $1.5 m_t$ [60]. Two alternative $t\bar{t}$ samples are used to estimate the effects of applying different matching prescriptions: one where the matrix element was calculated by MADGRAPH5_AMC@NLO 2.6.0 [35] instead of POWHEG BOX, and one where showering and hadronisation was performed by HERWIG 7.1.3 [45] instead of PYTHIA.

The $t\bar{t}$ samples were simulated inclusively, with events categorised according to the flavour content of additional jets not originating from the decay of the $t\bar{t}$ system (see Ref. [61] for details). Events containing at least one b -hadron are classified as $t\bar{t}+\geq 1b$. Among the remaining events, those containing at least one c -hadron are classified as $t\bar{t}+\geq 1c$. All other events, including those with no additional jets, are labelled as $t\bar{t}$ +light jets. An alternative $t\bar{t}b\bar{b}$ sample was simulated at NLO in the four-flavour scheme with POWHEG BOX RES [46, 47] interfaced to OPENLOOPS [62–64] and PYTHIA 8.309 [48], with the NNPDF3.1_{NNLO} [49] PDF set. Based on the studies of Ref. [65], the factorisation scale was set to $\frac{1}{2} \sum_{i=t,\bar{t},b,\bar{b},j} m_{T,i}$ and the renormalisation scale to $\frac{1}{2} \sqrt[4]{m_T(t) \cdot m_T(\bar{t}) \cdot m_T(b) \cdot m_T(\bar{b})}$. The h_{damp} parameter was set to $H_T/2$ and the POWHEG internal parameter h_{bzd} , which regulates the damping function in conjunction with h_{damp} , was set to 5. This sample is used to assess the effects of alternative $t\bar{t}+\geq 1b$ modelling, in particular the use of the four- rather than the five-flavour scheme and consequently $b\bar{b}$ pairs being included in the matrix element rather than being added by the parton shower.

Single-top-quark event samples for the Wt -, s -, and t -channel production mechanisms were simulated at NLO with POWHEG BOX v2 using a fixed renormalisation and factorisation scale and the NNPDF3.0_{NLO} PDF set, interfaced to PYTHIA 8.230 with the A14 tune and NNPDF2.3_{LO} PDF set. Overlaps between the $t\bar{t}$ and Wt final states were removed using the diagram removal scheme [66, 67]. To assess the impact of this choice, an alternative sample was produced applying the diagram subtraction scheme but otherwise identical event settings. Two alternative samples are used to estimate the effects of hard-process and parton-shower modelling, respectively: one where the matrix element was calculated by MADGRAPH5_AMC@NLO 2.6.2 instead of POWHEG BOX, and one where showering and hadronisation was performed by HERWIG 7.0.4 instead of PYTHIA.

The production of $t\bar{t}W$ and $t\bar{t}Z/\gamma^*$ events was modelled using MADGRAPH5_AMC@NLO 2.3.3 interfaced to PYTHIA 8.210 in the A14 tune. The production of $t\bar{t}H$ (tH) events was modelled using POWHEG BOX v2

(MADGRAPH5_AMC@NLO 2.3.3) interfaced to PYTHIA 8.230 in the A14 tune. All of these samples were simulated at NLO and using the NNPDF3.0_{NLO} PDF set. The production of tZ events was modelled at LO using MADGRAPH5_AMC@NLO 2.2.1 with the NNPDF2.3_{LO} PDF set, interfaced to PYTHIA 8.201 with the A14 tune. Four-top-quark production ($t\bar{t}t\bar{t}$) was simulated at LO using MADGRAPH5_AMC@NLO 2.2.2 with the NNPDF2.3_{LO} PDF set, interfaced to PYTHIA 8.186 with the A14 tune, and normalised to the NLO theoretical cross-section.

Samples of W +jets and Z +jets events (V +jets) were simulated using SHERPA 2.2.11, following the ATLAS V +jets modelling setup described in Ref. [68]. The matrix-element calculation was performed with up to two partons at NLO and up to five partons at LO using COMIX [69] and OPENLOOPS. The matrix-element calculation, performed using the NNPDF3.0_{NNLO} PDF set, was merged with the SHERPA parton shower [50] using the MEPS@NLO prescription [70].

Samples of diboson final states (VV), representing collectively WW , WZ , and ZZ samples, were simulated with SHERPA 2.2.1 or 2.2.2 depending on the process, including off-shell effects and Higgs-boson contributions where appropriate. Fully leptonic final states and semileptonic final states, where one boson decays leptonically and the other hadronically, were simulated at NLO in QCD for up to one additional parton and at LO for up to three additional parton emissions. Samples for the loop-induced processes $gg \rightarrow VV$ were simulated at LO for up to one additional parton emission for both, fully leptonic and semileptonic, final states. The matrix-element calculations and PDF choice were handled using the same procedure as in V +jets samples.

Multijet events were simulated at LO using PYTHIA 8.230 for dijet production and interfaced to a p_T -ordered parton shower [71].

4 Object reconstruction

The targeted final state, depicted in Figure 1, is characterised by exactly one electron or muon, multiple jets and b -tagged jets, and E_T^{miss} from the neutrinos. Hadronically decaying vector bosons, Higgs bosons and top quarks are reconstructed by reclustering and tagging jets. Leptonic W -boson candidates are constructed from the lepton and \vec{p}_T^{miss} . Leptonic top-quark candidates are then formed by combining the leptonic W -boson candidate with a b -tagged jet. T -quark candidates are constructed from reclustered jets and leptonic W -boson or top-quark candidates. The kinematics of all objects are used to construct sensitive input variables for the multivariate signal classifier and to define analysis regions. The detailed procedure for reconstructing all of these objects is described in the following.

Interaction vertices from proton–proton collisions are reconstructed from at least two tracks with $p_T > 500$ MeV that are consistent with originating from the beam collision region in the x – y plane. If more than one primary vertex candidate is found, the candidate whose associated tracks form the largest sum of squared p_T [72] is selected as the hard-scatter primary vertex.

Electron candidates [73] are reconstructed from energy clusters in the EM calorimeter associated with reconstructed tracks in the inner detector. They are required to have $p_T > 30$ GeV and $|\eta_{\text{cluster}}| < 2.47$, omitting the transition region between the EM barrel and endcap calorimeters ($1.37 < |\eta_{\text{cluster}}| < 1.52$). The ‘‘Tight’’ likelihood-based identification criteria using calorimeter, tracking, and combined variables are imposed to provide separation between electrons and jets. To further reduce the background from heavy-flavour decays and misidentified light hadrons, the electron candidates are required to be isolated in the tracking system and the calorimeter according to the ‘‘Loose’’ criteria.

Muon candidates [74] are reconstructed by matching tracks in the muon spectrometer to those found in the inner detector. The resulting muon candidates are re-fitted using the complete track information from both detector systems. They are required to have $p_T > 30$ GeV, $|\eta| < 2.5$, and satisfy the “Medium” (“High- p_T ”) identification criteria if their transverse momentum is smaller (larger) than 800 GeV. To further reduce the background from non-prompt muons, the muon candidates are required to be isolated in the tracking system and the calorimeter according to the “TightTrackOnly” criteria. Electron (muon) candidates are matched to the primary vertex by requiring that the significance of their transverse impact parameter, d_0 , satisfies $|d_0/\sigma(d_0)| < 5$ (3), where $\sigma(d_0)$ is the measured uncertainty in d_0 , and by requiring that their longitudinal impact parameter, z_0 , satisfies $|z_0 \sin \theta| < 0.5$ mm.

Jet candidates are reconstructed using the anti- k_t algorithm [75] as implemented in FASTJET [76] with a jet radius parameter $R = 0.4$. The inputs to this algorithm are particle-flow objects [77], which combine measurements from the ATLAS inner detector and calorimeters [78]. Candidate jets are required to have $p_T > 25$ GeV and $|\eta| < 2.5$, and are called small- R jets in the following. Quality criteria are imposed to reject events that contain any jet arising from non-collision sources or detector noise [79]. For jets with $p_T < 120$ GeV, the output score of the jet-vertex tagger (JVT) [80] algorithm is required to be larger than 0.59 if $|\eta| < 2.4$ and larger than 0.11 if $2.4 \leq |\eta| < 2.5$ to suppress contamination from jets that originate from pile-up interactions.

Overlaps between candidate objects are removed sequentially. To suppress misattribution of muon calorimeter deposits, small- R jets within $\Delta R = 0.4$ of a muon candidate are discarded if the muon has a significant fraction of the jet momentum or there is significant hadronic activity close to the muon. Similarly, electrons that share a track with a muon candidate are removed. Double-counting of clusters associated with electrons and small- R jets is avoided by discarding small- R jets within $\Delta R = 0.2$ of any electron. If the electron is within $\Delta R = 0.4$ of the axis of any small- R jet after this initial removal, the small- R jet is retained and the electron is removed. Jets arising from muon bremsstrahlung are characterised by having few matching inner-detector tracks. They are removed by discarding those small- R jet candidates within $\Delta R = 0.2$ of a muon that have less than three tracks originating from the primary vertex. Muons that satisfy $\Delta R(\mu, \text{jet}) < 0.04 + 10 \text{ GeV}/p_T^\mu$ are rejected to remove those muons that are likely to have arisen in the decay chain of hadrons.

Jets originating from b -hadrons are identified using anti- k_t variable-radius jets [81], reconstructed from inner-detector tracks, with an effective radius parameter $R_{\text{eff}} = 30 \text{ GeV}/p_T$ using the transverse momentum of the resulting jet, and minimum and maximum radius bounds of 0.02 and 0.4, respectively. Flavour tagging is performed with the multivariate DL1r algorithm [82], which exploits the jet kinematics, track-level impact parameter information, and the properties of reconstructed secondary and tertiary decay vertices. Jets are classified as b -tagged if their DL1r discriminant exceeds the threshold corresponding to a 77% b -hadron identification efficiency, at which the rejection factors for c -hadrons and light hadrons (from gluons, up, down, and strange quarks) are approximately 5 and 112, respectively. Selected b -tagged jets are required to satisfy $p_T > 20$ GeV and $|\eta| < 2.5$.

The missing transverse momentum \vec{p}_T^{miss} is calculated as the negative vector sum of the \vec{p}_T of all selected and calibrated objects in the event, including a term to account for energy from soft particles in the event that are not associated with any of the selected objects. This soft term is calculated from inner-detector tracks matched to the selected primary vertex to make it more resilient to contamination from pile-up interactions [83].

Candidate small- R jets with relaxed kinematic requirements of $p_T > 20$ GeV and $|\eta| < 4.5$ before overlap removal are used as input for jet reclustering [84]. Reclustering is performed with an anti- k_t variable-radius

Table 2: Selection criteria for mass-, V -, H -, and t -tagged jets, and their respective performances. N_{const} denotes the number of small- R jets retained as constituents of the reclustered variable- R jet after trimming. Dashes (–) refer to definitions that are not applicable to certain categories.

Jet tag	Selection			Performance	
	p_{T} [GeV]	m [GeV]	N_{const}	True-positive rate	False-positive rate
mass	> 300	> 70	–	–	–
V	> 350	(70, 105]	$= 2$ if $p_{\text{T}} < 450$ GeV ≤ 2 if $p_{\text{T}} \geq 450$ GeV	0.80	0.20
H	> 350	(105, 140]	$= 2$ if $p_{\text{T}} < 600$ GeV ≤ 2 if $p_{\text{T}} \geq 600$ GeV	0.65	0.10
t	> 400	> 140	≥ 2 if $p_{\text{T}} < 700$ GeV ≥ 1 if $p_{\text{T}} \geq 700$ GeV	0.70	0.25

algorithm [81] with $R_{\text{eff}} = \min(1.5, 550 \text{ GeV}/p_{\text{T}})$ using the transverse momentum of the resulting jet, and is found to more accurately capture the kinematics of hadronically decaying boosted heavy particles, such as top quarks and Higgs bosons, compared with fixed-radius jets with $R = 1.0$, particularly at $p_{\text{T}} < 600$ GeV. Contributions from pile-up interactions and soft radiation are suppressed by removing small- R subjets within each variable- R jet that carry less than 5% of its transverse momentum [85]. The resulting variable- R jets are required to satisfy $p_{\text{T}} > 200$ GeV and $|\eta| < 2.0$.

Hadronically decaying, boosted heavy-particle candidates are identified and mass-tagged as variable- R jets with $p_{\text{T}} > 300$ GeV and mass m larger than 70 GeV. These mass-tagged jets are further classified as originating from vector bosons, Higgs bosons, or top quarks using analysis-specific criteria optimised for signal acceptance and mistag rate. Vector-boson candidates (V -tagged jets) are mass-tagged jets with $70 \text{ GeV} < m \leq 105 \text{ GeV}$, $p_{\text{T}} > 350$ GeV, and exactly two small- R subjets (N_{const}) for $p_{\text{T}} < 450$ GeV or up to two subjets for higher p_{T} . Higgs-boson candidates (H -tagged jets) are mass-tagged jets with $105 \text{ GeV} < m \leq 140 \text{ GeV}$, $p_{\text{T}} > 350$ GeV, and $N_{\text{const}} = 2$ for $p_{\text{T}} < 600$ GeV or $N_{\text{const}} \leq 2$ for higher p_{T} . Top-quark candidates (t -tagged jets) are mass-tagged jets with $m > 140$ GeV, $p_{\text{T}} > 400$ GeV, and $N_{\text{const}} \geq 2$ for $p_{\text{T}} < 700$ GeV or $N_{\text{const}} \geq 1$ for higher p_{T} . The selection criteria and the tagging performance are summarised in Table 2. The performance is characterised by the true-positive rate, defined as the rate of correctly tagging a jet originating from a vector boson, Higgs boson, or top quark, and the false-positive rate, defined as the rate of incorrectly tagging a jet not originating from the corresponding particle, evaluated in $T\bar{T}$, $t\bar{t}$, and non- $t\bar{t}$ SM events as appropriate.

Leptonic W -boson candidates (W_{ℓ}^{reco}) are constructed from the lepton and the $\vec{p}_{\text{T}}^{\text{miss}}$ in the event: the azimuthal direction and p_{T} of the neutrino attributed to the W boson are chosen to be the same as the azimuthal direction and magnitude of $\vec{p}_{\text{T}}^{\text{miss}}$. The neutrino pseudorapidity η^{ν} is determined by imposing a W -boson mass constraint on the lepton–neutrino system. If multiple solutions exist, the lowest $|\eta^{\nu}|$ is chosen. If no solution exists, a unique solution is constructed by setting η^{ν} to be identical with the lepton pseudorapidity and the neutrino p_{T} such that the W -boson mass constraint is met.

Leptonic top-quark candidates (t_{ℓ}^{reco}) are constructed from W_{ℓ}^{reco} and a small- R jet geometrically matched to one originating from a b -hadron. First, the b -tagged jet closest in ΔR to the W_{ℓ}^{reco} is identified. The small- R jet closest in ΔR to this b -tagged jet is then combined with W_{ℓ}^{reco} to form t_{ℓ}^{reco} , provided that it lies within $\Delta R = 0.4$ of the b -tagged jet, within $\Delta R = 1.5$ of W_{ℓ}^{reco} , and not within $\Delta R = 1.0$ of a V -, H -, or t -tagged jet. The small- R jet is used, instead of the b -tagged jet directly, to avoid double-counting

four-momenta in the later construction of T -quark candidates. If no suitable small- R jet is found, no t_ℓ^{reco} candidate is constructed.

T -quark candidates are constructed from combinations of decay products. The input set consists of all variable- R jets and, when available, the leptonic top-quark candidate t_ℓ^{reco} . To avoid double counting, the four-momentum of the small- R jet associated with the t_ℓ^{reco} is subtracted from that of the nearest variable- R jet. If no t_ℓ^{reco} candidate is reconstructed, the leptonic W -boson candidate W_ℓ^{reco} is used instead. Two T -quark candidates, $T_1^{\text{var-}R}$ and $T_2^{\text{var-}R}$, are then formed by pairing the available decay candidates and selecting the two exclusive combinations with the largest ΔR separation, reflecting the expected back-to-back topology of the T -quark pair. An analogous set of T -quark candidates, T_1^{mass} and T_2^{mass} , is constructed based on mass-tagged jets in place of variable- R jets.

5 Analysis strategy

This search targets the pair production of T -quarks in events where at least one T -quark decays via $T \rightarrow Ht$, with subsequent $H \rightarrow b\bar{b}$ and a leptonic top-quark decay. These signal topologies are characterised by multiple small- R , b -tagged, and H -tagged jets, as well as moderate E_T^{miss} from neutrinos. The events frequently contain an additional t -tagged jet, corresponding to a hadronically decaying boosted top quark, or a reconstructed leptonic top-quark candidate. V -tagged jets can arise from hadronically decaying Z or W bosons produced in decays of T -quarks ($T \rightarrow Zt$, $T \rightarrow Wb$), Higgs bosons or top quarks.

Events are first required to satisfy a preselection targeting the general features of the signal topology, as described in Section 5.1. Selected background processes are then corrected using data-driven reweighting to improve their modelling (Section 5.2). A multivariate classifier (Section 5.3) is subsequently trained to discriminate signal from SM background. Its output, together with requirements on the b -tagged and H -tagged jet multiplicities, is used to categorise events into signal and control regions, as described in Section 5.4. The event yields in these regions as a function of the effective mass are used in the statistical analysis.

5.1 Preselection

A preselection is applied requiring events to satisfy the trigger selection and have at least one primary vertex candidate. Exactly one selected electron or muon is required, suppressing multijet background, while retaining signal events in which one W boson decays leptonically. For events satisfying a single-lepton trigger, the selected lepton must match the trigger-level object within $\Delta R < 0.15$. Events failing to meet the single-lepton trigger acceptance or matching conditions are retained if they satisfy the E_T^{miss} trigger and have an offline-reconstructed E_T^{miss} above 250 GeV, ensuring full trigger efficiency. At least five small- R jets ($N_{\text{jets}} \geq 5$) and at least two b -tagged jets ($N_{b\text{-jets}} \geq 2$) are required, reducing contributions from non- $t\bar{t}$ processes. Additional conditions suppress multijet background. The missing transverse momentum is required to satisfy $E_T^{\text{miss}} > 20$ GeV and $m_T^W + E_T^{\text{miss}} > 60$ GeV, where $m_T^W := \sqrt{2p_T^\ell E_T^{\text{miss}}(1 - \cos \Delta\phi)}$ is the transverse mass of the lepton and \vec{p}_T^{miss} system. Finally, to select events consistent with the decay of high-mass particles into many objects with large transverse momentum, the effective mass m_{eff} , defined as the scalar sum of the p_T of all selected small- R jets and the lepton as well as E_T^{miss} , is required to exceed 1000 GeV.

5.2 Data-driven background reweighting

The background samples as described in Section 3.2 overestimate the multijet production cross-section, and a reweighting procedure is applied to correct the normalisation. Reweighting factors are derived in a multijet-enriched region defined by inverting preselection requirements on E_T^{miss} and $E_T^{\text{miss}} + m_T^W$, and requiring the lepton p_T to be below 100 GeV, a selection under which the lepton candidate is predominantly non-prompt or misidentified. The resulting reweighting factors of approximately 0.55 are applied to normalise all multijet distributions in the following, while the shape is retained from the MC simulation.

The background samples furthermore overestimate the cross-section of $t\bar{t}$ processes at large p_T and underestimate it at large N_{jets} [86, 87]. Similarly, large uncertainties are observed for the modelling of V +jets processes at large jet multiplicities [68]. This is addressed with an iterative data-driven reweighting, similar to the technique used in Ref. [88], as outlined in the following.

First, a region enriched in $Z(\rightarrow \ell\ell)$ +jets events is defined to derive reweighting factors for V +jets processes. The region is designed to be kinematically close to the preselection, requiring $N_{\text{jets}} \geq 5$, $N_{b\text{-jets}} \geq 1$, exactly two same-flavour, oppositely charged leptons, and a dilepton invariant mass consistent with the Z boson. Contamination from $t\bar{t}$ processes is reduced by requiring $E_T^{\text{miss}} < 100$ GeV. Reweighting factors are then derived as a function of jet multiplicity; each factor is defined as the ratio of the difference between data and the predicted non- V +jets yields to predicted V +jets yields. They range from 1.0 at $N_{\text{jets}} = 5$ to 0.7 at $N_{\text{jets}} \geq 8$, and are applied to all V +jets processes according to their jet multiplicity.

Subsequently, a region enriched in $t\bar{t}$ events is defined to derive reweighting factors for $t\bar{t}$ and tW processes. The region is designed to be kinematically close to the preselection, requiring $N_{\text{jets}} \geq 3$, $N_{b\text{-jets}} = 2$, and exactly one lepton. Reweighting factors are first derived as a function of jet multiplicity, ranging from 0.9 at $N_{\text{jets}} = 5$ to 1.4 at $N_{\text{jets}} \geq 12$, and are applied to all $t\bar{t}$ and tW processes according to their jet multiplicity in the following. In a final step, reweighting factors are derived as a function of $m_{\text{eff}}^{\text{red}} := m_{\text{eff}} - (N_{\text{jets}} - 5) \cdot 40$ GeV, an observable in which m_{eff} is reduced by the average transverse momentum (i.e. 40 GeV) of each additional small- R jet in $t\bar{t}$ events. This renders $m_{\text{eff}}^{\text{red}}$ less dependent on N_{jets} than m_{eff} , though a residual dependence remains. To account for this, reweighting factors are derived separately for four jet multiplicities ($N_{\text{jets}} = 5, = 6, = 7, \geq 8$), where the binning is chosen to ensure sufficient statistical precision in the highest multiplicity bin. This motivates the successive rather than simultaneous derivation of the N_{jets} and $m_{\text{eff}}^{\text{red}}$ reweighting factors. The $m_{\text{eff}}^{\text{red}}$ reweighting factors are parameterised using sigmoid functions with the normalisation fixed to that determined in the preceding N_{jets} step. The resulting factors vary between 1.3 and 0.6 as a function of $m_{\text{eff}}^{\text{red}}$, with a mild increase with N_{jets} , and are applied to all $t\bar{t}$ and tW processes according to both observables in the following.

The expected and observed yields before and after the full reweighting procedure in the preselection phase space are given in Figure 2 as a function of m_{eff} , showing a significant improvement of the agreement between data and SM prediction after the reweighting. A similar improvement is observed in E_T^{miss} and the p_T and multiplicity of the other objects considered in the search such as the lepton, the leptonic W -boson and top-quark candidates, and the various jet collections.

5.3 Multivariate signal classifier

Signal events are discriminated from SM backgrounds using a feed-forward neural network (NN) implemented as a multilayer perceptron. The NN uses 30 input variables with low mutual correlation, encompassing both kinematic and topological event properties, chosen to maximise signal-to-background

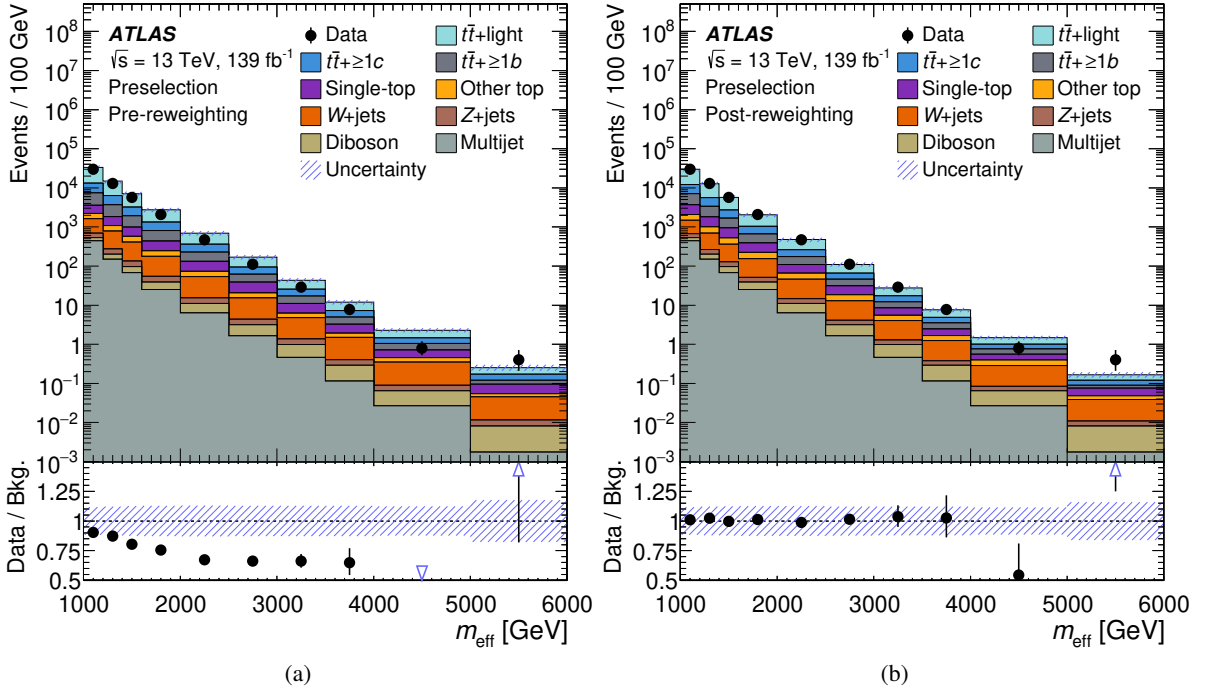


Figure 2: Distribution of the pre-fit expected yields for different SM processes and the observed data yields (black dots) after the preselection as a function of m_{eff} before (a) and after (b) the full reweighting procedure. The bottom panel shows the ratio of the observed data yield to the total SM yield. The blue hatched band indicates the pre-fit uncertainty in the background prediction including the statistical uncertainty, the theoretical cross-section uncertainties and the uncertainty in the integrated luminosity. The blue triangles indicate points that are outside the vertical range of the lower pad.

discrimination. The full list of input variables is given in Appendix A. The NN consists of four hidden layers with 30, 10, 10, and 5 nodes, respectively, and uses a sigmoid activation function. All simulated samples for signal and background processes described in Section 3 are used in the training, which is performed using a binary cross-entropy loss with five-fold cross-validation to mitigate statistical bias. Training regions are defined by requiring $N_{\text{jets}} \geq 6$, $N_{b\text{-jets}} \geq 3$, at least three variable- R jets ($N_{\text{jets}}^{\text{var-}R} \geq 3$), and at least two mass-tagged jets ($N_{\text{jets}}^{\text{mass}} \geq 2$), in addition to the preselection. The NN hyperparameters, including the architecture and activation function, are optimised by scanning multiple configurations and selecting the one that maximises the area under the receiver operating characteristic (ROC) curve in test data.

Figure 3 gives a comparison of the yields expected from SM and representative signal processes in the training region for the two NN input variables with the largest signal-to-background separation power, the effective mass m_{eff} and the transverse momentum of the third-most-energetic variable- R jet, $p_{\text{T}}^{\text{var-}R,3}$. The next most important input variables are the transverse momentum of the leptonic top-quark candidate, the multiplicity of variable- R jets, and the transverse momentum of the most energetic H -tagged jet, as shown in Appendix A. The NN score (h_{NN}) distributions for the different $T\bar{T}$ decay modes have similar shapes, as shown in Figure 4, indicating comparable discrimination power across the signal topologies considered. The NN performance is validated by verifying the agreement between data and SM predictions in both the preselection and training region for the NN input variables and output score.

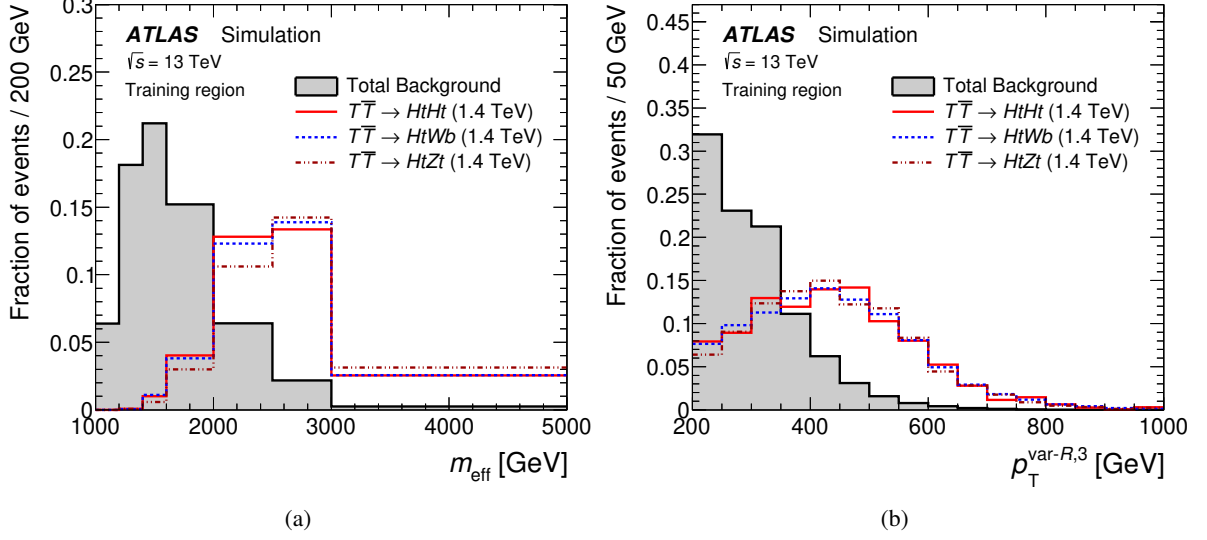


Figure 3: Normalised distributions for the total SM background (grey area) and representative signal processes (coloured lines) in the training region as a function of (a) effective mass and (b) p_{T} of the third-most-energetic variable- R jet, which are the two NN input variables with the largest signal-to-background separation power.

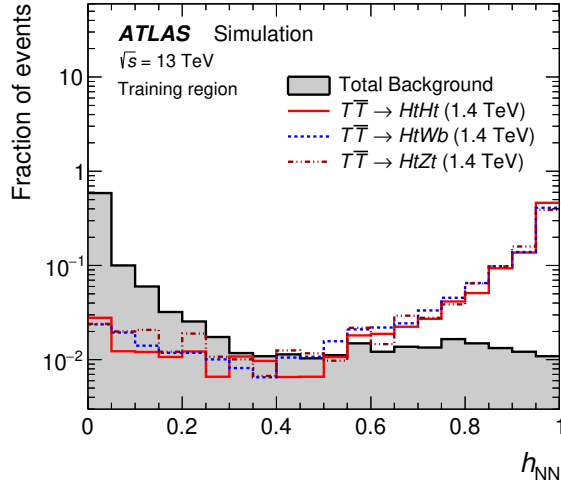


Figure 4: Normalised distributions for the total SM background (grey area) and representative signal processes (coloured lines) in the training region as a function of the NN score h_{NN} .

5.4 Event categorisation

For the statistical analysis, twelve signal regions (SRs) targeting the signal topology and one control region (CR) for estimating the $t\bar{t}$ +light jets background are constructed. The background modelling is further validated in two validation regions (VRs). These three region categories (SRs, CRs, and VRs) are collectively referred to as “analysis regions”. Their selection requirements in addition to the preselection criteria are summarised in Table 3.

The SRs exploit the NN and therefore follow the selection used for its training, as described in Section 5.3. To improve signal sensitivity, the jet multiplicity requirement is relaxed to the preselection level of $N_{\text{jets}} \geq 5$, with negligible impact on the NN performance. The signal regions are subdivided according to the NN score h_{NN} into three categories of decreasing signal purity. The high-NN (HNN) region, defined by $h_{\text{NN}} > 0.81$, achieves a background rejection factor above 20 for an $HtH\bar{t}$ signal efficiency of 79%. The mid-NN (MNN) region, defined by $0.16 \leq h_{\text{NN}} \leq 0.81$, retains 17% of $HtH\bar{t}$ signal events. The low-NN (LNN) region, defined by $h_{\text{NN}} < 0.16$, has a background rejection factor of 4 while accepting only 4% of $HtH\bar{t}$ signal events, resulting in a large fraction of $t\bar{t}+\geq 1c$ and $t\bar{t}+\geq 1b$ events that makes it well-suited for constraining these backgrounds in the fit. Since the NN is trained to be agnostic to the vector-like quark decay mode, sensitivity to the $T\bar{T} \rightarrow HtH\bar{t}$ signal is enhanced by further subdividing the signal regions according to the b -tagged jet multiplicity (3 or ≥ 4) and, independently, whether at least one H -tagged jet is present.

For the $t\bar{t}$ +light jets control region, events are required to satisfy the preselection, to contain exactly one reconstructed leptonic top-quark candidate t_{ℓ}^{reco} ($N_{t_{\ell}^{\text{reco}}} = 1$), and to have exactly one V -tagged or t -tagged jet ($N_{\text{jets}}^V + N_{\text{jets}}^t = 1$). Events containing H -tagged jets are vetoed ($N_{\text{jets}}^H = 0$). A high purity in $t\bar{t}$ +light jets events is achieved by requiring exactly two b -tagged jets. Two validation regions are defined to validate the modelling of the $t\bar{t}+\geq 1c$ and $t\bar{t}+\geq 1b$ backgrounds in the SRs. They follow the same selections as the control region, but require exactly three or at least four b -tagged jets, respectively. To increase statistical precision, no requirement on t_{ℓ}^{reco} is imposed. The validation regions are not orthogonal to the $0H$ signal regions and are therefore not used in the simultaneous fit.

Table 3: Summary of requirements for control, validation and signal regions in addition to the preselection requirements. Dashes (–) refer to selection requirements that are not applied.

Observable	Selection																	
	CR			VRs			LNN SRs				MNN SRs				HNN SRs			
	2b	3b	4b	3b		4b		3b		4b		3b		4b				
region name				0H	1H	0H	1H	0H	1H	0H	1H	0H	1H	0H	1H			
N_{jets}^H		= 0		= 0	≥ 1	= 0	≥ 1	= 0	≥ 1	= 0	≥ 1	= 0	≥ 1	= 0	≥ 1			
$N_{\text{jets}}^V + N_{\text{jets}}^t$		= 1		–	–	–	–	–	–	–	–	–	–	–	–			
$N_{b\text{-jets}}$	= 2	= 3	≥ 4	= 3		≥ 4		= 3		≥ 4		= 3		≥ 4				
$N_{t_{\ell}^{\text{reco}}}$	= 1	–	–	–	–	–	–	–	–	–	–	–	–	–	–			
$N_{\text{jets}}^{\text{var-R}}$	–	–	–							≥ 3								
$N_{\text{jets}}^{\text{mass}}$	–	–	–							≥ 2								
h_{NN}	–	–	–		< 0.16					$[0.16, 0.81]$				> 0.81				

6 Systematic uncertainties

Systematic uncertainties can be categorised into two main types: experimental uncertainties and modelling uncertainties. Experimental uncertainties arise from the detector response to the various physics objects. Modelling uncertainties encompass uncertainties related to theoretical predictions and the parameters chosen for those predictions, and to the data-driven corrections. The former arise from missing higher-order corrections, parton-shower modelling, alternative PDFs, and assumptions in the underlying theory models. Each systematic uncertainty is considered to be correlated across processes, channels, and bins of the signal discriminant, unless explicitly stated otherwise. Uncertainties from different sources are considered to be uncorrelated with each other.

The leading sources of uncertainty in this search arise from the modelling of the $t\bar{t}$ and single-top Wt backgrounds, the flavour-tagging efficiencies (b , c , and light), and the jet mass resolution. The relative contributions of these uncertainties vary across analysis regions, and since different signal processes populate the analysis regions in different proportions, their impact on the search sensitivity is signal-process dependent. The considered systematic uncertainties are detailed in the following.

6.1 Experimental uncertainties

Uncertainties associated with jets arise from the jet-energy scale (JES), jet-energy resolution (JER), the jet-mass scale (JMS), jet-mass resolution (JMR), and the efficiency of the JVT requirements. The JES and JER uncertainties are estimated by combining information from collision data, test-beam data, and simulation [89, 90]. The JES (JER) uncertainties are split into 30 (8) uncorrelated components, corresponding to different physical sources. The uncertainties in the JMS are measured using the ratio of calorimeter and track measurements of the jet mass, and are split into 8 uncorrelated components. The uncertainty in the JMR is estimated by comparing each nominal sample with an alternative event sample in which the mass of each jet is smeared by a Gaussian function whose width is increased by 20% relative to the nominal JMR. These jet-related uncertainties in small- R jets are propagated to the variable- R jets in the reclustering procedure.

The flavour-tagging efficiencies for b -, c -, and light-tagged jets in simulation are corrected to match those measured in $t\bar{t}$ - and Z +jets-enriched data, following the methods described in Refs. [91–93]. Uncertainties are evaluated using nine independent sources for b -tagged jets, five for c -tagged jets, and six for light-flavour jets. These sources are treated as uncorrelated between the different jet flavours. An additional extrapolation uncertainty is included for high- p_T jets beyond the kinematic reach of the calibration data. This uncertainty is assumed to be correlated across all jet flavours.

Uncertainties associated with leptons arise from the efficiencies of the trigger selection, reconstruction, identification, and isolation criteria, as well as the lepton momentum scale and resolution. These are measured in data using $Z \rightarrow \ell\ell$ and $J/\psi \rightarrow \ell\ell$ decays [73, 94].

The estimated uncertainty in the integrated luminosity of the combined 2015–2018 data is 1.7% [24]. Uncertainties associated with the resolution and scale of E_T^{miss} [83], as well as with the efficiency of the E_T^{miss} trigger are also considered. The uncertainty associated with the modelling of pile-up interactions is evaluated from variations of the pile-up reweighting applied to simulated events.

6.2 Theoretical modelling uncertainties

Some systematic uncertainties arise in the theoretical modelling of the signal and background processes detailed in Section 3. All simulated SM processes include predictions for alternative choices of the factorisation and renormalisation scales, and from standard PDF-set variations that capture the statistical and modelling uncertainties in the PDF fits.

Systematic uncertainties in the signal modelling arising from the choice of PDF set are evaluated following the PDF4LHC15 prescription [95], using the MSTW2008 NLO, CT10 NLO [96, 97], and NNPDF3.0_{NLO} PDF sets. No further systematic uncertainties in the signal modelling, in particular regarding the production cross-section, are considered.

An uncertainty of approximately $\pm 6\%$ is assigned to the inclusive $t\bar{t}$ production cross-section [56] for $t\bar{t}$ +light jets processes. For single-top processes, a $\pm 5\%$ uncertainty in the total cross-section, estimated as a weighted average of the theoretical uncertainties in Wt -, s -, and t -channel production [98–100], is included. Multiple additional sources of systematic uncertainty affecting the modelling of $t\bar{t}$ and single-top production are considered. Uncertainties due to the choice of the NLO generator are estimated by comparing the nominal POWHEG+PYTHIA samples with alternative samples generated by MADGRAPH5_AMC@NLO and showered by PYTHIA. The nominal samples are compared with POWHEG+HERWIG samples to estimate the uncertainties in the modelling of the parton showering and hadronisation processes. The alternative samples used to evaluate modelling uncertainties are detailed in Section 3.2. The uncertainty due to initial-state radiation is estimated by simultaneously varying the h_{damp} parameter and the renormalisation and factorisation scales, and choosing the Var3c up/down variants of the A14 set of tuned parameters as described in Ref. [60]. The impact of final-state radiation is evaluated by doubling or halving the renormalisation scale for emissions from the parton shower. The systematic uncertainties arising from the choice of PDF set are evaluated following the PDF4LHC15 prescription identical to those for the signal modelling. All $t\bar{t}$ and single-top uncertainties are considered to be uncorrelated among $t\bar{t}$ +light jets, $t\bar{t}+\geq 1c$, $t\bar{t}+\geq 1b$, and single-top samples, but correlated across the subcategories of the single-top background (Wt -, s -, or t -channel). An additional uncertainty is assigned for the modelling of $t\bar{t}+\geq 1b$ processes by comparing the nominal five-flavour scheme $t\bar{t}$ sample with the alternative $t\bar{t}b\bar{b}$ sample generated in the four-flavour scheme, in which $b\bar{b}$ pairs enter the matrix element. The magnitude of this uncertainty is negligible except in analysis regions with $\geq 4b$, where it ranges from 9% in VR $4b$ to 67% in SR $4b-1H$ -HNN, the latter reflecting the susceptibility of the NN to small kinematic changes and the limited statistical precision on the estimation procedure in this region. Despite the significant size of this uncertainty in certain low-yield bins, its impact on the exclusion limits remains negligible.

An additional systematic uncertainty in Wt -channel production, concerning the separation between $t\bar{t}$ and Wt at NLO [67], is assessed by comparing the nominal sample, which uses the diagram removal scheme, with the alternative sample using the diagram subtraction scheme but otherwise identical event generation settings.

The uncertainties in the modelling of the V +jets backgrounds are estimated by varying the values of the internal renormalisation and factorisation scale parameters in SHERPA. An additional $\pm 30\%$ normalisation uncertainty for the V +jets background is considered for events in analysis regions with different b -tag multiplicity (2, 3, ≥ 4), uncorrelated among b -tag multiplicities. This uncertainty is based on variations of the factorisation and renormalisation scales and SHERPA matching parameters [101], and is considered to be correlated between W +jets and Z +jets processes.

The kinematic reweighting of the main background processes (described in Section 5.2) is derived separately for each modelling uncertainty. This ensures that each alternative background model reproduces the data in the regions used to derive the reweighting factors. After reweighting, the modelling uncertainties therefore primarily account for extrapolations in kinematics and background composition from the derivation regions to the analysis regions. Additional uncertainties arise from the reweighting procedure itself. For the multijet reweighting, a $\pm 11\%$ normalisation uncertainty is assigned based on the statistical precision in the derivation region; its impact on the sensitivity is negligible due to the small multijet contribution. For the $t\bar{t}$ and V +jets reweightings as a function of N_{jets} , the uncertainty is given by the bin-by-bin statistical uncertainties in the derivation regions. For the $m_{\text{eff}}^{\text{red}}$ -dependent reweighting, the uncertainty is obtained by propagating the fit parameter uncertainties according to their covariance matrix, thereby accounting for their correlations. The functional form is kept fixed as a sigmoid function. To obtain a conservative estimate that covers both normalisation and shape variations, a shift of two standard deviations is applied. The resulting uncertainty ranges from ± 0.5 to $\pm 12\%$, depending on the jet multiplicity and reweighted process, and is largest for events with $N_{\text{jets}} \geq 8$.

Diboson, $t\bar{t}W$, $t\bar{t}Z/\gamma^*$, $t\bar{t}H$, tH and tZ processes contribute only a small fraction of events in the analysis regions. Their shape uncertainties are therefore neglected, and only normalisation uncertainties are considered. These are taken from PDF and scale variations in NLO calculations, resulting in $\pm 15\%$ for $t\bar{t}W$, $t\bar{t}Z/\gamma^*$, tH and tZ , $+9/-12\%$ for $t\bar{t}H$, and $\pm 30\%$ for the four-top production. For the diboson background, a $\pm 5\%$ uncertainty is assigned to the inclusive cross-section at NLO [102]. An additional uncorrelated $\pm 24\%$ uncertainty per additional jet is included to account for modelling of additional radiation, based on comparisons of different LO matrix-element and parton-shower merging schemes [103]. This is evaluated at the average jet multiplicity in the analysis regions, which is five jets, corresponding to three additional jets from radiation. A further $\pm 30\%$ normalisation uncertainty is assigned to the production of additional heavy-flavour jets, following the treatment used for V +jets [101]. The total normalisation uncertainty for diboson processes amounts to $\pm 56\%$. As the two leading b -tagged jets in diboson events predominantly originate from $W \rightarrow cs$ or $Z \rightarrow bb$ decays, this uncertainty is applied only in analysis regions with ≥ 3 b -tagged jets. All of these uncertainties are added in quadrature within each region, and the resulting uncertainty is treated as uncorrelated between the $2b$ and $\geq 3b$ analysis regions.

7 Statistical analysis

For each benchmark scenario considered in this search, the m_{eff} distributions across all signal and control regions are jointly studied to test for the presence of the predicted signal. A binned likelihood function $\mathcal{L}(\mu, \kappa, \theta)$ [104] is constructed as a product of Poisson probability terms over all m_{eff} bins considered in the search. The likelihood function depends on the signal-strength parameter μ , which multiplies the predicted production cross-section for the signal, free normalisation factors κ , and θ , a set of nuisance parameters that encode the effect of systematic uncertainties in the signal and background expectations. The normalisation factors κ are applied separately for the $t\bar{t}+\geq 1c$ and $t\bar{t}+\geq 1b$ backgrounds, which proved beneficial in other ATLAS analyses with three or more b -tagged jets [105–107]. Nuisance parameters accounting for statistical uncertainties from the limited size of the simulated samples are modelled in the likelihood function using Poisson constraints. All other nuisance parameters are modelled with Gaussian constraints.

For a given value of μ , variations in the normalisation factors κ and nuisance parameters θ allow the expectations for signal and background to change according to the corresponding systematic uncertainties.

Table 4: Summary of the different sources of uncertainty in μ , shown for a vector-like T -quark with mass 1.4 TeV under the SU(2) singlet, SU(2) doublet, and $\mathcal{B}(T \rightarrow Ht) = 100\%$ scenarios. The impact of a group of nuisance parameters is obtained by summing in quadrature the impacts of all nuisance parameters in this category. The fractional contribution of an uncertainty source gives the ratio of the uncertainty in μ resulting from the fit when fixing the nuisance parameters corresponding to each category to the uncertainty in the best-fit value of μ .

Uncertainty source	Fractional contribution [%], $m_T = 1.4$ TeV		
	SU(2) singlet	SU(2) doublet	$\mathcal{B}(T \rightarrow Ht) = 100\%$
Theory uncertainties (per process group)			
$t\bar{t}$			
Modelling	21	24	26
Reweighting	27	24	21
Single-top	14	10	6.3
Non-top	6.2	4.7	4.0
Other top	4.9	4.6	3.8
Experimental uncertainties			
Jets	17	15	15
Flavour-tagging	8.0	8.0	8.2
Leptons, pile-up, E_T^{miss} & luminosity	1.9	1.7	1.8
Total systematic uncertainty	42	40	38
Data statistical uncertainty	90	90	91
MC statistical uncertainty			
Background	14	14	14
Signal	1.4	3.0	5.3
$t\bar{t}$ normalisation	3.8	3.7	4.1
Total statistical uncertainty	91	92	92

The fitted values of κ and θ correspond to deviations from the nominal expectations that globally provide the best fit to the data. This procedure reduces the impact of systematic uncertainties on the search sensitivity and improves the background prediction by taking advantage of the highly populated, background-dominated control region and LNN signal regions included in the likelihood fit.

The test statistic q_μ , as implemented in the TRExFITTER framework [108] based on RooSTATS [109, 110], is defined as the profile likelihood ratio: $q_\mu := -2 \ln(\mathcal{L}(\mu, \hat{\kappa}_\mu, \hat{\theta}_\mu) / \mathcal{L}(\hat{\mu}, \hat{\kappa}, \hat{\theta}))$. Here, $\hat{\mu}$, $\hat{\kappa}$, and $\hat{\theta}$ are the values of the parameters μ , κ and θ , respectively, which simultaneously maximise the likelihood function $\mathcal{L}(\mu, \kappa, \theta)$. The values of the normalisation factors and nuisance parameters which maximise the likelihood function for a given value of μ are denoted by $\hat{\kappa}_\mu$ and $\hat{\theta}_\mu$, respectively. The statistic used for the discovery test, i.e. to determine the compatibility of the observed data with the background-only hypothesis, is obtained by setting $\mu = 0$ in the profile likelihood ratio and leaving $\hat{\mu}$ unconstrained: $q_0 = -2 \ln(\mathcal{L}(0, \hat{\kappa}_0, \hat{\theta}_0) / \mathcal{L}(\hat{\mu}, \hat{\kappa}, \hat{\theta}))$. The p -value of the discovery test is given by the integral of the probability distribution of q_0 above the observed q_0 value when assuming the background-only hypothesis, computed using the asymptotic approximation detailed in Refs. [111, 112]. The test statistic for deriving the upper limits on the signal production cross-section for each signal scenario considered sets $0 \leq \hat{\mu} \leq \mu$ and is computed using q_μ in the CL_s method [113, 114], also in the asymptotic approximation. For a given signal scenario, values of the production cross-section (parameterised by μ) yielding $\text{CL}_s < 0.05$ are

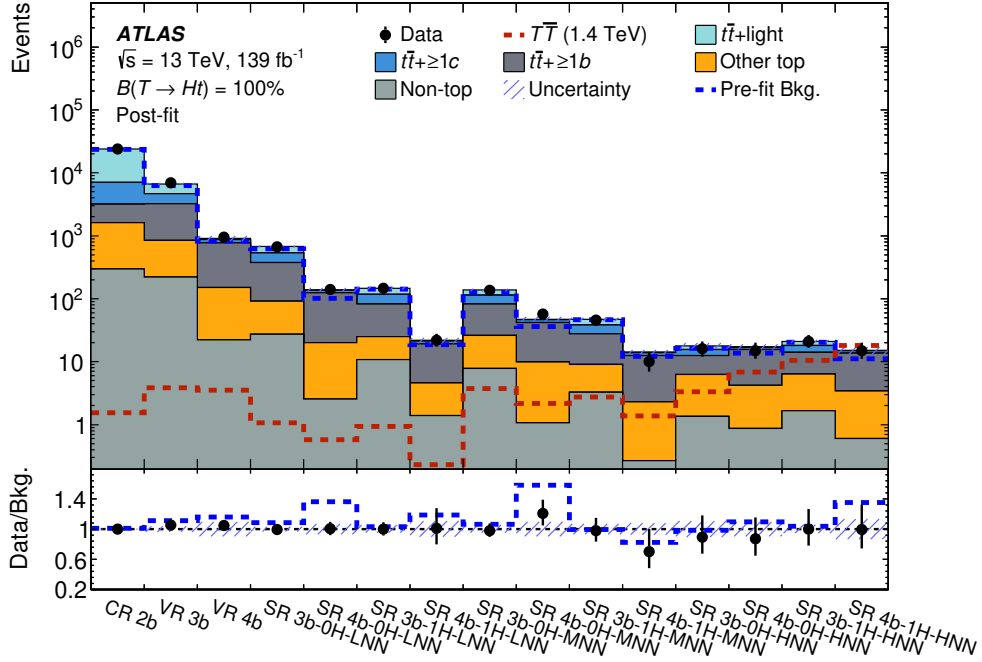


Figure 5: Comparison between total observed yields (black dots) and expected SM yields (coloured areas) in all analysis regions after a fit under the background-only hypothesis in the control and signal regions. The fit result is extrapolated to the validation regions, which are not included in the fit. The bottom panel displays the ratio of data and total SM background. The size of the combined statistical and systematic uncertainty in the background prediction is indicated by a blue hatched band, including all sources of systematic uncertainty described in Section 6. In the upper panel, the dashed blue (red) lines give the total expected SM yield (expected yield from a $\mathcal{B}(T \rightarrow Ht) = 100\%$ signal with $m_T = 1.4$ TeV) before the fit. In the lower panel, the dashed blue line gives the ratio of the observed yield to the total expected SM yield before the fit.

excluded at $\geq 95\%$ confidence level (CL).

8 Results

8.1 Likelihood fit

A likelihood fit is performed under the signal-plus-background hypothesis for each of the generated signal points. No significant excess of the data over the SM prediction, indicative of a signal, is observed. Figure 5 shows results for a likelihood fit under the background-only hypothesis, giving the comparison between the total observed and expected yields in each analysis region after the fit. The combined impact of the systematic uncertainties is constrained in the fit, making use of the information from the large statistics in the signal-depleted control region and LNN signal regions. The normalisation factors for the $t\bar{t} + \geq 1c$ and $t\bar{t} + \geq 1b$ backgrounds are estimated from the fit to be $\kappa_{t\bar{t} + \geq 1c} = 0.97 \pm 0.40$ and $\kappa_{t\bar{t} + \geq 1b} = 1.20 \pm 0.23$, respectively, which is compatible with the findings of comparable ATLAS analyses [105–107]. The fit result is extrapolated to the validation regions, which are not included in the fit, to verify the reliability of the background modelling.

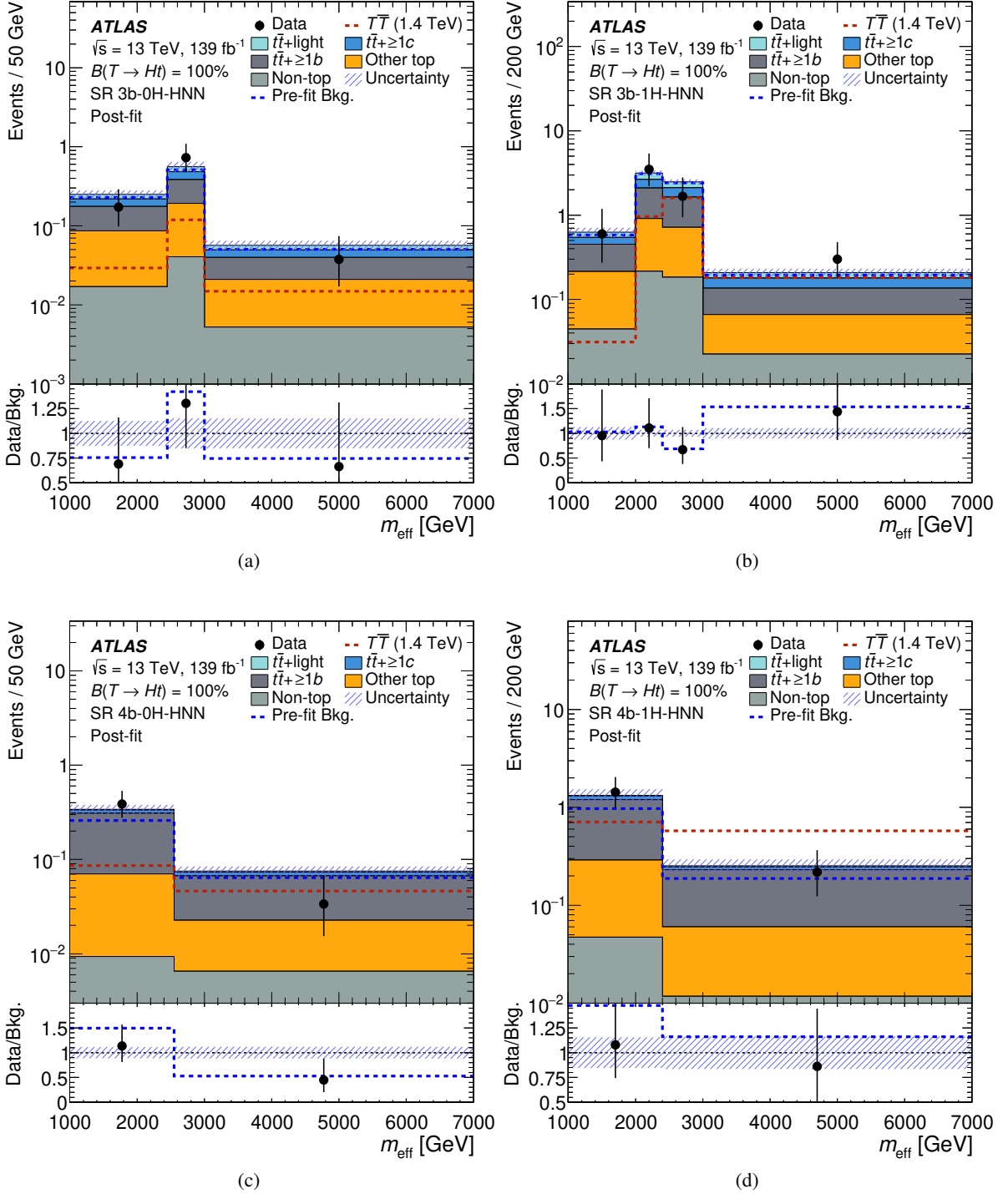


Figure 6: Comparison between observed yields (black dots) and expected SM yields (coloured areas) as a function of m_{eff} for the HNN signal regions (a) SR 3b-0H-HNN, (b) SR 3b-1H-HNN, (c) SR 4b-0H-HNN, and (d) SR 4b-1H-HNN. The expected yields are shown after a fit under the background-only hypothesis in the control and signal regions. The bottom panels display the ratio of data and total SM background. The size of the combined statistical and systematic uncertainty in the background prediction is indicated by a blue hatched band, including all sources of systematic uncertainty described in Section 6. In the upper panel, the total expected SM yield (expected yield from a $\mathcal{B}(T \rightarrow Ht) = 100\%$ signal with $m_T = 1.4$ TeV) before the fit is shown as a dashed blue (red) line. In the lower panel, the ratio of the observed yield to the total expected SM yield before the fit is shown as a dashed blue line.

Table 5: Summary of observed (expected) 95% CL lower limits on the mass of pair-produced vector-like T -quarks under the SU(2) singlet, SU(2) doublet, and $\mathcal{B}(T \rightarrow Ht) = 100\%$ scenarios for this and other related results.

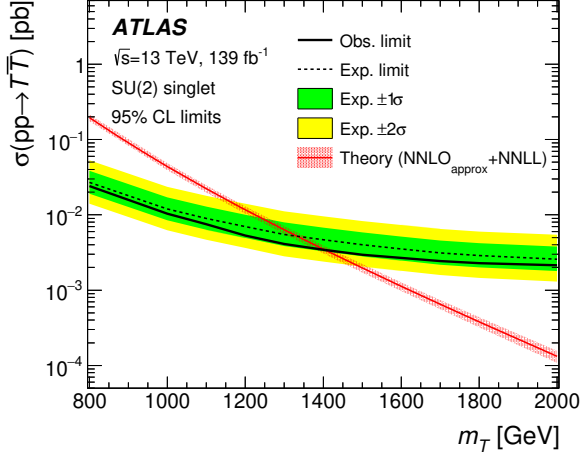
Reference	Analysis		Exclusion limits [TeV]		
	Experiment	Integrated luminosity [fb ⁻¹]	SU(2) singlet	SU(2) doublet	$\mathcal{B}(T \rightarrow Ht) = 100\%$
This result	ATLAS	139	1.40 (1.33)	1.56 (1.48)	1.66 (1.61)
[13]	ATLAS	36.1	1.19 (1.11)	1.31 (1.26)	1.43 (1.34)
[14]	ATLAS	36.1	1.31 (1.23)	1.37 (1.32)	1.43 (1.34)
[15]	ATLAS	139	1.27 (1.28)	1.46 (1.44)	–
[17]	ATLAS	140	1.36 (1.36)	–	–
[19]	CMS	138	1.48 (1.41)	1.49 (1.50)	1.50 (1.55)

Distributions as a function of m_{eff} for the analysis regions most sensitive to a hypothetical signal are shown in Figure 6, with all remaining analysis regions delegated to Appendix B. Good post-fit agreement between observed data and SM background prediction is obtained in all control and signal regions after the fit, including those in which the largest fraction of signal events is expected.

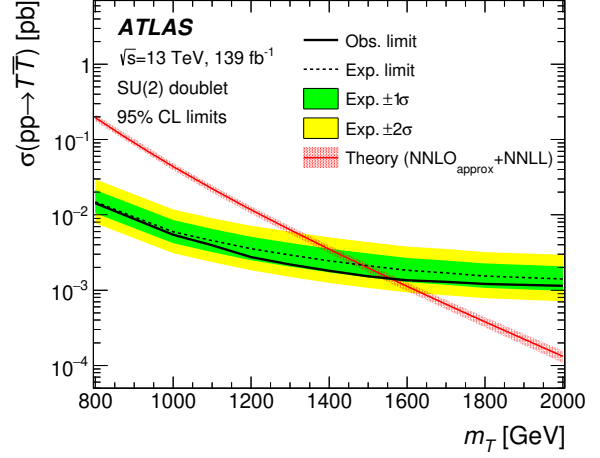
The impact of the different sources of uncertainty on the signal strength parameter μ is summarised in Table 4 for vector-like T -quarks with $m_T = 1.4$ TeV in the SU(2) singlet, SU(2) doublet, and $\mathcal{B}(T \rightarrow Ht) = 100\%$ scenarios. The results are dominated by the statistical uncertainties on the data. Among the systematic uncertainties, the largest contribution arises from the modelling of SM backgrounds, in particular $t\bar{t}$ production. The background reweighting uncertainty, although individually small, has a sizeable impact because its effect mirrors that of the signal: it is suppressed at low m_{eff} and enhanced at high m_{eff} , allowing it to either obscure or amplify signal contributions. Considered alongside other modelling uncertainties, however, the background reweighting impacts are of comparable magnitude, indicating that the fit is robust against variations of the pre-fit background model. Among experimental uncertainties, those related to jets have the largest impact. While the absolute impact of the uncertainties varies between signal scenarios, their relative hierarchy remains similar.

8.2 Exclusion limits on pair-production of vector-like quarks

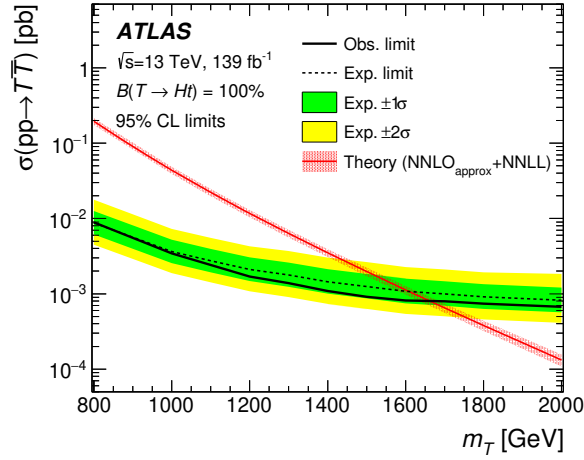
Upper limits on the $T\bar{T}$ production cross-section as a function of the T -quark mass are derived. These are shown in Figure 7 for the three different benchmark scenarios. The observed (expected) 95% CL lower limits on the mass of pair-produced vector-like T -quarks are 1.40 TeV (1.33 TeV) in the SU(2) singlet, 1.56 TeV (1.48 TeV) in the SU(2) doublet, and 1.66 TeV (1.61 TeV) in the $\mathcal{B}(T \rightarrow Ht) = 100\%$ scenario. These are the most stringent limits in the SU(2) doublet and $\mathcal{B}(T \rightarrow Ht) = 100\%$ scenarios to date, extending the exclusion by 0.07 TeV and 0.16 TeV, respectively, compared with the current strongest limits set by a CMS search [19]. They are also the most stringent limits set by the ATLAS Collaboration for all three scenarios, extending the exclusion by 0.04 TeV in the SU(2) singlet scenario [17], 0.10 TeV in the SU(2) doublet scenario [15], and 0.23 TeV in the $\mathcal{B}(T \rightarrow Ht) = 100\%$ scenario [13]. An overview of the lower limits on the mass of pair-produced vector-like T -quarks from this and related works is given in Table 5.



(a)



(b)



(c)

Figure 7: Observed and expected 95% CL upper limits on the $T\bar{T}$ pair-production cross-section as a function of the T -quark mass for the (a) SU(2) singlet, (b) SU(2) doublet, and (c) $\mathcal{B}(T \rightarrow Ht) = 100\%$ benchmark scenarios. The inner green (outer yellow) band corresponds to the $\pm 1\sigma$ ($\pm 2\sigma$) uncertainty around the expected limits. The theoretical cross-section prediction, and its corresponding uncertainty are also shown with a red line and light red band, respectively.

9 Conclusion

A search for the pair production of up-type vector-like T -quarks, where at least one T -quark decays via the $T \rightarrow Ht$ channel with subsequent $H \rightarrow b\bar{b}$ decay, is presented. The search uses 139 fb^{-1} of pp collisions at $\sqrt{s} = 13 \text{ TeV}$, collected by the ATLAS detector at the LHC during the 2015–2018 Run 2 data-taking period. Events are analysed in the lepton-plus-jets final state, characterised by the presence of a single electron or muon, multiple jets and b -tagged jets in the event. The search makes use of the presence of boosted, hadronically decaying Higgs and vector bosons, and hadronically or leptonically decaying top quarks in signal events. No significant excess above the SM expectation is observed, and exclusion limits at 95% CL are set on the production cross-section of pair-produced T -quarks. In the SU(2) singlet (doublet) scenario, T -quarks with masses below 1.40 TeV (1.56 TeV) are excluded. If $\mathcal{B}(T \rightarrow Ht) = 100\%$, T -quarks with masses below 1.66 TeV are excluded. These are the most stringent limits in the SU(2) doublet and $\mathcal{B}(T \rightarrow Ht) = 100\%$ scenarios to date. As the search remains limited by statistical uncertainties, the substantially increased data from Run 3 and the High-Luminosity LHC offer significant potential for extending the sensitivity beyond the mass ranges probed here. To facilitate reinterpretation and future studies, event yields, systematic uncertainties, exclusion limits, and the statistical workspace are provided on HEPDATA [115], along with the NN weights in both their original form and a portable format produced using PETRIFYML [116]. A RIVET [117, 118] analysis routine is also provided to enable direct comparison of the result with theoretical predictions.

Acknowledgements

We thank CERN for the very successful operation of the LHC and its injectors, as well as the support staff at CERN and at our institutions worldwide without whom ATLAS could not be operated efficiently.

The crucial computing support from all WLCG partners is acknowledged gratefully, in particular from CERN, the ATLAS Tier-1 facilities at TRIUMF/SFU (Canada), NDGF (Denmark, Norway, Sweden), CC-IN2P3 (France), KIT/GridKA (Germany), INFN-CNAF (Italy), NL-T1 (Netherlands), PIC (Spain), RAL (UK) and BNL (USA), the Tier-2 facilities worldwide and large non-WLCG resource providers. Major contributors of computing resources are listed in Ref. [119].

We gratefully acknowledge the support of ANPCyT, Argentina; YerPhI, Armenia; ARC, Australia; BMWFW and FWF, Austria; ANAS, Azerbaijan; CNPq and FAPESP, Brazil; NSERC, NRC and CFI, Canada; CERN; ANID, Chile; CAS, MOST and NSFC, China; Minciencias, Colombia; MEYS CR, Czech Republic; DNRF and DNSRC, Denmark; IN2P3-CNRS and CEA-DRF/IRFU, France; SRNSFG, Georgia; BMFTR, HGF and MPG, Germany; GSRI, Greece; RGC and Hong Kong SAR, China; ICHEP and Academy of Sciences and Humanities, Israel; INFN, Italy; MEXT and JSPS, Japan; CNRST, Morocco; NWO, Netherlands; RCN, Norway; MNiSW, Poland; FCT, Portugal; MNE/IFA, Romania; MSTDI, Serbia; MSSR, Slovakia; ARIS and MVZI, Slovenia; DSI/NRF, South Africa; MICIU/AEI, Spain; SRC and Wallenberg Foundation, Sweden; SERI, SNSF and Cantons of Bern and Geneva, Switzerland; NSTC, Taipei; TENMAK, Türkiye; STFC/UKRI, United Kingdom; DOE and NSF, United States of America.

Individual groups and members have received support from BCKDF, CANARIE, CRC and DRAC, Canada; CERN-CZ, FORTE and PRIMUS, Czech Republic; COST, ERC, ERDF, Horizon 2020 and Marie Skłodowska-Curie Actions, European Union; Investissements d’Avenir Labex, Investissements d’Avenir IDEX and ANR, France; DFG and AvH Foundation, Germany; Herakleitos, Thales and Aristeia programmes

co-financed by EU-ESF and the Greek NSRF, Greece; BSF-NSF and MINERVA, Israel; NCN and NAWA, Poland; La Caixa Banking Foundation, CERCA and AGAUR programs from Generalitat de Catalunya and PROMETEO and GenT Programmes Generalitat Valenciana, Spain; Göran Gustafssons Stiftelse, Sweden; The Royal Society and Leverhulme Trust, United Kingdom; Eric and Wendy Schmidt Fund for Strategic Innovation, United States of America.

In addition, individual members wish to acknowledge support from Chile: Agencia Nacional de Investigación y Desarrollo (ANID FONDECYT reg. 1230987, FONDECYT 1230812, FONDECYT 1240864, Fondecyt 3240661, Fondecyt Regular 1240721); China: Chinese Ministry of Science and Technology (MOST-2023YFA1605700, MOST-2023YFA1609300), National Natural Science Foundation of China (NSFC 12275265, NSFC-W2543005); Czech Republic: Czech Science Foundation (GACR - 24-11373S), Ministry of Education Youth and Sports (ERC-CZ-LL2327, FORTE CZ.02.01.01/00/22_008/0004632), PRIMUS Research Programme (PRIMUS/21/SCI/017); EU: H2020 European Research Council (ERC - 101002463); European Union: European Research Council (BARD No. 101116429, ERC - 101219398, ERC - 948254, ERC 101089007), European Regional Development Fund (HE COFUND GA No.101081355, ERDF), Marie Skłodowska-Curie Actions (GAP-101168829); France: Agence Nationale de la Recherche (ANR-21-CE31-0013, ANR-22-EDIR-0002, ANR-24-CE31-0504-01); Germany: Deutsche Forschungsgemeinschaft (DFG - 469666862); China: Research Grants Council (GRF); Italy: Ministero dell'Università e della Ricerca (NextGenEU 153D23001490006 M4C2.1.1, NextGenEU I53D23000820006 M4C2.1.1, NextGenEU I53D23001490006 M4C2.1.1, SOE2024_0000023); Japan: Japan Society for the Promotion of Science (JSPS KAKENHI JP25H0063, JSPS KAKENHI JP22H01227, JSPS KAKENHI JP22H04944, JSPS KAKENHI JP22KK0227, JSPS KAKENHI JP24K23939, JSPS KAKENHI JP24KK0251, JSPS KAKENHI JP25H00650, JSPS KAKENHI JP25H01291, JSPS KAKENHI JP25K01011, JSPS KAKENHI JP25K01023); Norway: Research Council of Norway (RCN-314472); Poland: Polish National Science Centre (NCN 2021/42/E/ST2/00350, NCN OPUS 2023/51/B/ST2/02507, NCN OPUS nr 2022/47/B/ST2/03059, NCN UMO-2019/34/E/ST2/00393, UMO-2022/47/O/ST2/00148, UMO-2023/49/B/ST2/04085, UMO-2023/51/B/ST2/00920, UMO-2024/53/N/ST2/00869); Spain: Agència de Gestió d'Ajuts Universitaris i de Recerca. (AGAUR - 2023 BP 00141), Ministry of Science and Innovation (RYC2019-028510-I, RYC2020-030254-I, RYC2021-031273-I, RYC2022-038164-I), Ministerio de Ciencia, Innovación y Universidades/Agencia Estatal de Investigación (EU NextGenerationEU (PRTR-C17.I1), PID2022-142604OB-C22); Sweden: Carl Trygger Foundation (Carl Trygger Foundation CTS 22:2312), Swedish Research Council (Swedish Research Council 2023-04654, VR 2021-03651, VR 2022-03845, VR 2022-04683, VR 2023-03403, VR 2024-05451, VR 2025-05940), Knut and Alice Wallenberg Foundation (KAW 2023.0366); Switzerland: Swiss National Science Foundation (SNSF - PCEFP2_194658); United Kingdom: The Binks Trust, Royal Society (NIF-R1-231091); United States of America: U.S. Department of Energy (ECA DE-AC02-76SF00515), John Templeton Foundation (John Templeton Foundation 63206), Neubauer Family Foundation.

Appendix

A Complete list of neural network input variables

Table 6: Input variables for the multilayer perceptron ranked according to their importance and separation power.

Number	Variable	Description
1.	m_{eff}	effective mass: scalar sum of the p_T of all selected small- R jets and the lepton as well as E_T^{miss}
2.	$p_T^{\text{var-}R,3}$	p_T of third-leading variable- R jet
3.	$p_T^{t_{\ell}^{\text{reco}}}$	p_T of t_{ℓ}^{reco}
4.	$N_{\text{jets}}^{\text{var-}R}$	number of variable- R jets
5.	$p_T^{H,1}$	p_T of leading H -tagged jet
6.	$\Delta\phi_{\text{avg}}^{\text{var-}R}$	average pairwise $\Delta\phi$ separation between all variable- R jets
7.	$m_{T_2}^{\text{mass}}$	mass of the T -quark candidate built from mass-tagged jets with the second-largest ΔR separation between its constituents
8.	$N_{\text{const}}^{H,1}$	number of constituents of leading H -tagged jet
9.	$N_{b\text{-const}}^{H,1}$	number of b -tagged constituents of leading H -tagged jet
10.	$\Delta R_{\text{min}}^{\text{mass}}$	minimum pairwise ΔR separation between all mass-tagged jets
11.	$\Delta R_{\text{min}}^{\text{var-}R}$	minimum pairwise ΔR separation between all variable- R jets
12.	$m_{T_2}^{\text{var-}R}$	mass of the T -quark candidate built from variable- R jets with the second-largest ΔR separation between its constituents
13.	$m_{T,\text{min}}^b$	minimum transverse mass between E_T^{miss} and any of the three leading b -tagged jets
14.	E_T^{miss}	missing transverse energy
15.	$N_{b\text{-jets}}$	number of b -tagged jets
16.	$\Delta\phi_{\text{min}}^{\text{mass}}$	minimum pairwise $\Delta\phi$ separation between all mass-tagged jets
17.	$\Delta R_{\text{avg}}^{\text{var-}R}$	average pairwise ΔR separation between all variable- R jets
18.	$\Delta\phi_{\text{min}}^{\text{var-}R}$	minimum pairwise $\Delta\phi$ separation between all variable- R jets
19.	$N_{\text{const}}^{V,1}$	number of constituents of leading V -tagged jet
20.	$p_T^{V,1}$	p_T of leading V -tagged jet
21.	$E_T^{\text{miss, res}}$	residual E_T^{miss} : difference between E_T^{miss} and the neutrino p_T as determined in the W_{ℓ}^{reco} reconstruction
22.	$\Delta\eta_{\text{min}}^{\text{mass}}$	minimum pairwise $\Delta\eta$ separation between all mass-tagged jets
23.	$p_T^{t,1}$	p_T of leading t -tagged jet
24.	$m_{T_1}^{\text{mass}}$	mass of the T -quark candidate built from mass-tagged jets with the largest ΔR separation between its constituents
25.	$\Delta\eta_{\text{min}}^{\text{var-}R}$	minimum pairwise $\Delta\eta$ separation between all variable- R jets
26.	$\Delta\eta_{\text{lead}}^{\text{var-}R}$	$\Delta\eta$ separation between two leading variable- R jets
27.	m_T^W	transverse mass of lepton- \vec{p}_T^{miss} system
28.	$\Delta R_{\text{lead}}^{\text{var-}R}$	ΔR separation between two leading variable- R jets
29.	$p_T^{H,2}$	p_T of subleading H -tagged jet
30.	$\Delta R_{\text{lead}}^{\text{mass}}$	ΔR separation between two leading mass-tagged jets

B Complete set of data and predicted yields in analysis regions

A full set of tables with the expected and observed yields in all control, validation and signal regions, after a background-only fit to data in the control and signal regions, is provided in Tables 7 to 10. To complete the results in Section 8.1, Figures 8 to 10 show the pre- and post-fit distributions of data and predicted yields as a function of m_{eff} in the remaining regions used in the search.

Table 7: Expected and observed yields in the control and validation regions after a background-only fit to the data. The ‘‘Other top’’ category includes contributions from $t\bar{t}W$, $t\bar{t}Z/\gamma^*$, $t\bar{t}H$, tH , tZ and four-top events. The signal yields are shown before the fit (assuming $\mu = 1$) for a selection of signal scenarios and mass points.

	CR 2b		VR 3b		VR 4b	
$T\bar{T}$ (SU(2) singlet, 1.4 TeV, $\mu = 1$)	1.81	± 0.17	3.47	± 0.27	1.51	± 0.28
$T\bar{T}$ (SU(2) doublet, 1.4 TeV, $\mu = 1$)	2.09	± 0.24	3.4	± 0.4	2.3	± 0.4
$T\bar{T}$ ($\mathcal{B}(T \rightarrow Ht) = 100\%$, 1.0 TeV, $\mu = 1$)	27	± 4	86	± 13	91	± 9
$T\bar{T}$ ($\mathcal{B}(T \rightarrow Ht) = 100\%$, 1.4 TeV, $\mu = 1$)	1.53	± 0.22	3.8	± 0.4	3.5	± 0.8
$T\bar{T}$ ($\mathcal{B}(T \rightarrow Ht) = 100\%$, 1.8 TeV, $\mu = 1$)	0.08	± 0.03	0.26	± 0.06	0.23	± 0.05
$t\bar{t}$ +light jets	16 900	± 1300	2010	± 190	34	± 4
$t\bar{t}+\geq 1c$	3900	± 1500	1400	± 600	100	± 40
$t\bar{t}+\geq 1b$	1570	± 300	2400	± 400	620	± 110
Single-top	920	± 110	340	± 40	32	± 11
Other top	390	± 50	286	± 28	97	± 9
W+jets	128	± 10	120	± 40	9.9	± 3.2
Z+jets	25.7	± 2.3	17	± 5	1.7	± 0.6
Diboson	27.4	± 1.8	19	± 11	2.2	± 1.3
Multijet	115	± 13	65	± 7	8.4	± 0.9
Total background	23 950	± 160	6650	± 240	900	± 90
Data	23 958		6982		945	

Table 8: Expected and observed yields in the LNN signal regions after a background-only fit to the data. The “Other top” category includes contributions from $t\bar{t}W$, $t\bar{t}Z/\gamma^*$, $t\bar{t}H$, tH , tZ and four-top events. The signal yields are shown before the fit (assuming $\mu = 1$) for a selection of signal scenarios and mass points.

	SR 3b-0H-LNN	SR 4b-0H-LNN	SR 3b-1H-LNN	SR 4b-1H-LNN
$T\bar{T}$ (SU(2) singlet, 1.4 TeV, $\mu = 1$)	0.62 \pm 0.07	0.17 \pm 0.03	0.30 \pm 0.05	0.04 \pm 0.02
$T\bar{T}$ (SU(2) doublet, 1.4 TeV, $\mu = 1$)	0.92 \pm 0.13	0.37 \pm 0.10	0.49 \pm 0.09	0.11 \pm 0.05
$T\bar{T}$ ($\mathcal{B}(T \rightarrow Ht) = 100\%$, 1.0 TeV, $\mu = 1$)	43 \pm 5	32.3 \pm 2.8	23 \pm 4	11.7 \pm 2.5
$T\bar{T}$ ($\mathcal{B}(T \rightarrow Ht) = 100\%$, 1.4 TeV, $\mu = 1$)	1.1 \pm 0.3	0.57 \pm 0.15	1.0 \pm 0.2	0.2 \pm 0.1
$T\bar{T}$ ($\mathcal{B}(T \rightarrow Ht) = 100\%$, 1.8 TeV, $\mu = 1$)	0.09 \pm 0.04	0.05 \pm 0.01	0.09 \pm 0.02	0.01 \pm 0.01
$t\bar{t}$ +light jets	141 \pm 18	2.8 \pm 0.7	30.6 \pm 3.0	0.5 \pm 0.1
$t\bar{t}+\geq 1c$	160 \pm 60	12 \pm 5	34 \pm 13	2.0 \pm 0.8
$t\bar{t}+\geq 1b$	280 \pm 50	104 \pm 11	58 \pm 11	14.7 \pm 2.1
Single-top	24 \pm 8	3.9 \pm 0.7	5.5 \pm 1.2	0.77 \pm 0.28
Other top	40 \pm 4	13.6 \pm 1.7	8.6 \pm 1.1	2.43 \pm 0.33
W+jets	15 \pm 5	1.7 \pm 0.6	3.6 \pm 1.2	0.40 \pm 0.18
Z+jets	2.2 \pm 0.7	0.27 \pm 0.09	0.67 \pm 0.23	0.05 \pm 0.02
Diboson	2.4 \pm 1.4	0.37 \pm 0.22	0.6 \pm 0.4	0.04 \pm 0.04
Multijet	8.2 \pm 0.9	0.22 \pm 0.03	5.8 \pm 0.7	0.91 \pm 0.15
Total background	673 \pm 21	138 \pm 10	147 \pm 8	22 \pm 2
Data	670	139	147	22

Table 9: Expected and observed yields in the MNN signal regions after a background-only fit to the data. The “Other top” category includes contributions from $t\bar{t}W$, $t\bar{t}Z/\gamma^*$, $t\bar{t}H$, tH , tZ and four-top events. The signal yields are shown before the fit (assuming $\mu = 1$) for a selection of signal scenarios and mass points.

	SR 3b-0H-MNN	SR 4b-0H-MNN	SR 3b-1H-MNN	SR 4b-1H-MNN
$T\bar{T}$ (SU(2) singlet, 1.4 TeV, $\mu = 1$)	2.28 \pm 0.25	0.75 \pm 0.11	0.97 \pm 0.10	0.29 \pm 0.04
$T\bar{T}$ (SU(2) doublet, 1.4 TeV, $\mu = 1$)	3.40 \pm 0.33	1.49 \pm 0.31	1.63 \pm 0.22	0.66 \pm 0.11
$T\bar{T}$ ($\mathcal{B}(T \rightarrow Ht) = 100\%$, 1.0 TeV, $\mu = 1$)	41 \pm 7	44 \pm 7	36 \pm 8	28.9 \pm 3.4
$T\bar{T}$ ($\mathcal{B}(T \rightarrow Ht) = 100\%$, 1.4 TeV, $\mu = 1$)	3.8 \pm 1.0	2.2 \pm 0.8	2.7 \pm 0.5	1.4 \pm 0.3
$T\bar{T}$ ($\mathcal{B}(T \rightarrow Ht) = 100\%$, 1.8 TeV, $\mu = 1$)	0.33 \pm 0.13	0.18 \pm 0.05	0.26 \pm 0.04	0.09 \pm 0.04
$t\bar{t}$ +light jets	24.1 \pm 3.0	1.01 \pm 0.23	8.6 \pm 0.8	0.34 \pm 0.08
$t\bar{t}+\geq 1c$	31 \pm 12	4.2 \pm 1.7	11 \pm 4	1.4 \pm 0.5
$t\bar{t}+\geq 1b$	56 \pm 10	32 \pm 4	19 \pm 4	10.3 \pm 1.3
Single-top	6.8 \pm 3.5	2.5 \pm 3.2	2.3 \pm 0.6	0.43 \pm 0.22
Other top	11.5 \pm 1.5	6.3 \pm 1.0	3.4 \pm 0.5	1.61 \pm 0.27
W+jets	4.6 \pm 1.6	0.68 \pm 0.23	2.2 \pm 0.7	0.21 \pm 0.14
Z+jets	0.58 \pm 0.19	0.12 \pm 0.04	0.27 \pm 0.09	0.04 \pm 0.02
Diboson	1.2 \pm 0.7	0.14 \pm 0.09	0.54 \pm 0.32	0.02 \pm 0.02
Multijet	1.47 \pm 0.16	0.13 \pm 0.01	0.24 \pm 0.03	–
Total background	138 \pm 7	47 \pm 4	47 \pm 3	14 \pm 1
Data	135	57	46	10

Table 10: Expected and observed yields in the HNN signal regions after a background-only fit to the data. The “Other top” category includes contributions from $t\bar{t}W$, $t\bar{t}Z/\gamma^*$, $t\bar{t}H$, tH , tZ and four-top events. The signal yields are shown before the fit (assuming $\mu = 1$) for a selection of signal scenarios and mass points.

	SR 3b-0H-HNN	SR 4b-0H-HNN	SR 3b-1H-HNN	SR 4b-1H-HNN
$T\bar{T}$ (SU(2) singlet, 1.4 TeV, $\mu = 1$)	2.90 \pm 0.34	2.6 \pm 0.4	4.03 \pm 0.34	3.9 \pm 0.5
$T\bar{T}$ (SU(2) doublet, 1.4 TeV, $\mu = 1$)	3.8 \pm 0.7	5.2 \pm 0.9	6.7 \pm 0.7	9.1 \pm 1.2
$T\bar{T}$ ($\mathcal{B}(T \rightarrow Ht) = 100\%$, 1.0 TeV, $\mu = 1$)	20 \pm 5	52 \pm 12	49 \pm 9	106 \pm 14
$T\bar{T}$ ($\mathcal{B}(T \rightarrow Ht) = 100\%$, 1.4 TeV, $\mu = 1$)	3.3 \pm 1.2	6.8 \pm 2.1	10.5 \pm 1.8	18.2 \pm 2.9
$T\bar{T}$ ($\mathcal{B}(T \rightarrow Ht) = 100\%$, 1.8 TeV, $\mu = 1$)	0.44 \pm 0.16	0.67 \pm 0.31	1.65 \pm 0.30	2.43 \pm 0.34
$t\bar{t}$ +light jets	2.3 \pm 0.4	0.37 \pm 0.14	3.1 \pm 0.5	0.25 \pm 0.06
$t\bar{t}+\geq 1c$	3.1 \pm 1.2	1.4 \pm 0.6	3.9 \pm 1.5	1.1 \pm 0.6
$t\bar{t}+\geq 1b$	6.2 \pm 1.2	11.3 \pm 1.6	7.7 \pm 1.5	10.3 \pm 1.9
Single-top	2.6 \pm 1.1	0.56 \pm 0.31	2.4 \pm 0.5	0.78 \pm 0.31
Other top	2.4 \pm 0.4	2.7 \pm 0.6	2.3 \pm 0.3	2.0 \pm 0.4
W+jets	0.95 \pm 0.35	0.39 \pm 0.13	1.1 \pm 0.4	0.31 \pm 0.13
Z+jets	0.12 \pm 0.05	0.04 \pm 0.02	0.11 \pm 0.05	0.03 \pm 0.02
Diboson	0.14 \pm 0.18	0.08 \pm 0.05	0.21 \pm 0.13	0.09 \pm 0.06
Multijet	0.15 \pm 0.02	0.36 \pm 0.05	0.19 \pm 0.02	0.16 \pm 0.02
Total background	18 \pm 2	17 \pm 2	21 \pm 1	15 \pm 2
Data	16	15	21	15

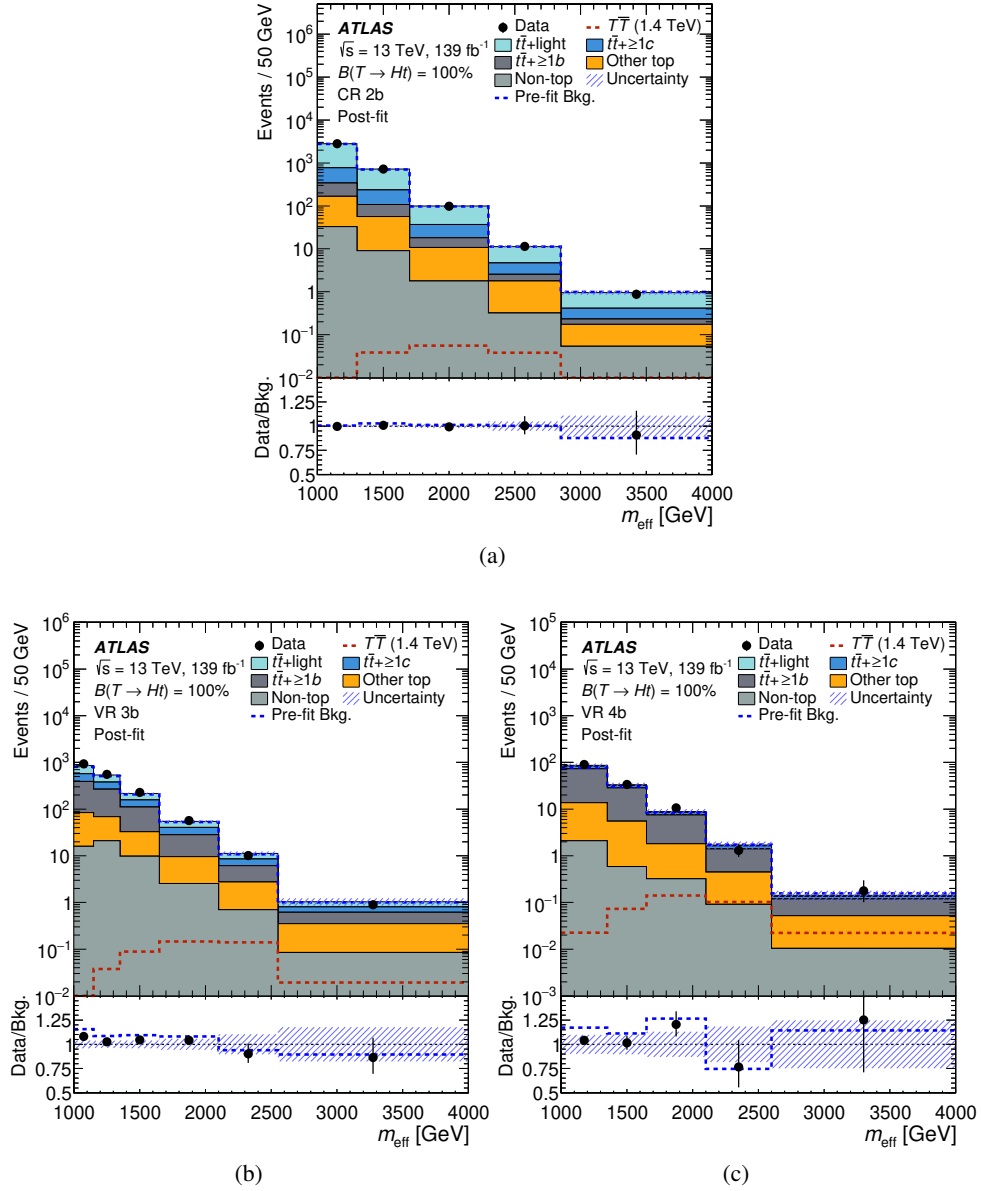


Figure 8: Comparison between observed yields (black dots) and expected SM yields (coloured areas) as a function of m_{eff} for (a) the control region CR 2b and the validation regions (b) VR 3b and (c) VR 4b. The expected yields are shown after a fit under the background-only hypothesis in the control and signal regions. The bottom panels display the ratio of data and total SM background. The size of the combined statistical and systematic uncertainty in the background prediction is indicated by a blue hatched band, including all sources of systematic uncertainty described in Section 6. In the upper panel, the total expected SM yield (expected yield from a $\mathcal{B}(T \rightarrow Ht) = 100\%$ scenario with $m_T = 1.4$ TeV) before the fit is shown as a dashed blue (red) line. In the lower panel, the ratio of the observed yield to the total expected SM yield before the fit is shown as a dashed blue line.

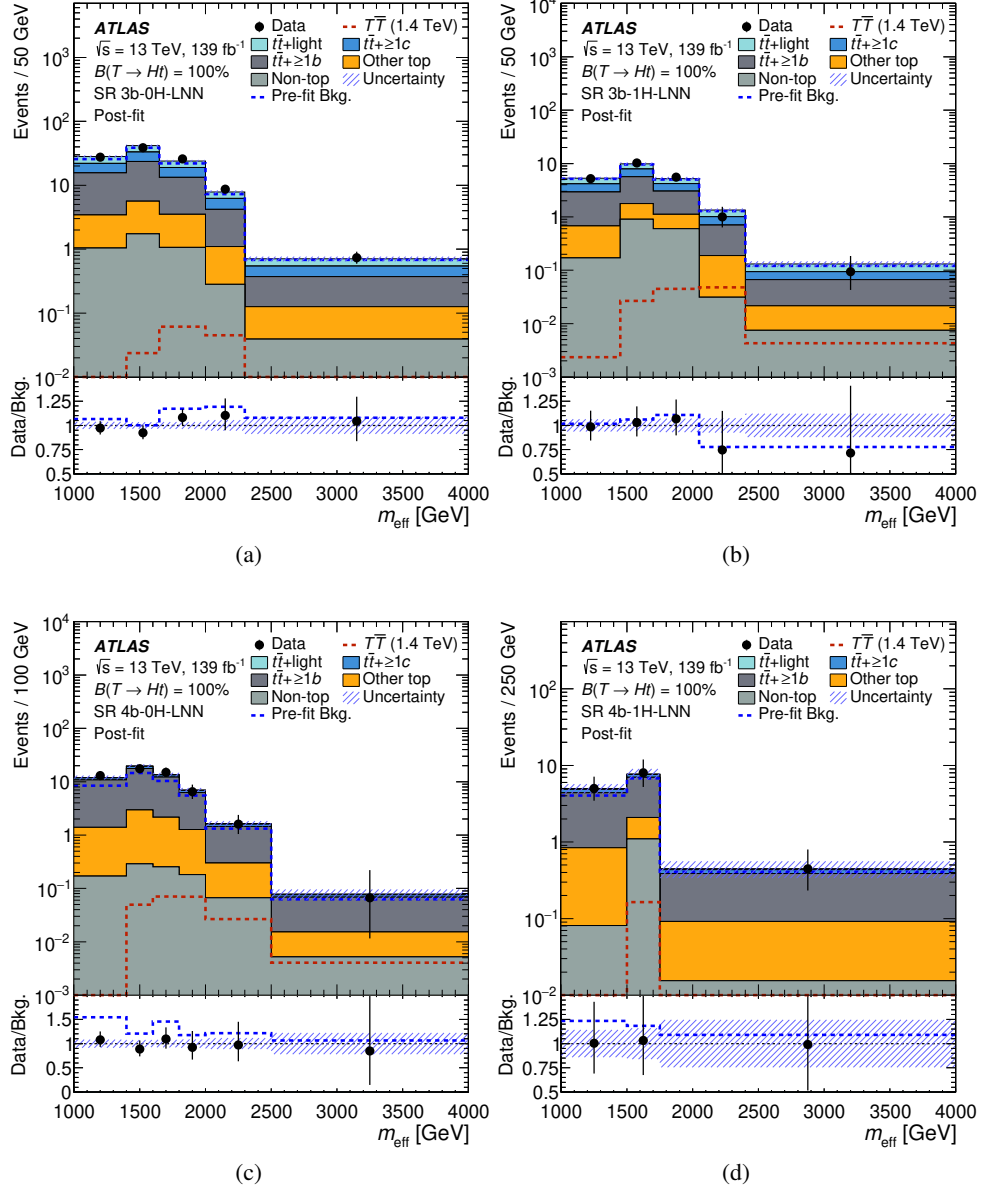


Figure 9: Comparison between observed yields (black dots) and expected SM yields (coloured areas) as a function of m_{eff} for the LNN signal regions (a) SR 3b-0H-LNN, (b) SR 3b-1H-LNN, (c) SR 4b-0H-LNN, and (d) SR 4b-1H-LNN. The expected yields are shown after a fit under the background-only hypothesis in the control and signal regions. The bottom panels display the ratio of data and total SM background. The size of the combined statistical and systematic uncertainty in the background prediction is indicated by a blue hatched band, including all sources of systematic uncertainty described in Section 6. In the upper panel, the total expected SM yield (expected yield from a $\mathcal{B}(T \rightarrow Ht) = 100\%$ scenario with $m_T = 1.4$ TeV) before the fit is shown as a dashed blue (red) line. In the lower panel, the ratio of the observed yield to the total expected SM yield before the fit is shown as a dashed blue line.

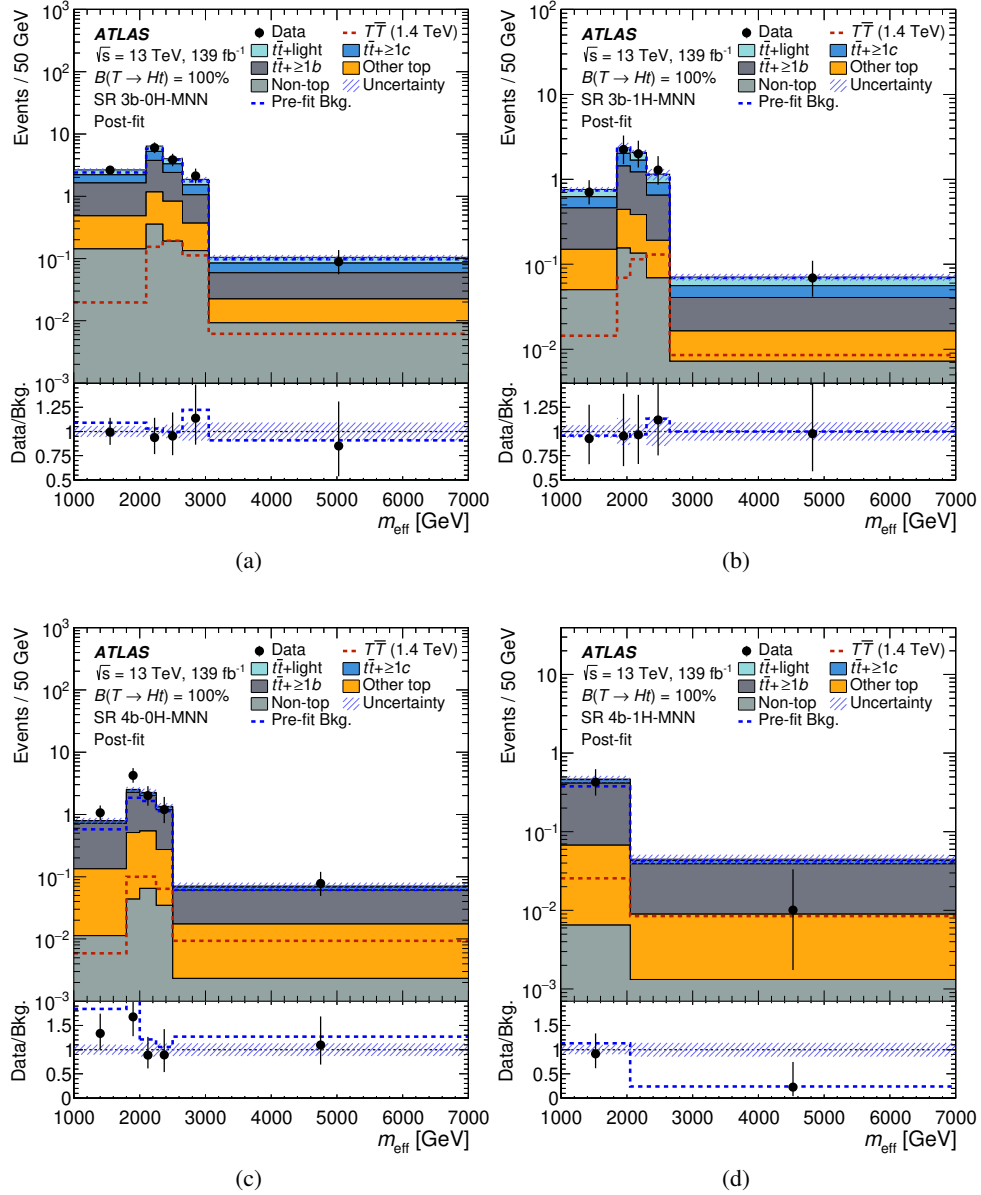


Figure 10: Comparison between observed yields (black dots) and expected SM yields (coloured areas) as a function of m_{eff} for the MNN signal regions (a) SR 3b-0H-MNN, (b) SR 3b-1H-MNN, (c) SR 4b-0H-MNN, and (d) SR 4b-1H-MNN. The expected yields are shown after a fit under the background-only hypothesis in the control and signal regions. The bottom panels display the ratio of data and total SM background. The size of the combined statistical and systematic uncertainty in the background prediction is indicated by a blue hatched band, including all sources of systematic uncertainty described in Section 6. In the upper panel, the total expected SM yield (expected yield from a $\mathcal{B}(T \rightarrow Ht) = 100\%$ scenario with $m_T = 1.4$ TeV) before the fit is shown as a dashed blue (red) line. In the lower panel, the ratio of the observed yield to the total expected SM yield before the fit is shown as a dashed blue line.

References

- [1] S. Dimopoulos and J. Preskill, *Massless Composites With Massive Constituents*, [*Nucl. Phys. B* **199** \(1982\) 206](#).
- [2] D. B. Kaplan and H. Georgi, *SU(2) x U(1) Breaking by Vacuum Misalignment*, [*Phys. Lett. B* **136** \(1984\) 183](#).
- [3] D. B. Kaplan, H. Georgi and S. Dimopoulos, *Composite Higgs Scalars*, [*Phys. Lett. B* **136** \(1984\) 187](#).
- [4] M. Schmaltz and D. Tucker-Smith, *Little Higgs Theories*, [*Ann. Rev. Nucl. Part. Sci.* **55** \(2005\) 229](#), arXiv: [hep-ph/0502182](#).
- [5] M. Perelstein, M. E. Peskin and A. Pierce, *Top quarks and electroweak symmetry breaking in little Higgs models*, [*Phys. Rev. D* **69** \(2004\) 075002](#), arXiv: [hep-ph/0310039](#).
- [6] T. Gherghetta and A. Pomarol, *Bulk fields and supersymmetry in a slice of AdS*, [*Nucl. Phys. B* **586** \(2000\) 141](#), arXiv: [hep-ph/0003129](#).
- [7] S. P. Martin, *Extra vectorlike matter and the lightest Higgs scalar boson mass in low-energy supersymmetry*, [*Phys. Rev. D* **81** \(2010\) 035004](#), arXiv: [0910.2732 \[hep-ph\]](#).
- [8] F. del Aguila and M. J. Bowick, *The Possibility of New Fermions With $\Delta I = 0$ Mass*, [*Nucl. Phys. B* **224** \(1983\) 107](#).
- [9] J. A. Aguilar-Saavedra, *Mixing with vector-like quarks: constraints and expectations*, [*EPJ Web Conf.* **60** \(2013\) 16012](#), arXiv: [1306.4432 \[hep-ph\]](#).
- [10] J. A. Aguilar-Saavedra, *Identifying top partners at LHC*, [*JHEP* **11** \(2009\) 030](#), arXiv: [0907.3155 \[hep-ph\]](#).
- [11] M. Buchkremer, G. Cacciapaglia, A. Deandrea and L. Panizzi, *Model-Independent framework for Searches of top partners*, [*Nucl. Phys. B* **876** \(2013\) 376](#), arXiv: [1305.4172 \[hep-ph\]](#).
- [12] ATLAS Collaboration, *The ATLAS Experiment at the CERN Large Hadron Collider*, [*JINST* **3** \(2008\) S08003](#).
- [13] ATLAS Collaboration, *Search for pair production of up-type vector-like quarks and for four-top-quark events in final states with multiple b-jets with the ATLAS detector*, [*JHEP* **07** \(2018\) 089](#), arXiv: [1803.09678 \[hep-ex\]](#).
- [14] ATLAS Collaboration, *Combination of the Searches for Pair-Produced Vectorlike Partners of the Third-Generation Quarks at $\sqrt{s} = 13$ TeV with the ATLAS Detector*, [*Phys. Rev. Lett.* **121** \(2018\) 211801](#), arXiv: [1808.02343 \[hep-ex\]](#).
- [15] ATLAS Collaboration, *Search for pair-production of vector-like quarks in pp collision events at $\sqrt{s} = 13$ TeV with at least one leptonically decaying Z boson and a third-generation quark with the ATLAS detector*, [*Phys. Lett. B* **843** \(2023\) 138019](#), arXiv: [2210.15413 \[hep-ex\]](#).
- [16] ATLAS Collaboration, *Search for pair-produced vector-like top and bottom partners in events with large missing transverse momentum in pp collisions with the ATLAS detector*, [*Eur. Phys. J. C* **83** \(2023\) 719](#), arXiv: [2212.05263 \[hep-ex\]](#).

- [17] ATLAS Collaboration, *Search for pair-production of vector-like quarks in lepton+jets final states containing at least one b-tagged jet using the Run 2 data from the ATLAS experiment*, *Phys. Lett. B* **854** (2024) 138743, arXiv: 2401.17165 [hep-ex].
- [18] ATLAS Collaboration, *Search for pair-produced vectorlike quarks coupling to light quarks in the lepton plus jets final state using 13 TeV pp collisions with the ATLAS detector*, *Phys. Rev. D* **110** (2024) 052009, arXiv: 2405.19862 [hep-ex].
- [19] CMS Collaboration, *Search for pair production of vector-like quarks in leptonic final states in proton–proton collisions at $\sqrt{s} = 13$ TeV*, *JHEP* **07** (2023) 020, arXiv: 2209.07327 [hep-ex].
- [20] G. Avoni et al., *The new LUCID-2 detector for luminosity measurement and monitoring in ATLAS*, *JINST* **13** (2018) P07017.
- [21] ATLAS Collaboration, *Performance of the ATLAS trigger system in 2015*, *Eur. Phys. J. C* **77** (2017) 317, arXiv: 1611.09661 [hep-ex].
- [22] ATLAS Collaboration, *Software and computing for Run 3 of the ATLAS experiment at the LHC*, *Eur. Phys. J. C* **85** (2025) 234, arXiv: 2404.06335 [hep-ex],
Erratum: *Eur. Phys. J. C* **85** (2025) 907.
- [23] ATLAS Collaboration, *Luminosity determination in pp collisions at $\sqrt{s} = 13$ TeV using the ATLAS detector at the LHC*, *Eur. Phys. J. C* **83** (2023) 982, arXiv: 2212.09379 [hep-ex].
- [24] ATLAS Collaboration, *Luminosity determination in pp collisions at $\sqrt{s} = 13$ TeV using the ATLAS detector at the LHC*, ATLAS-CONF-2019-021, 2019, URL: <https://cds.cern.ch/record/2677054>.
- [25] ATLAS Collaboration, *ATLAS data quality operations and performance for 2015–2018 data-taking*, *JINST* **15** (2020) P04003, arXiv: 1911.04632 [physics.ins-det].
- [26] ATLAS Collaboration, *Performance of the ATLAS muon triggers in Run 2*, *JINST* **15** (2020) P09015, arXiv: 2004.13447 [physics.ins-det].
- [27] ATLAS Collaboration, *Performance of electron and photon triggers in ATLAS during LHC Run 2*, *Eur. Phys. J. C* **80** (2020) 47, arXiv: 1909.00761 [hep-ex].
- [28] ATLAS Collaboration, *Performance of the missing transverse momentum triggers for the ATLAS detector during Run-2 data taking*, *JHEP* **08** (2020) 080, arXiv: 2005.09554 [hep-ex].
- [29] ATLAS Collaboration, *The ATLAS Simulation Infrastructure*, *Eur. Phys. J. C* **70** (2010) 823, arXiv: 1005.4568 [physics.ins-det].
- [30] S. Agostinelli et al., *GEANT4 – a simulation toolkit*, *Nucl. Instrum. Meth. A* **506** (2003) 250.
- [31] S. Höche, F. Krauss, S. Schumann and F. Siegert, *QCD matrix elements and truncated showers*, *JHEP* **05** (2009) 053, arXiv: 0903.1219 [hep-ph].
- [32] D. J. Lange, *The EvtGen particle decay simulation package*, *Nucl. Instrum. Meth. A* **462** (2001) 152.
- [33] T. Sjöstrand, S. Mrenna and P. Skands, *A brief introduction to PYTHIA 8.1*, *Comput. Phys. Commun.* **178** (2008) 852, arXiv: 0710.3820 [hep-ph].
- [34] ATLAS Collaboration, *Further ATLAS tunes of PYTHIA 6 and Pythia 8*, ATL-PHYS-PUB-2011-014, 2011, URL: <https://cds.cern.ch/record/1400677>.

- [35] J. Alwall et al., *The automated computation of tree-level and next-to-leading order differential cross sections, and their matching to parton shower simulations*, *JHEP* **07** (2014) 079, arXiv: [1405.0301 \[hep-ph\]](#).
- [36] P. Golonka and Z. Was, *PHOTOS Monte Carlo: a precision tool for QED corrections in Z and W decays*, *Eur. Phys. J. C* **45** (2006) 97, arXiv: [hep-ph/0506026](#).
- [37] J. A. Aguilar-Saavedra, *PROTOS, a PROgram for TOp Simulations*, <http://jaguilar.web.cern.ch/jaguilar/protos/>.
- [38] NNPDF Collaboration, R. D. Ball et al., *Parton distributions with LHC data*, *Nucl. Phys. B* **867** (2013) 244, arXiv: [1207.1303 \[hep-ph\]](#).
- [39] ATLAS Collaboration, *ATLAS Pythia 8 tunes to 7 TeV data*, ATL-PHYS-PUB-2014-021, 2014, URL: <https://cds.cern.ch/record/1966419>.
- [40] P. Nason, *A new method for combining NLO QCD with shower Monte Carlo algorithms*, *JHEP* **11** (2004) 040, arXiv: [hep-ph/0409146](#).
- [41] S. Frixione, P. Nason and C. Oleari, *Matching NLO QCD computations with parton shower simulations: the POWHEG method*, *JHEP* **11** (2007) 070, arXiv: [0709.2092 \[hep-ph\]](#).
- [42] S. Alioli, P. Nason, C. Oleari and E. Re, *A general framework for implementing NLO calculations in shower Monte Carlo programs: the POWHEG BOX*, *JHEP* **06** (2010) 043, arXiv: [1002.2581 \[hep-ph\]](#).
- [43] T. Sjöstrand et al., *An introduction to PYTHIA 8.2*, *Comput. Phys. Commun.* **191** (2015) 159, arXiv: [1410.3012 \[hep-ph\]](#).
- [44] NNPDF Collaboration, R. D. Ball et al., *Parton distributions for the LHC run II*, *JHEP* **04** (2015) 040, arXiv: [1410.8849 \[hep-ph\]](#).
- [45] M. Bähr et al., *Herwig++ physics and manual*, *Eur. Phys. J. C* **58** (2008) 639, arXiv: [0803.0883 \[hep-ph\]](#).
- [46] T. Ježo, J. M. Lindert, N. Moretti and S. Pozzorini, *New NLOPS predictions for $t\bar{t} + b$ -jet production at the LHC*, *Eur. Phys. J. C* **78** (2018) 502, arXiv: [1802.00426 \[hep-ph\]](#).
- [47] T. Ježo, *Powheg-Box-Res ttbb source code*, 2019, URL: https://gitlab.cern.ch/tjezo/powheg-box-res_ttbb/.
- [48] C. Bierlich et al., *A comprehensive guide to the physics and usage of PYTHIA 8.3*, *SciPost Phys. Codebases* (2022) 8, arXiv: [2203.11601 \[hep-ph\]](#).
- [49] R. D. Ball et al., *Parton distributions from high-precision collider data*, *Eur. Phys. J. C* **77** (2017) 663, arXiv: [1706.00428 \[hep-ph\]](#).
- [50] S. Schumann and F. Krauss, *A parton shower algorithm based on Catani–Seymour dipole factorisation*, *JHEP* **03** (2008) 038, arXiv: [0709.1027 \[hep-ph\]](#).
- [51] M. Cacciari, M. Czakon, M. Mangano, A. Mitov and P. Nason, *Top-pair production at hadron colliders with next-to-next-to-leading logarithmic soft-gluon resummation*, *Phys. Lett. B* **710** (2012) 612, arXiv: [1111.5869 \[hep-ph\]](#).

- [52] M. Beneke, P. Falgari, S. Klein and C. Schwinn, *Hadronic top-quark pair production with NNLL threshold resummation*, *Nucl. Phys. B* **855** (2012) 695, arXiv: [1109.1536 \[hep-ph\]](#).
- [53] P. Bärnreuther, M. Czakon and A. Mitov, *Percent-Level-Precision Physics at the Tevatron: Next-to-Next-to-Leading Order QCD Corrections to $q\bar{q} \rightarrow t\bar{t} + X$* , *Phys. Rev. Lett.* **109** (2012) 132001, arXiv: [1204.5201 \[hep-ph\]](#).
- [54] M. Czakon and A. Mitov, *NNLO corrections to top-pair production at hadron colliders: the all-fermionic scattering channels*, *JHEP* **12** (2012) 054, arXiv: [1207.0236 \[hep-ph\]](#).
- [55] M. Czakon, P. Fiedler and A. Mitov, *Total Top-Quark Pair-Production Cross Section at Hadron Colliders Through $O(\alpha_S^4)$* , *Phys. Rev. Lett.* **110** (2013) 252004, arXiv: [1303.6254 \[hep-ph\]](#).
- [56] M. Czakon and A. Mitov, *Top++: A program for the calculation of the top-pair cross-section at hadron colliders*, *Comput. Phys. Commun.* **185** (2014) 2930, arXiv: [1112.5675 \[hep-ph\]](#).
- [57] A. D. Martin, W. J. Stirling, R. S. Thorne and G. Watt, *Parton distributions for the LHC*, *Eur. Phys. J. C* **63** (2009) 189, arXiv: [0901.0002 \[hep-ph\]](#).
- [58] A. D. Martin, W. J. Stirling, R. S. Thorne and G. Watt, *Uncertainties on α_S in global PDF analyses and implications for predicted hadronic cross sections*, *Eur. Phys. J. C* **64** (2009) 653, arXiv: [0905.3531 \[hep-ph\]](#).
- [59] S. Frixione, G. Ridolfi and P. Nason, *A positive-weight next-to-leading-order Monte Carlo for heavy flavour hadroproduction*, *JHEP* **09** (2007) 126, arXiv: [0707.3088 \[hep-ph\]](#).
- [60] ATLAS Collaboration, *Studies on top-quark Monte Carlo modelling with Sherpa and MG5_aMC@NLO*, ATL-PHYS-PUB-2017-007, 2017, URL: <https://cds.cern.ch/record/2261938>.
- [61] ATLAS Collaboration, *Search for the Standard Model Higgs boson produced in association with top quarks and decaying into $b\bar{b}$ in pp collisions at $\sqrt{s} = 8$ TeV with the ATLAS detector*, *Eur. Phys. J. C* **75** (2015) 349, arXiv: [1503.05066 \[hep-ex\]](#).
- [62] F. Buccioni et al., *OpenLoops 2*, *Eur. Phys. J. C* **79** (2019) 866, arXiv: [1907.13071 \[hep-ph\]](#).
- [63] F. Cascioli, P. Maierhöfer and S. Pozzorini, *Scattering Amplitudes with Open Loops*, *Phys. Rev. Lett.* **108** (2012) 111601, arXiv: [1111.5206 \[hep-ph\]](#).
- [64] A. Denner, S. Dittmaier and L. Hofer, *COLLIER: A fortran-based complex one-loop library in extended regularizations*, *Comput. Phys. Commun.* **212** (2017) 220, arXiv: [1604.06792 \[hep-ph\]](#).
- [65] ATLAS Collaboration, *Studies of Monte Carlo predictions for the $t\bar{t}b\bar{b}$ process*, ATL-PHYS-PUB-2022-006, 2022, URL: <https://cds.cern.ch/record/2802806>.
- [66] S. Frixione, E. Laenen, P. Motylinski and B. R. Webber, *Single-top production in MC@NLO*, *JHEP* **03** (2006) 092, arXiv: [hep-ph/0512250](#).
- [67] S. Frixione, E. Laenen, P. Motylinski, C. White and B. R. Webber, *Single-top hadroproduction in association with a W boson*, *JHEP* **07** (2008) 029, arXiv: [0805.3067 \[hep-ph\]](#).

- [68] ATLAS Collaboration, *Modelling and computational improvements to the simulation of single vector-boson plus jet processes for the ATLAS experiment*, **JHEP** **08** (2022) 089, arXiv: [2112.09588 \[hep-ex\]](#).
- [69] T. Gleisberg and S. Höche, *Comix, a new matrix element generator*, **JHEP** **12** (2008) 039, arXiv: [0808.3674 \[hep-ph\]](#).
- [70] S. Höche, F. Krauss, M. Schönherr and F. Siegert, *QCD matrix elements + parton showers. The NLO case*, **JHEP** **04** (2013) 027, arXiv: [1207.5030 \[hep-ph\]](#).
- [71] ATLAS Collaboration, *Multijet simulation for 13 TeV ATLAS Analyses*, ATL-PHYS-PUB-2019-017, 2019, URL: <https://cds.cern.ch/record/2672252>.
- [72] ATLAS Collaboration, *Vertex Reconstruction Performance of the ATLAS Detector at $\sqrt{s} = 13$ TeV*, ATL-PHYS-PUB-2015-026, 2015, URL: <https://cds.cern.ch/record/2037717>.
- [73] ATLAS Collaboration, *Electron and photon performance measurements with the ATLAS detector using the 2015–2017 LHC proton–proton collision data*, **JINST** **14** (2019) P12006, arXiv: [1908.00005 \[hep-ex\]](#).
- [74] ATLAS Collaboration, *Muon reconstruction and identification efficiency in ATLAS using the full Run 2 pp collision data set at $\sqrt{s} = 13$ TeV*, **Eur. Phys. J. C** **81** (2021) 578, arXiv: [2012.00578 \[hep-ex\]](#).
- [75] M. Cacciari, G. P. Salam and G. Soyez, *The anti- k_t jet clustering algorithm*, **JHEP** **04** (2008) 063, arXiv: [0802.1189 \[hep-ph\]](#).
- [76] M. Cacciari, G. P. Salam and G. Soyez, *FastJet user manual*, **Eur. Phys. J. C** **72** (2012) 1896, arXiv: [1111.6097 \[hep-ph\]](#).
- [77] ATLAS Collaboration, *Jet reconstruction and performance using particle flow with the ATLAS Detector*, **Eur. Phys. J. C** **77** (2017) 466, arXiv: [1703.10485 \[hep-ex\]](#).
- [78] ATLAS Collaboration, *Topological cell clustering in the ATLAS calorimeters and its performance in LHC Run 1*, **Eur. Phys. J. C** **77** (2017) 490, arXiv: [1603.02934 \[hep-ex\]](#).
- [79] ATLAS Collaboration, *Selection of jets produced in 13 TeV proton–proton collisions with the ATLAS detector*, ATL-CONF-2015-029, 2015, URL: <https://cds.cern.ch/record/2037702>.
- [80] ATLAS Collaboration, *Performance of pile-up mitigation techniques for jets in pp collisions at $\sqrt{s} = 8$ TeV using the ATLAS detector*, **Eur. Phys. J. C** **76** (2016) 581, arXiv: [1510.03823 \[hep-ex\]](#).
- [81] D. Krohn, J. Thaler and L.-T. Wang, *Jets with Variable R*, **JHEP** **06** (2009) 059, arXiv: [0903.0392 \[hep-ph\]](#).
- [82] ATLAS Collaboration, *ATLAS flavour-tagging algorithms for the LHC Run 2 pp collision dataset*, **Eur. Phys. J. C** **83** (2023) 681, arXiv: [2211.16345 \[physics.data-an\]](#).
- [83] ATLAS Collaboration, *Performance of missing transverse momentum reconstruction with the ATLAS detector using proton–proton collisions at $\sqrt{s} = 13$ TeV*, **Eur. Phys. J. C** **78** (2018) 903, arXiv: [1802.08168 \[hep-ex\]](#).

- [84] B. Nachman, P. Nef, A. Schwartzman, M. Swiatlowski and C. Wanotayaroj, *Jets from Jets: Re-clustering as a tool for large radius jet reconstruction and grooming at the LHC*, [JHEP **02** \(2015\) 075](#), arXiv: [1407.2922 \[hep-ph\]](#).
- [85] D. Krohn, J. Thaler and L.-T. Wang, *Jet Trimming*, [JHEP **02** \(2010\) 084](#), arXiv: [0912.1342 \[hep-ph\]](#).
- [86] ATLAS Collaboration, *Measurements of top-quark pair differential and double-differential cross-sections in the ℓ +jets channel with pp collisions at $\sqrt{s} = 13$ TeV using the ATLAS detector*, [Eur. Phys. J. C **79** \(2019\) 1028](#), arXiv: [1908.07305 \[hep-ex\]](#),
Erratum: [Eur. Phys. J. C **80** \(2020\) 1092](#).
- [87] ATLAS Collaboration, *Measurement of the $t\bar{t}$ production cross-section and lepton differential distributions in $e\mu$ dilepton events from pp collisions at $\sqrt{s} = 13$ TeV with the ATLAS detector*, [Eur. Phys. J. C **80** \(2020\) 528](#), arXiv: [1910.08819 \[hep-ex\]](#).
- [88] ATLAS Collaboration, *Search for single production of vector-like T quarks decaying into Ht or Zt in pp collisions at $\sqrt{s} = 13$ TeV with the ATLAS detector*, [JHEP **08** \(2023\) 153](#), arXiv: [2305.03401 \[hep-ex\]](#).
- [89] ATLAS Collaboration, *Jet energy scale and resolution measured in proton–proton collisions at $\sqrt{s} = 13$ TeV with the ATLAS detector*, [Eur. Phys. J. C **81** \(2021\) 689](#), arXiv: [2007.02645 \[hep-ex\]](#).
- [90] ATLAS Collaboration, *In situ calibration of large-radius jet energy and mass in 13 TeV proton–proton collisions with the ATLAS detector*, [Eur. Phys. J. C **79** \(2019\) 135](#), arXiv: [1807.09477 \[hep-ex\]](#).
- [91] ATLAS Collaboration, *ATLAS b -jet identification performance and efficiency measurement with $t\bar{t}$ events in pp collisions at $\sqrt{s} = 13$ TeV*, [Eur. Phys. J. C **79** \(2019\) 970](#), arXiv: [1907.05120 \[hep-ex\]](#).
- [92] ATLAS Collaboration, *Measurement of the c -jet mistagging efficiency in $t\bar{t}$ events using pp collision data at $\sqrt{s} = 13$ TeV collected with the ATLAS detector*, [Eur. Phys. J. C **82** \(2022\) 95](#), arXiv: [2109.10627 \[hep-ex\]](#).
- [93] ATLAS Collaboration, *Calibration of the light-flavour jet mistagging efficiency of the b -tagging algorithms with Z +jets events using 139 fb^{-1} of ATLAS proton–proton collision data at $\sqrt{s} = 13$ TeV*, [Eur. Phys. J. C **83** \(2023\) 728](#), arXiv: [2301.06319 \[hep-ex\]](#).
- [94] ATLAS Collaboration, *Muon reconstruction performance of the ATLAS detector in proton–proton collision data at $\sqrt{s} = 13$ TeV*, [Eur. Phys. J. C **76** \(2016\) 292](#), arXiv: [1603.05598 \[hep-ex\]](#).
- [95] J. Butterworth et al., *PDF4LHC recommendations for LHC Run II*, [J. Phys. G **43** \(2016\) 023001](#), arXiv: [1510.03865 \[hep-ph\]](#).
- [96] H.-L. Lai et al., *New parton distributions for collider physics*, [Phys. Rev. D **82** \(2010\) 074024](#), arXiv: [1007.2241 \[hep-ph\]](#).
- [97] J. Gao et al., *CT10 next-to-next-to-leading order global analysis of QCD*, [Phys. Rev. D **89** \(2014\) 033009](#), arXiv: [1302.6246 \[hep-ph\]](#).
- [98] N. Kidonakis, *Next-to-next-to-leading-order collinear and soft gluon corrections for t -channel single top quark production*, [Phys. Rev. D **83** \(2011\) 091503](#), arXiv: [1103.2792 \[hep-ph\]](#).

- [99] N. Kidonakis, *Two-loop soft anomalous dimensions for single top quark associated production with a W^- or H^-* , [Phys. Rev. D **82** \(2010\) 054018](#), arXiv: [1005.4451 \[hep-ph\]](#).
- [100] N. Kidonakis, *Next-to-next-to-leading logarithm resummation for s -channel single top quark production*, [Phys. Rev. D **81** \(2010\) 054028](#), arXiv: [1001.5034 \[hep-ph\]](#).
- [101] ATLAS Collaboration, *Measurement of Higgs boson decay into b -quarks in associated production with a top-quark pair in pp collisions at $\sqrt{s} = 13$ TeV with the ATLAS detector*, [JHEP **06** \(2022\) 097](#), arXiv: [2111.06712 \[hep-ex\]](#).
- [102] J. M. Campbell and R. K. Ellis, *Update on vector boson pair production at hadron colliders*, [Phys. Rev. D **60** \(1999\) 113006](#), arXiv: [hep-ph/9905386](#).
- [103] J. Alwall et al., *Comparative study of various algorithms for the merging of parton showers and matrix elements in hadronic collisions*, [Eur. Phys. J. C **53** \(2008\) 473](#), arXiv: [0706.2569 \[hep-ph\]](#).
- [104] W. A. Rolke, A. M. López and J. Conrad, *Limits and confidence intervals in the presence of nuisance parameters*, [Nucl. Instrum. Meth. A **551** \(2005\) 493](#), ed. by L. Lyons and M. Karagoz, arXiv: [physics/0403059](#).
- [105] ATLAS Collaboration, *Search for the standard model Higgs boson produced in association with top quarks and decaying into a $b\bar{b}$ pair in pp collisions at $\sqrt{s} = 13$ TeV with the ATLAS detector*, [Phys. Rev. D **97** \(2018\) 072016](#), arXiv: [1712.08895 \[hep-ex\]](#).
- [106] ATLAS Collaboration, *Measurement of $t\bar{t}$ production in association with additional b -jets in the $e\mu$ final state in proton–proton collisions at $\sqrt{s} = 13$ TeV with the ATLAS detector*, [JHEP **01** \(2025\) 068](#), arXiv: [2407.13473 \[hep-ex\]](#).
- [107] ATLAS Collaboration, *Search for a new pseudoscalar decaying into a pair of bottom and antibottom quarks in top-associated production in $\sqrt{s} = 13$ TeV proton–proton collisions with the ATLAS detector*, [Eur. Phys. J. C **85** \(2025\) 886](#), arXiv: [2503.17254 \[hep-ex\]](#).
- [108] ATLAS Collaboration, *TRExFitter*, URL: <https://doi.org/10.5281/zenodo.14845712>.
- [109] W. Verkerke and D. Kirkby, *The RooFit toolkit for data modeling*, eConf [C0303241](#) (2003) MOLT007, ed. by L. Lyons and M. Karagoz, arXiv: [physics/0306116](#).
- [110] L. Moneta et al., *The RooStats Project*, [PoS ACAT2010 \(2010\) 057](#), ed. by T. Speer et al., arXiv: [1009.1003 \[physics.data-an\]](#).
- [111] G. Cowan, K. Cranmer, E. Gross and O. Vitells, *Asymptotic formulae for likelihood-based tests of new physics*, [Eur. Phys. J. C **71** \(2011\) 1554](#), arXiv: [1007.1727 \[physics.data-an\]](#), Erratum: [Eur. Phys. J. C **73** \(2013\) 2501](#).
- [112] G. Cowan, K. Cranmer, E. Gross and O. Vitells, *Erratum to: Asymptotic formulae for likelihood-based tests of new physics*, [Eur. Phys. J. C **73** \(2013\)](#).
- [113] T. Junk, *Confidence level computation for combining searches with small statistics*, [Nucl. Instrum. Meth. A **434** \(1999\) 435](#), arXiv: [hep-ex/9902006](#).
- [114] A. L. Read, *Presentation of search results: the CL_s technique*, [J. Phys. G **28** \(2002\) 2693](#).

- [115] E. Maguire, L. Heinrich and G. Watt, *HEPData: a repository for high energy physics data*, *J. Phys. Conf. Ser.* **898** (2017) 102006, ed. by R. Mount and C. Tull, arXiv: [1704.05473](https://arxiv.org/abs/1704.05473) [[hep-ex](#)].
- [116] A. Buckley, L. Corpe, M. Habedank and T. Procter, *Enabling stable preservation of ML algorithms in high-energy physics with petrifyML*, (2025), arXiv: [2509.11830](https://arxiv.org/abs/2509.11830) [[hep-ph](#)].
- [117] C. Bierlich et al., *Robust Independent Validation of Experiment and Theory: Rivet version 3*, *SciPost Phys.* **8** (2020) 026, arXiv: [1912.05451](https://arxiv.org/abs/1912.05451) [[hep-ph](#)].
- [118] C. Bierlich et al., *Robust independent validation of experiment and theory: Rivet version 4 release note*, *SciPost Phys. Codeb.* **36** (2024) 1, arXiv: [2404.15984](https://arxiv.org/abs/2404.15984) [[hep-ph](#)].
- [119] ATLAS Collaboration, *ATLAS Computing Acknowledgements*, ATL-SOFT-PUB-2026-001, 2026, URL: <https://cds.cern.ch/record/2952666>.

The ATLAS Collaboration

G. Aad ¹⁰², E. Aakvaag ¹⁷, B. Abbott ¹²¹, S. Abdelhameed ^{83b}, K. Abeling ⁵⁴, N.J. Abicht ⁴⁸, S.H. Abidi ³⁰, M. Aboeela ⁴⁴, A. Aboulhorma ^{36e}, H. Abramowicz ¹⁵⁴, B.S. Acharya ^{68a,68b,m}, A. Ackermann ^{62a}, C. Adam Bourdarios ⁴, L. Adamczyk ^{85a}, S.V. Addepalli ¹⁴⁶, M.J. Addison ¹⁰¹, J. Adelman ¹¹⁷, A. Adiguzel ^{22c}, T. Adye ¹³⁵, A.A. Affolder ¹³⁷, Y. Afik ³⁹, M.N. Agaras ¹³, A. Aggarwal ¹⁰⁰, C. Agheorghiesei ^{28c}, A. Ahmad ^{83a}, F. Ahmadov ^{38,ad}, S. Ahuja ⁹⁵, S. Ahuja ¹⁶⁵, X. Ai ^{113c}, G. Aielli ^{75a,75b}, A. Aikot ¹⁶⁵, M. Ait Tamlihat ^{36e}, T.P.A. Åkesson ⁹⁸, D. Akiyama ¹⁷⁰, N.N. Akolkar ²⁵, S. Aktas ¹⁶⁸, G.L. Alberghi ^{24b}, J. Albert ¹⁶⁷, U. Alberti ²⁰, P. Albicocco ⁵², S. Alderweireldt ⁵¹, Z.L. Alegria ¹²², M. Aleksa ³⁷, I.N. Aleksandrov ³⁸, C. Alexa ^{28b}, T. Alexopoulos ¹⁰, F. Alfonsi ^{24b}, M. Algren ⁵⁵, M. Alhroob ¹⁶⁹, B. Ali ¹³³, H.M.J. Ali ^{91,v}, S. Ali ³², S.W. Alibocus ⁹², M. Aliev ^{34c}, G. Alimonti ^{70a}, C. Allaire ⁶⁵, B.M.M. Allbrooke ¹⁴⁹, D.R. Allen ¹²², J.S. Allen ¹⁰¹, J.F. Allen ⁵¹, C.S. Alley ¹, E.R. Almazan ¹³⁷, A. Aloisio ^{71a,71b}, F. Alonso ⁹⁰, C. Alpigiani ¹⁴⁰, A. Alvarez Fernandez ¹⁰⁰, M. Alves Cardoso ⁵⁵, M.G. Alviggi ^{71a,71b}, M. Aly ¹⁰¹, Y. Amaral Coutinho ^{81b}, A. Ambler ¹⁰⁴, C. Amelung ³⁷, M. Amerl ¹⁰¹, T. Amezza ¹²⁸, B. Amini ⁵³, K. Amirie ¹⁵⁸, A. Amirkhanov ³⁸, D. Amperidou ¹⁵⁵, S. An ⁸², C. Anastopoulos ¹⁴², T. Andeen ¹¹, J.K. Anders ⁹², A.C. Anderson ⁵⁸, A. Andreazza ^{70a,70b}, S. Angelidakis ⁹, A. Angerami ⁴¹, A.V. Anisenkov ³⁸, A. Annovi ^{73a}, C. Antel ³⁷, E. Antipov ¹⁴⁸, M. Antonelli ⁵², F. Anulli ^{74a}, M. Aoki ⁸², T. Aoki ¹⁵⁶, M.A. Aparo ¹³, L. Aperio Bella ⁴⁷, M. Apicella ³¹, C. Appelt ¹⁵⁴, A. Apyan ²⁷, M. Arampatzi ¹⁰, S.J. Arbiol Val ⁸⁶, C. Arcangeletti ⁵², A.T.H. Arce ⁵⁰, J-F. Arguin ¹⁰⁸, S. Argyropoulos ¹⁵⁵, J.-H. Arling ⁴⁷, O. Arnaez ⁴, H. Arnold ¹⁴⁸, G. Artoni ^{74a,74b}, H. Asada ¹¹¹, S. Asatryan ¹⁷⁵, N.A. Asbah ³⁷, R.A. Ashby Pickering ¹⁶⁹, A.M. Aslam ⁹⁵, J. Assahsah ^{36d}, K. Assamagan ³⁰, R. Astalos ^{29a}, K.S.V. Astrand ⁹⁸, S. Atashi ¹⁶², R.J. Atkin ^{34a}, H. Atmani ^{36f}, P.A. Atmasiddha ¹²⁹, K. Augsten ¹³³, A.D. Auriol ⁴⁰, V.A. Austrup ¹⁰¹, A.S. Avad ⁹⁴, G. Avolio ³⁷, K. Axiotis ⁵⁵, A. Azzam ¹³, D. Babal ^{29b}, H. Bachacou ¹³⁶, K. Bachas ^{155,p}, A. Bachi ³⁵, E. Bachmann ⁴⁹, M.J. Backes ^{62a}, A. Badea ³⁹, T.M. Baer ¹⁰⁶, M. Bahmani ¹⁹, D. Bahner ⁵³, K. Bai ¹²⁴, L. Baines ⁹⁴, O.K. Baker ¹⁷⁴, D. Bakshi Gupta ⁸, L.E. Balabram Filho ^{81b}, V. Balakrishnan ¹²¹, R. Balasubramanian ⁴, P. Balek ^{85a}, E. Ballabene ^{24b,24a}, F. Balli ¹³⁶, L.M. Baltes ^{62a}, W.K. Balunas ¹²⁷, I. Bamwidhi ^{83c}, E. Banas ⁸⁶, M. Bandieramonte ¹³⁰, A. Bandyopadhyay ²⁵, S. Bansal ²⁵, L. Barak ¹⁵⁴, M. Barakat ⁴⁷, E.L. Barberio ¹⁰⁵, D. Barberis ^{18b}, M. Barbero ¹⁰², M.Z. Barel ¹¹⁶, T. Barillari ¹¹⁰, M-S. Barisits ³⁷, T. Barklow ¹⁴⁶, P. Baron ¹³⁴, D.A. Baron Moreno ¹⁰¹, A. Baroncelli ⁶¹, A.J. Barr ¹²⁷, J.D. Barr ⁹⁶, F. Barreiro ⁹⁹, J. Barreiro Guimarães da Costa ¹⁴, M.G. Barros Teixeira ^{131a}, F. Bartels ^{62a}, R. Bartoldus ¹⁴⁶, A.E. Barton ⁹¹, P. Bartos ^{29a}, M. Baselga ⁴⁸, S. Bashiri ⁸⁶, A. Bassalat ^{65,b}, M.J. Basso ^{159a}, S. Bataju ⁴⁴, R. Bate ¹⁶⁶, R.L. Bates ⁵⁸, S. Batlamous ⁹⁹, M. Battaglia ¹³⁷, D. Battulga ¹⁹, M. Baucé ^{74a,74b}, L. Bauckhage ⁴⁷, P. Bauer ²⁵, L.T. Bayer ⁴⁷, L.T. Bazzano Hurrell ³¹, T. Beau ¹²⁸, J.Y. Beaucamp ⁹⁰, S. Beauceron ¹²⁸, P.H. Beauchemin ¹⁶¹, P. Bechtel ²⁵, H.P. Beck ^{20,o}, K. Becker ¹⁶⁹, A.J. Beddall ⁸⁰, V.A. Bednyakov ³⁸, C.P. Bee ¹⁴⁸, L.J. Beemster ¹⁶, M. Begalli ^{81d}, M. Beger ³⁰, J.K. Behr ⁴⁷, J.F. Beirer ³⁷, F. Beisiegel ²⁵, M. Belfkir ^{83c}, G. Bella ¹⁵⁴, L. Bellagamba ^{24b}, A. Bellerive ³⁵, C.D. Bellgraph ⁶⁷, P. Bellos ²¹, I. Benaoumeur ²¹, D. Bencheikroun ^{36a}, F. Bendebba ^{36a}, Y. Benhammou ¹⁵⁴, K.C. Benkendorfer ¹⁶⁷, L. Beresford ⁴⁷, M. Beretta ⁵², E. Bergeas Kuutmann ¹⁶³, N. Berger ⁴, B. Bergmann ¹³³, J. Beringer ^{18a}, M. Berkat ¹³⁶, G. Bernardi ⁵, C. Bernius ¹⁴⁶, F.U. Bernlochner ²⁵, A. Berrocal Guardia ¹³, T. Berry ⁹⁵, P. Berta ¹³⁴, A. Berti ^{131a},

R. Bertrand [ID102](#), S. Bethke [ID110](#), A. Betti [ID74a,74b](#), T.F. Beumker [ID173](#), A.J. Bevan [ID94](#), L. Bezio [ID55](#), N.K. Bhalla [ID53](#), S. Bharthuar [ID110](#), S. Bhatta [ID148](#), P. Bhattacharai [ID146](#), Z.M. Bhatti [ID118](#), K.D. Bhide [ID53](#), V.S. Bhopatkar [ID122](#), R.M. Bianchi [ID130](#), G. Bianco [ID24b,24a](#), O. Biebel [ID109](#), M. Biglietti [ID76a](#), P. Bijl [ID53](#), C.S. Billingsley [ID44](#), Y. Bimondi [ID36f](#), M. Bindi [ID54](#), A. Bingham [ID173](#), A. Bingul [ID22b](#), C. Bini [ID74a,74b](#), G.A. Bird [ID33](#), M. Biroš [ID134](#), S. Biryukov [ID149](#), T. Bisanz [ID48](#), E. Bisceglie [ID24b,24a](#), J.P. Biswal [ID135](#), D. Biswas [ID144](#), M. Biyabi [ID14](#), I. Bloch [ID47](#), A. Blue [ID58](#), U. Blumenschein [ID94](#), V.S. Bobrovnikov [ID38](#), L. Boccardo [ID56b,56a](#), M. Boehler [ID53](#), B. Boehm [ID168](#), D. Bogavac [ID13](#), L.S. Boggia [ID128](#), V. Boisvert [ID95](#), P. Bokan [ID163](#), T. Bold [ID85a](#), M. Bomben [ID5](#), M. Bona [ID94](#), M. Boonekamp [ID136](#), A.G. Borbély [ID58](#), G. Borissov [ID91](#), A. Borkar [ID168](#), D. Bortoletto [ID127](#), D. Boscherini [ID24b](#), M. Bosman [ID13](#), K. Bouaouda [ID36a](#), L. Boudet [ID136](#), J. Boudreau [ID130](#), E.V. Bouhova-Thacker [ID91](#), D. Boumediene [ID40](#), R. Bouquet [ID56b,56a](#), A. Boveia [ID120](#), D. Boye [ID30](#), I.R. Boyko [ID38](#), L. Bozianu [ID55](#), J. Bracinik [ID21](#), N. Brahimi [ID4](#), G. Brandt [ID173](#), O. Brandt [ID33](#), B. Brau [ID103](#), R. Brenner [ID171](#), L. Brenner [ID116](#), R. Brenner [ID163](#), S. Bressler [ID171](#), M. Brettell [ID96](#), G. Brianti [ID116](#), D. Britton [ID58](#), D. Britzger [ID110](#), I. Brock [ID25](#), R. Brock [ID107](#), H. Bronson [ID129](#), G. Brooijmans [ID41](#), A.J. Brooks [ID67](#), E.M. Brooks [ID159b](#), E. Brost [ID30](#), L.M. Brown [ID167,159a](#), L.E. Bruce [ID60](#), T.L. Bruckler [ID127](#), P.A. Bruckman de Renstrom [ID86](#), B. Brüers [ID47](#), A. Bruni [ID24b](#), G. Bruni [ID24b](#), D. Brunner [ID46a,46b](#), M. Bruschi [ID24b](#), N. Bruscinò [ID74a,74b](#), T. Buanes [ID17](#), Q. Buat [ID140](#), D. Buchin [ID110](#), A.G. Buckley [ID58](#), J. Bucko [ID134](#), M. Bühring [ID49](#), O. Bulekov [ID80](#), B.A. Bullard [ID146](#), T.O. Buratovich [ID90](#), S. Burdin [ID92](#), C.D. Burgard [ID48](#), A.M. Burger [ID89](#), B. Burghgrave [ID8](#), O. Burlayenko [ID53](#), J. Burleson [ID164](#), J.C. Burzynski [ID121](#), V. Büscher [ID100](#), P.J. Bussey [ID58](#), O. But [ID25](#), J.M. Butler [ID26](#), C.M. Buttar [ID58](#), J.M. Butterworth [ID96](#), P. Butti [ID37](#), W. Buttinger [ID135](#), C.J. Buxo Vazquez [ID107](#), A.R. Buzykaev [ID38](#), S. Cabrera Urbán [ID165](#), L. Cadamuro [ID65](#), H. Cai [ID37](#), Y. Cai [ID24b,112c,24a](#), Y. Cai [ID112a](#), M.A. Cairo [ID129](#), V.M.M. Cairo [ID37](#), O. Cakir [ID3a](#), N. Calace [ID37](#), P. Calafiura [ID18a](#), G. Calderini [ID128](#), P. Calfayan [ID35](#), L. Calic [ID98](#), G. Callea [ID58](#), L.P. Caloba [ID81b](#), D. Calvet [ID40](#), S. Calvet [ID40](#), R. Camacho Toro [ID128](#), S. Camarda [ID37](#), D. Camarero Munoz [ID27](#), P. Camarri [ID75a,75b](#), C. Camincher [ID37](#), M. Campanelli [ID96](#), A. Camplani [ID42](#), V. Canale [ID71a,71b](#), A.C. Canbay [ID3a](#), E. Canonero [ID95](#), J. Cantero [ID165](#), F. Capocasa [ID27](#), P. Cappelli [ID27](#), M. Capua [ID43b,43a](#), A. Carbone [ID70a,70b](#), R. Cardarelli [ID75a](#), J.C.J. Cardenas [ID8](#), M.P. Cardiff [ID27](#), G. Carducci [ID43b,43a](#), T. Carli [ID37](#), G. Carlino [ID71a](#), J.I. Carlotto [ID13](#), B.T. Carlson [ID130,q](#), E.M. Carlson [ID167](#), L. Carminati [ID70a,70b](#), A. Carnelli [ID4](#), M. Carnesale [ID37](#), S. Caron [ID115](#), E. Carquin [ID138g](#), I.B. Carr [ID105](#), S. Carrá [ID72a,72b](#), G. Carratta [ID24b,24a](#), C. Carrion Martinez [ID165](#), A.M. Carroll [ID124](#), N. Cartalade [ID40](#), M.P. Casado [ID13,h](#), P. Casolaro [ID71a,71b](#), M. Caspar [ID47](#), F. Cassinese [ID90](#), W.R. Castiglioni [ID39](#), F.L. Castillo [ID4](#), L. Castillo Garcia [ID13](#), V. Castillo Gimenez [ID165](#), N.F. Castro [ID131a,131e](#), A. Catinaccio [ID37](#), J.R. Catmore [ID126](#), T. Cavaliere [ID4](#), V. Cavaliere [ID30](#), E. Celebi [ID80](#), S. Cella [ID30](#), V. Cepaitis [ID55](#), K. Cerny [ID123](#), A.S. Cerqueira [ID81a](#), A. Cerri [ID73a,ap](#), L. Cerrito [ID75a,75b](#), F. Cerutti [ID18a](#), B. Cervato [ID70a,70b](#), A. Cervelli [ID24b](#), G. Cesarini [ID52](#), S.A. Cetin [ID80](#), P.M. Chabrilat [ID128](#), R. Chakkappai [ID65](#), S. Chakraborty [ID169](#), A. Chambers [ID60](#), J. Chan [ID18a](#), J.D. Chapman [ID33](#), E. Chapon [ID136](#), B. Chargeishvili [ID152b](#), D.G. Charlton [ID21](#), C. Chauhan [ID132](#), Y. Che [ID112a](#), S. Chekanov [ID6](#), G.A. Chelkov [ID38,a](#), H. Chen [ID30](#), J. Chen [ID141a](#), J. Chen [ID145](#), M. Chen [ID59](#), S. Chen [ID87](#), S.J. Chen [ID112a](#), X. Chen [ID141a](#), X. Chen [ID15,ai](#), Z. Chen [ID61](#), C.L. Cheng [ID146](#), H.C. Cheng [ID63a](#), S. Cheong [ID146](#), A. Cheplakov [ID38](#), E. Cherepanova [ID116](#), E. Cheu [ID7](#), K. Cheung [ID64](#), L. Chevalier [ID136](#), G. Chiarelli [ID73a](#), G. Chiodini [ID69a](#), A.S. Chisholm [ID21](#), J.L. Chisholm [ID166](#), A. Chitan [ID28b](#), M. Chitishvili [ID165](#), M.V. Chizhov [ID38,r](#), K. Choi [ID11](#), Y. Chou [ID140](#), E.Y.S. Chow [ID115](#), G. Christou [ID51](#), K.L. Chu [ID171](#), M.C. Chu [ID63a](#), Z. Chubinidze [ID52](#), J. Chudoba [ID132](#), J.J. Chwastowski [ID86](#), D. Cieri [ID110](#), K.M. Ciesla [ID85a](#), V. Cindro [ID93](#), A. Ciocio [ID18a](#), F. Ciotto [ID71a,71b](#), Z.H. Citron [ID171](#), M. Citterio [ID70a](#), D.A. Ciubotaru [ID28b](#), A. Clark [ID55](#), P.J. Clark [ID51](#), N. Clarke Hall [ID96](#), C. Clarry [ID158](#), S.E. Clawson [ID47](#), C. Clement [ID46a,46b](#), L. Clissa [ID24b,24a](#), Y. Coadou [ID102](#), M. Cobal [ID68a,68c](#), A. Coccaro [ID56b](#),

M.G. Cochran Branson [ID140](#), R.F. Coelho Barrue [ID131a](#), R. Coelho Lopes De Sa [ID103](#), S. Coelli [ID70a](#),
M.M. Cohen [ID129](#), L.S. Colangeli [ID158](#), B. Cole [ID41](#), P. Collado Soto [ID99](#), J. Collot [ID59](#),
M.R. Coluccia [ID69a](#), I. Combes [ID65](#), P. Conde Muiño [ID131a,131g](#), L.H.J. Condren [ID162](#), M.P. Connell [ID34c](#),
S.H. Connell [ID34c](#), E.I. Conroy [ID127](#), M. Contreras Cossio [ID11](#), F. Conventi [ID71a,ak](#),
A.M. Cooper-Sarkar [ID127](#), L. Corazzina [ID74a,74b](#), F.A. Corchia [ID24b,24a](#), A. Cordeiro Oudot Choi [ID140](#),
L.D. Corpe [ID40](#), M. Corradi [ID74a,74b](#), F. Corriveau [ID104,ab](#), A. Cortes-Gonzalez [ID156](#), M.J. Costa [ID165](#),
F. Costanza [ID4](#), D. Costanzo [ID142](#), J. Couthures [ID4](#), G. Cowan [ID95](#), K. Cranmer [ID172](#), L. Cremer [ID48](#),
D. Cremonini [ID24b,24a](#), S. Crépe-Renaudin [ID59](#), F. Crescioli [ID128](#), T. Cresta [ID72a,72b](#), M. Cristinziani [ID144](#),
M. Cristoforetti [ID77a,77b](#), T.M. Critchley [ID55](#), E. Critelli [ID96](#), A. Cueto [ID99](#), H. Cui [ID96](#), Z. Cui [ID7](#),
B.M. Cunnett [ID149](#), W.R. Cunningham [ID58](#), E. Cuppini [ID110](#), F. Curcio [ID165](#), J.R. Curran [ID51](#),
M.J. Da Cunha Sargedas De Sousa [ID56b,56a](#), J.V. Da Fonseca Pinto [ID81b](#), C. Da Via [ID101](#),
W. Dabrowski [ID85a](#), T. Dado [ID37](#), S. Dahbi [ID151](#), T. Dai [ID106](#), D. Dal Santo [ID20](#), C. Dallapiccola [ID103](#),
M. Dam [ID42](#), G. D'amen [ID30](#), V. D'Amico [ID109](#), J.R. Dandoy [ID35](#), M. D'Andrea [ID56b,56a](#),
D. Dannheim [ID37](#), G. D'anniballe [ID73a,73b](#), M. Danninger [ID145](#), V. Dao [ID148](#), G. Darbo [ID56b](#),
F. Dattola [ID47](#), S. D'Auria [ID70a,70b](#), A. D'Avanzo [ID71a,71b](#), T. Davidek [ID134](#), J. Davidson [ID169](#),
I. Dawson [ID94](#), K. De [ID8](#), C. De Almeida Rossi [ID158](#), N. De Biase [ID47](#), S. De Castro [ID24b,24a](#),
N. De Groot [ID115](#), P. de Jong [ID116](#), H. De la Torre [ID117](#), A. De Maria [ID112a](#), S. De Miranda Rimes [ID81d](#),
A. De Salvo [ID74a](#), U. De Sanctis [ID75a,75b](#), F. De Santis [ID69a,69b](#), A. De Santo [ID149](#),
J.B. De Vivie De Regie [ID59](#), K.G. De Vries [ID116](#), J. Debevc [ID93](#), D.V. Dedovich [ID38](#), J. Degens [ID92](#),
A.M. Deiana [ID44](#), J. Del Peso [ID99](#), L. Delagrangé [ID27](#), F. Deliot [ID136](#), C.M. Delitzsch [ID48](#),
M. Della Pietra [ID71a,71b](#), D. Della Volpe [ID55](#), A. Dell'Acqua [ID37](#), L. Dell'Asta [ID70a,70b](#), M. Delmastro [ID4](#),
C.C. Delogu [ID56b,56a](#), P.A. Delsart [ID59](#), S. Demers [ID174](#), M. Demichev [ID38](#), H. Denizli [ID22a,1](#),
M.G. Depala [ID92](#), L. D'Eramo [ID40](#), D. Derendarz [ID86](#), L. Derin [ID56b,56a](#), F. Derue [ID128](#), P. Dervan [ID92,*](#),
A.M. Desai [ID1](#), K. Desch [ID25](#), F.A. Di Bello [ID73a,73b](#), A. Di Ciaccio [ID75a,75b](#), L. Di Ciaccio [ID4](#),
D. Di Croce [ID37](#), C. Di Donato [ID71a,71b](#), A. Di Girolamo [ID37](#), G. Di Gregorio [ID65](#), A. Di Luca [ID77a,77b](#),
B. Di Micco [ID76a,76b](#), R. Di Nardo [ID76a,76b](#), K.F. Di Petrillo [ID39](#), M. Diamantopoulou [ID35](#), F.A. Dias [ID116](#),
M.A. Diaz [ID138a,138b](#), A.R. Didenko [ID38](#), M. Didenko [ID165](#), S.D. Diefenbacher [ID18a](#), E.B. Diehl [ID106](#),
S. Díez Cornell [ID47](#), C. Díez Pardos [ID144](#), C. Dimitriadi [ID147](#), A. Dimitrievska [ID21](#), A. Dimri [ID148](#),
Y. Ding [ID61](#), J. Dingfelder [ID25](#), T. Dingley [ID127](#), I-M. Dinu [ID28b](#), S.J. Dittmeier [ID62b](#), F. Dittus [ID37](#),
M. Divisek [ID134](#), B. Dixit [ID92](#), F. Djama [ID102](#), T. Djobava [ID152b](#), C. Doglioni [ID101,98](#), A. Dohnalova [ID29a](#),
Z. Dolezal [ID134](#), K. Domijan [ID85a](#), K.M. Dona [ID39](#), M. Donadelli [ID81d](#), B. Dong [ID107](#), J. Donini [ID40](#),
A. D'Onofrio [ID71a,71b](#), M. D'Onofrio [ID92](#), J. Dopke [ID135](#), A. Doria [ID71a](#), N. Dos Santos Fernandes [ID131a](#),
I.A. Dos Santos Luz [ID81e](#), P. Dougan [ID44](#), M.T. Dova [ID90](#), A.T. Doyle [ID58](#), M.P. Drescher [ID54](#),
E. Dreyer [ID171](#), I. Drivas-koulouris [ID10](#), M. Drnevich [ID118](#), D. Du [ID61](#), T. Du [ID39](#), T.A. du Pree [ID116](#),
Z. Duan [ID112a](#), M. Dubau [ID4](#), F. Dubinin [ID38](#), M. Dubovsky [ID29a](#), E. Duchovni [ID171](#), G. Duckeck [ID109](#),
P.K. Duckett [ID96](#), O.A. Ducu [ID28b](#), D. Duda [ID51](#), A. Dudarev [ID37](#), M.M. Dudek [ID86](#), E.R. Duden [ID27](#),
M. D'uffizi [ID101](#), L. Dufflot [ID65](#), M. Dührssen [ID37](#), I. Duminica [ID28g](#), A.E. Dumitriu [ID28b](#),
M. Dunford [ID62a](#), T. Duong [ID4](#), A. Duperrin [ID102](#), A.F. Duque Bran [ID40](#), H. Duran Yildiz [ID3a](#),
A. Durglishvili [ID152b](#), G.I. Dyckes [ID18a](#), M. Dyndal [ID85a](#), B.S. Dziedzic [ID37](#), G.H. Eberwein [ID127](#),
B. Eckerova [ID29a](#), J.C. Egan [ID96](#), S. Eggebrecht [ID54](#), E. Egidio Purcino De Souza [ID81e](#), G. Eigen [ID17](#),
K. Einsweiler [ID18a](#), T. Ekelof [ID163](#), P.A. Ekman [ID98](#), S. El Farkh [ID36b](#), Y. El Ghazali [ID61](#),
H. El Jarrari [ID104](#), A. El Moussaouy [ID36a](#), I. Elbaz [ID154](#), D. Elitez [ID37](#), M. Ellert [ID163](#),
F. Ellinghaus [ID173](#), T.A. Elliot [ID95](#), J. Elmsheuser [ID30](#), M. Elsayy [ID83b](#), M. Elsing [ID37](#),
D. Emelianov [ID135](#), Y. Enari [ID82](#), S. Epari [ID108](#), D. Ernani Martins Neto [ID86](#), F. Ernst [ID37](#),
M. Escalier [ID65](#), C. Escobar [ID165](#), R. Estevam De Paula [ID81c](#), E. Etzion [ID154](#), G. Evans [ID131a,131b](#),
H. Evans [ID67](#), L.S. Evans [ID47](#), S. Ezzarqtouni [ID36a](#), F. Fabbri [ID24b,24a](#), L. Fabbri [ID24b,24a](#), G. Facini [ID96](#),
V. Fadeyev [ID137](#), D. Fakoudis [ID100](#), S. Falciano [ID74a](#), L.F. Falda Ulhoa Coelho [ID27](#), F. Fallavollita [ID110](#),

G. Falsetti ^{43b,43a}, J. Faltova ¹³⁴, C. Fan ¹⁶⁴, K.Y. Fan ^{63b}, Y. Fan ¹⁴, Y. Fang ^{14,112c}, M. Fanti ^{70a,70b}, M. Faraj ^{68a,68c}, Z. Farazpay ⁹⁷, A. Farbin ⁸, A. Farilla ^{76a}, K. Farman ¹⁵¹, J.N. Farr ¹⁷⁴, M.S. Farrington ⁶⁰, S.M. Farrington ^{135,51}, F. Fassi ^{36e}, D. Fassouliotis ⁹, L. Fayard ⁶⁵, G. Fazzino ^{62b}, P. Federic ¹³⁴, P. Federicova ¹³², M. Feickert ¹⁷², L. Feligioni ¹⁰², D.E. Fellers ^{18a}, C. Feng ^{113b}, Y. Feng ¹⁴, Z. Feng ⁶⁵, B. Fernandez Barbadillo ⁹¹, P. Fernandez Martinez ⁶⁶, C. Fernandez Ruiz ³³, J. Ferrando ⁹¹, A. Ferrari ¹⁶³, P. Ferrari ^{116,115}, R. Ferrari ^{72a}, D. Ferrere ⁵⁵, C. Ferretti ¹⁰⁶, M.P. Fewell ¹, D. Fiacco ^{74a,74b}, F. Fiedler ¹⁰⁰, P. Fiedler ¹³³, S. Filimonov ³⁸, M.S. Filip ^{28b,s}, A. Filipčič ⁹³, E.K. Filmer ^{159a}, F. Filthaut ¹¹⁵, M.C.N. Fiolhais ^{131a,131c,c}, L. Fiorini ¹⁶⁵, W.C. Fisher ¹⁰⁷, T. Fitschen ¹⁰¹, I. Fleck ¹⁴⁴, P. Fleischmann ¹⁰⁶, T. Flick ¹⁷³, M. Flores ^{34d,ag}, L.R. Flores Castillo ^{63a}, M. Foll ¹²⁶, F.M. Follega ^{77a,77b}, N. Fomin ³³, J.H. Foo ¹⁵⁸, A. Formica ¹³⁶, M. Fornasiero ¹⁴⁹, A.C. Forti ¹⁰¹, N. Forti ^{24b,24a}, E. Fortin ¹⁰², A.W. Fortman ^{18a}, L. Foster ^{18a}, L. Fountas ⁹, H. Fox ⁹¹, P. Francavilla ^{73a,73b}, S. Francescato ⁶⁰, S. Franchellucci ²⁰, M. Franchini ^{24b,24a}, S. Franchino ^{62a}, D. Francis ³⁷, L. Franco ⁴⁷, L. Franconi ⁴⁷, M. Franklin ⁶⁰, G. Frattari ²⁷, Y.Y. Frid ¹⁵⁴, N. Fritzsche ³⁷, A. Froch ⁵⁵, D. Froidevaux ³⁷, J.A. Frost ¹³⁵, Y. Fu ¹⁰⁷, S. Fuenzalida Garrido ^{138g}, Y.C. Fujikake ¹³⁷, M. Fujimoto ¹⁴⁸, K.Y. Fung ^{63a}, E. Furtado De Simas Filho ^{81e}, M. Furukawa ¹⁵⁶, M. Fuste Costa ⁴⁷, J. Fuster ¹⁶⁵, A. Gaa ⁵⁴, A. Gabrielli ^{24b,24a}, A. Gabrielli ¹⁵⁸, G. Gagliardi ^{56b,56a}, L.G. Gagnon ^{18a}, S. Galantzan ¹⁵⁴, J. Gallagher ¹, E.J. Gallas ¹²⁷, A.L. Gallen ¹⁶³, B.J. Gallop ¹³⁵, K.K. Gan ¹²⁰, Y. Gao ⁵¹, Z. Gao ^{112a}, A. Garabaglu ¹⁴⁰, F.M. Garay Walls ^{138a,138b}, C. García ¹⁶⁵, A. Garcia Alonso ¹¹⁶, A.G. Garcia Caffaro ¹⁷⁴, J.E. García Navarro ¹⁶⁵, M.A. Garcia Ruiz ^{23b}, M. Garcia-Sciveres ^{18a}, G.L. Gardner ¹²⁹, R.W. Gardner ³⁹, N. Garelli ¹⁶¹, R.B. Garg ¹⁴⁶, J.M. Gargan ³³, C.A. Garner ¹⁵⁸, C.M. Garvey ^{34a}, V.K. Gassmann ¹⁶¹, G. Gaudio ^{72a}, A.J. Gavin ⁹⁴, J. Gavranovic ⁹³, I.L. Gavrilenko ^{131a}, C. Gay ¹⁶⁶, G. Gaycken ¹²⁴, A. Gekow ¹²⁰, C. Gemme ^{56b}, M.H. Genest ⁵⁹, A.D. Gentry ¹¹⁴, S. George ⁹⁵, T. Geralis ⁴⁵, A.A. Gerwin ¹²¹, P. Gessinger-Befurt ³⁷, M. Ghani ¹⁶⁹, K. Ghorbanian ⁹⁴, A. Ghosal ¹⁴⁴, A. Ghosh ¹⁶², A. Ghosh ⁷, B. Giacobbe ^{24b}, S. Giagu ^{74a,74b}, A. Giannini ⁶¹, S.M. Gibson ⁹⁵, D.T. Gil ^{85b}, A.K. Gilbert ^{85a}, B.J. Gilbert ⁴¹, D. Gillberg ³⁵, G. Gilles ¹¹⁶, D.M. Gingrich ^{2,aj}, M.P. Giordani ^{68a,68c}, P.F. Giraud ¹³⁶, G. Giugliarelli ^{68a,68c}, D. Giugni ^{70a}, F. Giuli ^{75a,75b,al}, I. Gkialas ^{9,i}, C. Glasman ⁹⁹, M. Glazewska ²⁰, R.M. Gleason ¹⁶², G. Glemža ⁴⁷, I. Gnesi ^{24b,24a,am}, Y. Go ³⁰, M. Goblirsch-Kolb ³⁷, B. Gocke ⁴⁸, D. Godin ¹⁰⁸, B. Gokturk ^{22a}, S. Goldfarb ¹⁰⁵, T. Golling ⁵⁵, M.G.D. Gololo ^{34c}, A. Golub ¹⁴⁰, J.P. Gombas ¹⁰⁷, A. Gomes ^{131a,131b}, G. Gomes Da Silva ¹⁴⁴, A.J. Gomez Delegido ³⁷, R. Gonçalves ^{131a}, A. Gongadze ^{152c}, F. Gonnella ²¹, J.L. Gonski ¹⁴⁶, R.Y. González Andana ⁵¹, S. González de la Hoz ¹⁶⁵, M.V. Gonzalez Rodrigues ⁴⁷, R. Gonzalez Suarez ¹⁶³, S. Gonzalez-Sevilla ⁵⁵, L. Goossens ³⁷, B. Gorini ³⁷, E. Gorini ^{69a,69b}, A. Gorišek ⁹³, T.C. Gosart ¹²⁹, A.T. Goshaw ⁵⁰, M.I. Gostkin ³⁸, S. Goswami ¹²², C.A. Gottardo ³⁷, S.A. Gotz ¹⁰⁹, M. Goughri ^{36b}, A.G. Goussiou ¹⁴⁰, N. Govender ^{34c}, R.P. Grabarczyk ¹²⁷, I. Grabowska-Bold ^{85a}, K. Graham ³⁵, E. Gramstad ¹²⁶, S. Grancagnolo ^{69a,69b}, C.M. Grant ¹, P.M. Gravila ^{28f}, F.G. Gravili ^{69a,69b}, H.M. Gray ^{18a}, M. Greco ¹¹⁰, M.J. Green ¹, C. Grefe ²⁵, A.S. Grefsrud ¹⁷, I.M. Gregor ⁴⁷, K.T. Greif ¹⁶², P. Grenier ¹⁴⁶, S.G. Grewe ¹¹⁰, K. Grimm ³², S. Grinstein ^{13,x}, E. Gross ¹⁷¹, J. Grosse-Knetter ⁵⁴, L.H. Grossman ^{18b}, L. Guan ¹⁰⁶, G. Guerrieri ³⁷, R. Guevara ¹²⁶, R. Gugel ¹⁰⁰, J.A.M. Guhit ¹⁰⁶, A. Guida ¹⁹, E. Guilloton ¹⁶⁹, S. Guindon ³⁷, F. Guo ^{14,112c}, J. Guo ^{141a}, L. Guo ⁴⁷, L. Guo ^{112b,u}, Y. Guo ¹⁰⁶, Y. Guo ⁴¹, A. Gupta ⁴⁸, R. Gupta ¹³⁰, S. Gupta ²⁷, S. Gurbuz ²⁵, S.S. Gurdasani ⁴⁷, G. Gustavino ^{74a,74b}, P. Gutierrez ¹²¹, L.F. Gutierrez Zagazeta ¹²⁹, M. Gutsche ⁴⁹, C. Gutschow ⁹⁶, W. Guérin ⁸⁹, C. Gwenlan ¹²⁷, C.B. Gwilliam ⁹², E.S. Haaland ¹²⁶, A. Haas ¹¹⁸, M. Habedank ⁵⁸, C. Haber ^{18a},

R.J. Haberle ¹⁷¹, H.K. Hadavand ⁸, A. Haddad ⁴⁰, A. Hadeef ⁴⁹, A.I. Hagan ⁹¹, J.J. Hahn ¹⁴⁴, M. Haleem ¹⁶⁸, J. Haley ¹²², G.D. Hallelwell ¹⁰², J.A. Hallford ⁴⁷, K. Hamano ¹⁶⁷, H. Hamdaoui ¹⁶³, M. Hamer ²⁵, S.E.D. Hammoud ⁶⁵, E.J. Hampshire ⁹⁵, L. Han ^{112a}, L. Han ⁶¹, S. Han ¹⁴, K. Hanagaki ⁸², M. Hance ¹³⁷, D.A. Hangal ⁴¹, H. Hanif ¹⁴⁵, M.D. Hank ¹²⁹, J.B. Hansen ⁴², P.H. Hansen ⁴², T. Harenberg ¹⁷³, S. Harkusha ¹⁷⁵, M.L. Harris ¹⁰³, Y.T. Harris ²⁵, J. Harrison ¹³, P.F. Harrison ¹⁶⁹, M.L.E. Hart ⁹⁶, N.M. Hartman ¹¹⁰, N.M. Hartmann ¹⁰⁹, R.Z. Hasan ^{95,135}, Y. Hasegawa ¹⁴³, D. Hashimoto ¹¹¹, F. Haslbeck ³⁷, S. Hassan ¹²⁶, R. Hauser ¹⁰⁷, M. Haviernik ¹³⁴, C.M. Hawkes ²¹, R.J. Hawkings ³⁷, Y. Hayashi ¹⁵⁶, D. Hayden ¹⁰⁷, R.L. Hayes ¹¹⁶, C.P. Hays ¹²⁷, J.M. Hays ⁹⁴, H.S. Hayward ⁹², M. He ^{14,112c}, Y. He ⁴⁷, Y. He ⁹⁶, N.B. Heatley ⁹⁴, V. Hedberg ⁹⁸, J. Heilman ³⁵, S. Heim ⁴⁷, T. Heim ^{18a}, J.J. Heinrich ¹²⁴, L. Heinrich ¹¹⁰, J. Hejbal ¹³², M. Helbig ⁴⁹, A. Held ¹⁷², S. Hellesund ¹⁷, C.M. Helling ¹⁶⁶, F.N.E. Henry ⁵⁸, H. Herde ⁹⁸, Y. Hernández Jiménez ¹⁴⁸, G. Herten ⁵³, R. Hertenberger ¹⁰⁹, L. Hervas ³⁷, M.E. Hespings ¹⁰⁰, N.P. Hessey ^{159a}, J. Hessler ¹¹⁰, R. Hicks ¹²⁹, M. Hidaoui ^{36b}, N. Hidic ¹³⁴, E. Hill ¹⁵⁸, T.S. Hillersoy ¹⁷, S.J. Hillier ²¹, J.R. Hinds ¹⁰⁷, F. Hinterkeuser ²⁵, M. Hirose ¹²⁵, S. Hirose ¹⁶⁰, D. Hirschbuehl ¹⁷³, B. Hiti ⁹³, J. Hobbs ¹⁴⁸, R. Hobincu ^{28e}, N. Hod ¹⁷¹, A.M. Hodges ¹⁶⁴, M.C. Hodgkinson ¹⁴², B.H. Hodgkinson ¹²⁷, A. Hoecker ³⁷, D.D. Hofer ¹⁰⁶, J. Hofer ¹⁶⁵, J. Hofner ¹⁰⁰, M. Holzbock ³⁷, L.B.A.H. Hommels ³³, V. Homsak ¹²⁷, J.J. Hong ⁶⁷, T.M. Hong ¹³⁰, B.H. Hooberman ¹⁶⁴, W.H. Hopkins ⁶, M.C. Hoppesch ¹⁶⁴, Y. Horii ¹¹¹, M.E. Horstmann ¹¹⁰, M.M. Horzela ⁵⁴, S. Hou ¹⁵¹, M.R. Housenga ¹⁶⁴, J. Howarth ⁵⁸, J. Hoya ⁶, M. Hrabovsky ¹²³, T. Hryn'ova ⁴, P.J. Hsu ⁶⁴, S.-C. Hsu ¹⁴⁰, T. Hsu ⁶⁵, M. Hu ^{18a}, P. Hu ^{63b}, Q. Hu ⁶¹, S. Huang ³³, X. Huang ^{14,112c}, Y. Huang ¹³⁴, Y. Huang ^{112b}, Y. Huang ¹⁴, Z. Huang ⁶⁵, Z. Hubacek ¹³³, F. Huegging ²⁵, T.B. Huffman ¹²⁷, M. Hufnagel Maranha De Faria ^{81a}, C.A. Hugli ⁴⁷, M. Huhtinen ³⁷, S.K. Huiberts ¹⁷, R. Hulsken ¹⁰⁴, C.E. Hultquist ^{18a}, D.L. Humphreys ¹⁰³, N. Huseynov ¹², J. Huston ¹⁰⁷, B. Huth ³⁷, J. Huth ⁶⁰, L. Huth ⁴⁷, R. Hyneman ⁷, G. Iacobucci ⁵⁵, G. Iakovidis ³⁰, L. Iconomidou-Fayard ⁶⁵, J.P. Iddon ³⁷, P. Iengo ^{71a,71b}, Y. Iiyama ¹⁵⁶, T. Iizawa ¹⁵⁶, Y. Ikegami ⁸², D. Iliadis ¹⁵⁵, N. Ilic ¹⁵⁸, H. Imam ^{36a}, G. Inacio Goncalves ^{81d}, S.A. Infante Cabanas ^{138c}, T. Ingebretsen Carlson ^{46a,46b}, J.M. Inglis ⁹⁴, G. Introzzi ^{72a,72b}, M. Iodice ^{76a}, V. Ippolito ^{74a,74b}, R.K. Irwin ⁹², M. Ishino ¹⁵⁶, W. Islam ¹⁷², C. Issever ¹⁹, S. Istin ^{22a,ar}, K. Itabashi ¹²⁵, H. Ito ¹⁷⁰, R. Iuppa ^{77a,77b}, A. Ivina ¹⁷¹, F. Ivone ³⁷, S. Izumiyama ¹¹¹, V. Izzo ^{71a}, P. Jacka ¹³³, P. Jackson ¹, P.R. Jacobson ⁵⁰, P. Jain ⁴⁷, K. Jakobs ⁵³, J. Jamieson ⁵⁸, W. Jang ¹⁵⁶, S. Jankovych ¹¹⁶, B.K. Jashal ¹³⁵, M. Javurkova ¹⁰³, P. Jawahar ¹⁰¹, L. Jeanty ¹²⁴, J. Jejelava ^{152a,ae}, P. Jenni ^{53,f}, L. Jerala ⁹³, C.E. Jessiman ³⁵, H. Jia ¹⁶⁶, J. Jia ¹⁴⁸, X. Jia ^{110,112c}, C. Jiang ⁵¹, Q. Jiang ^{63b}, S. Jiggins ⁴⁷, M. Jimenez Ortega ¹⁶⁵, J. Jimenez Pena ¹³, S. Jin ^{112a}, A. Jinaru ^{28b}, O. Jinnouchi ¹³⁹, P. Johansson ¹⁴², K.A. Johns ⁷, J.W. Johnson ¹³⁷, F.A. Jolly ⁴⁷, D.M. Jones ¹⁴⁹, E. Jones ⁴⁷, K.S. Jones ⁸, P. Jones ³³, R.W.L. Jones ⁹¹, T.J. Jones ⁹², H.L. Joos ³⁷, R. Joshi ¹²⁰, J. Jovicevic ¹⁶, X. Ju ^{18a}, J.J. Junggeburth ³⁷, T. Junkermann ^{62a}, A. Juste Rozas ^{13,x}, M.K. Juzek ⁸⁶, S. Kabana ^{138f}, A. Kaczmaraska ⁸⁶, S.A. Kadir ¹⁴⁶, M. Kado ¹¹⁰, H. Kagan ¹²⁰, M. Kagan ¹⁴⁶, A. Kahn ¹²⁹, C. Kahra ¹⁰⁰, T. Kaji ¹⁵⁶, E. Kajomovitz ¹⁵³, N. Kakati ¹⁷¹, N. Kakoty ¹³, S. Kandel ⁸, N. Kanellos ¹⁰, D. Kar ^{34,*}, E. Karentzos ²⁵, K. Karki ⁸, O. Karkout ¹¹⁶, S.N. Karpov ³⁸, Z.M. Karpova ³⁸, V. Kartvelishvili ^{91,152b}, E. Kasimi ¹⁵⁵, J. Katzy ⁴⁷, S. Kaur ³⁵, R. Kavak ¹⁶⁴, K. Kawade ¹⁴³, M.P. Kawale ¹²¹, C. Kawamoto ⁸⁷, E.F. Kay ³⁷, S. Kazakos ¹⁰⁷, K. Kazakova ¹⁰², J.M. Keaveney ^{34a}, R. Keeler ¹⁶⁷, G.V. Kehris ⁶⁰, J.S. Keller ³⁵, J.M. Kelly ¹⁶⁷, J.J. Kempster ¹⁴⁹, O. Kepka ¹³², J. Kerr ^{159b}, B.P. Kerridge ¹³⁵, B.P. Kerševan ⁹³, L. Keszeghova ^{29a}, R.A. Khan ¹³⁰, A. Khanov ¹²², M. Kholodenko ^{131a},

T.J. Khoo ¹⁹, G. Khoraiuli ¹⁶⁸, Y. Khoulaki ^{36a}, Y.A.R. Khwaira ¹²⁸, D. Kim ⁶, D.W. Kim ^{18b}, Y.K. Kim ³⁹, N. Kimura ⁹⁶, M.K. Kingston ⁵⁴, F. Kirfel ²⁵, J. Kirk ¹³⁵, A.E. Kiryunin ¹¹⁰, S. Kita ¹⁶⁰, O. Kivernyk ²⁵, M. Klassen ¹⁶¹, C. Klein ³⁵, L. Klein ¹⁶⁸, M.H. Klein ⁴⁴, S.B. Klein ⁵⁵, U. Klein ⁹², A. Klimentov ³⁰, P. Kluit ¹¹⁶, S. Kluth ¹¹⁰, E. Kneringer ⁷⁸, T.M. Knight ¹⁵⁸, A. Knue ⁴⁸, M. Kobel ⁴⁹, D. Kobylianskii ¹⁷¹, S.F. Koch ³⁷, M. Kocian ¹⁴⁶, P. Kodyš ¹³⁴, D.M. Koeck ¹²⁴, T. Koffas ³⁵, K. Kojima ⁸², O. Kolay ⁴⁹, I. Koletsou ⁴, T. Komarek ⁸⁶, S. Kondo ¹⁵⁶, K. Köneke ⁵⁴, A.X.Y. Kong ¹, T. Kono ¹¹⁹, N. Konstantinidis ⁹⁶, P. Kontaxakis ⁵⁵, B. Konya ⁹⁸, R. Kopeliansky ⁴¹, S. Koperny ^{35a}, R. Koppenhofer ⁵³, K. Korcyl ⁸⁶, K. Kordas ^{155,d}, A. Korn ⁹⁶, S. Korn ⁵⁴, I. Korolkov ¹³, B. Kortman ¹¹⁶, O. Kortner ¹¹⁰, S. Kortner ¹¹⁰, W.H. Kostecka ¹¹⁷, M. Kostov ^{29a}, V.V. Kostyukhin ¹⁴⁴, A. Kotsokechagia ³⁷, A. Kotwal ⁵⁰, A. Koulouris ³⁷, A. Kourkoumeli-Charalampidi ^{72a,72b}, O. Kovanda ¹²⁴, R. Kowalewski ¹⁶⁷, W. Kozanecki ¹²⁴, G. Kramberger ⁹³, P. Kramer ²⁵, A. Krasznahorkay ¹⁰³, A.C. Kraus ¹¹⁷, J.W. Kraus ¹⁷³, J.A. Kremer ⁴⁷, N.B. Kregel ¹⁴⁴, T. Kresse ¹⁵⁸, L. Kretschmann ¹⁷³, J. Kretschmar ⁹², P. Krieger ¹⁵⁸, K. Krizka ²¹, K. Kroeninger ⁴⁸, H. Kroha ¹¹⁰, J. Kroll ¹³², J. Kroll ¹²⁹, K.S. Krowpman ¹⁰⁷, U. Kruchonak ³⁸, H. Krüger ²⁵, N. Krumnack ⁷⁹, J. Krupa ¹⁴⁶, M.C. Kruse ⁵⁰, O. Kuchinskaia ³⁸, S. Kuday ^{3a}, S. Kuehn ³⁷, R. Kuesters ⁵³, T. Kuhl ⁴⁷, V. Kukhtin ³⁸, Y. Kulchitsky ³⁸, S. Kuleshov ^{138d,138b}, J. Kull ¹, E.V. Kumar ¹⁰⁹, M. Kumar ^{34j}, N. Kumari ⁴⁷, P. Kumari ^{159b}, A. Kupco ¹³², O. Kuprash ⁵³, H. Kurashige ⁸⁴, L.L. Kurchaninov ^{159a}, O. Kurdysh ⁴, M. Kuze ¹³⁹, A.K. Kvam ¹⁰³, J. Kvita ¹²³, N.G. Kyriacou ¹⁴⁰, M. Laassiri ³⁰, C. Lacasta ¹⁶⁵, H. Lacker ¹⁹, D. Lacour ¹²⁸, E. Ladygin ³⁸, A. Lafarge ⁴⁰, B. Laforge ¹²⁸, T. Lagouri ¹⁷⁴, F.Z. Lahbabi ^{36a}, S. Lai ⁵⁴, W.S. Lai ⁹⁶, I.K. Lakomic ⁵⁴, J.E. Lambert ¹⁶⁷, S. Lammers ⁶⁷, W. Lampl ⁷, C. Lampoudis ¹⁵⁵, G. Lamprinoudis ¹⁶⁸, A.N. Lancaster ¹¹⁷, U. Landgraf ⁵³, M.P.J. Landon ⁹⁴, V.S. Lang ⁵³, A.J. Lankford ¹⁶², F. Lanni ³⁷, C.S. Lantz ¹⁶⁴, K. Lantzsch ²⁵, A. Lanza ^{72a}, M. Lanzac Berrocal ¹⁶⁵, T. Lari ^{70a}, D. Larsen ¹⁷, L. Larson ¹¹, F. Lasagni Manghi ^{24b}, M. Lassnig ³⁷, H.C. Lau ¹⁶⁷, S.D. Lawlor ¹⁴², R. Lazaridou ¹⁶², M. Lazzaroni ^{70a,70b}, E.T.T. Le ¹⁶², H.D.M. Le ¹⁰⁷, E.M. Le Boulicaut ¹⁷⁴, L.T. Le Pottier ^{18a}, B. Leban ^{24b,24a}, F. Ledroit-Guillon ⁵⁹, T.F. Lee ^{159b}, L.L. Leeuw ^{34h}, M. Lefebvre ¹⁶⁷, C. Leggett ^{18a}, L.M. Lehmann ¹¹⁶, G. Lehmann Miotto ³⁷, M. Leigh ⁵⁵, W.A. Leight ¹⁰³, W. Leinonen ¹¹⁵, A. Leisos ^{155,t}, M.A.L. Leite ^{81c}, C.E. Leitgeb ¹⁹, R. Leitner ¹³⁴, K.J.C. Leney ⁴⁴, T. Lenz ²⁵, S. Leone ^{73a}, C. Leonidopoulos ⁵¹, A. Leopold ¹⁴⁷, J. LePage-Bourbonnais ³⁵, R. Les ¹⁰⁷, C.G. Lester ³³, J. Levêque ⁴, L.J. Levinson ¹⁷¹, G. Levrini ^{24b,24a}, M.P. Lewicki ⁸⁶, C. Lewis ¹⁴⁰, D.J. Lewis ⁴, L. Lewitt ¹⁴², A. Li ³⁰, B. Li ^{113b}, C. Li ¹⁰⁶, C-Q. Li ¹¹⁰, H. Li ^{113b}, H. Li ¹⁰¹, H. Li ¹⁵, H. Li ⁶¹, H. Li ^{113b}, J. Li ^{141a}, L. Li ^{141a}, R. Li ¹⁷⁴, S. Li ^{141b,141a}, T. Li ⁵, Y. Li ¹⁴, Z. Li ^{14,112c}, Z. Li ⁶¹, S. Liang ^{14,112c}, Z. Liang ¹⁴, M. Liberatore ¹³⁶, B. Liberti ^{75a}, G.B. Libotte ^{81d}, K. Lie ^{63c}, J. Lieber Marin ^{81e}, H. Lien ⁶⁷, H. Lin ¹⁰⁶, S.F. Lin ¹⁴⁸, L. Linden ¹⁰⁹, R.E. Lindley ⁷, J.H. Lindon ³⁷, J. Ling ⁶⁰, E. Lipeles ¹²⁹, A. Lipniacka ¹⁷, A. Lister ¹⁶⁶, J.D. Little ⁶⁷, B. Liu ^{113a}, B.X. Liu ^{112b}, D. Liu ¹⁵³, D. Liu ¹³⁷, E.H.L. Liu ²¹, H. Liu ^{112b}, J.K.K. Liu ¹¹⁸, K. Liu ^{141b}, K. Liu ^{141b}, M. Liu ⁶¹, M.Y. Liu ⁶¹, P. Liu ^{113b}, Q. Liu ¹⁴⁶, S. Liu ¹⁴⁸, X. Liu ^{113b}, Y. Liu ^{112b,112c}, Y. Liu ¹⁶⁴, Y.L. Liu ^{113b}, Y.W. Liu ⁶¹, Z. Liu ^{65j}, S.L. Lloyd ⁹⁴, E.M. Lobodzinska ⁴⁷, P. Loch ⁷, E. Lodhi ¹⁵⁸, K. Lohwasser ¹⁴², E. Loiacono ¹²², J.D. Lomas ²¹, I. Longarini ¹⁶², R. Longo ^{24b,24a,am}, A. Lopez Solis ¹³, N.A. Lopez-canelas ⁷, N. Lorenzo Martinez ⁴, A.M. Lory ¹⁰⁹, M. Losada ^{83b}, G. Löschke Centeno ⁴, X. Lou ^{14,112c}, P.A. Love ⁹¹, M. Lu ⁶⁵, S. Lu ¹²⁹, Y.J. Lu ¹⁵¹, H.J. Lubatti ¹⁴⁰, C. Luci ^{74a,74b}, F.L. Lucio Alves ^{112a}, F. Luehring ⁶⁷, B.S. Lunday ¹²⁹, O. Lundberg ¹⁴⁷, J. Lunde ³⁷, N.A. Luongo ⁶, M.S. Lutz ¹⁵⁸, A.B. Lux ²⁶, D. Lynn ³⁰, R. Lysak ¹³², V. Lysenko ¹³³, E. Lytken ⁹⁸, V. Lyubushkin ³⁸, T. Lyubushkina ³⁸,

M.M. Lyukova [id148](#), H. Ma [id30](#), K. Ma [id61](#), L.L. Ma [id113b](#), W. Ma [id61](#), Y. Ma [id113b](#),
J.C. MacDonald [id100](#), P.C. Machado De Abreu Farias [id81e](#), D. Macina [id37](#), R. Madar [id40](#),
T. Madula [id96](#), J. Maeda [id84](#), T. Maeno [id30](#), P.T. Mafa [id34f](#), H. Maguire [id142](#), M. Maheshwari [id33](#),
V. Maiboroda [id65](#), A. Maio [id131a,131b,131d](#), K. Maj [id85a](#), O. Majersky [id47](#), S. Majewski [id124](#),
A. Makita [id156](#), N. Makovec [id65](#), V. Maksimovic [id16](#), B. Malaescu [id128](#), J. Malamant [id126](#),
Pa. Malecki [id86](#), F. Malek [id59,n](#), M. Mali [id93](#), D. Malito [id95](#), A. Maloizel [id5](#), A. Malvezzi Lopes [id81d](#),
S. Malyukov [id38](#), J. Mamuzic [id93](#), G. Mancini [id52](#), M.N. Mancini [id27](#), G. Manco [id72a,72b](#),
S.S. Mandarry [id149](#), I. Mandić [id93](#), L. Manhaes de Andrade Filho [id81a](#), I.M. Maniatis [id171](#),
J. Manjarres Ramos [id89](#), D.C. Mankad [id171](#), A. Mann [id109](#), T. Manoussos [id37](#), M.N. Mantinan [id39](#),
S. Manzoni [id37](#), L. Mao [id141a](#), X. Mapekula [id34c](#), A. Marantis [id155](#), R.R. Marcelo Gregorio [id1](#),
G. Marchiori [id5](#), C. Marcon [id70a](#), E. Maricic [id16](#), M. Marinescu [id47](#), S. Marium [id47](#),
M. Marjanovic [id121](#), A. Markhoos [id53](#), M. Markovitch [id65](#), M.K. Maroun [id103](#), M.C. Marr [id145](#),
G.T. Marsden [id101](#), Z. Marshall [id18a](#), S. Marti-Garcia [id165](#), J. Martin [id96](#), T.A. Martin [id135](#),
V.J. Martin [id51](#), B. Martin dit Latour [id17](#), L. Martinelli [id74a,74b](#), V.I. Martinez Outschoorn [id103](#),
P. Martinez Suarez [id37](#), S. Martin-Haugh [id135](#), G. Martinovicova [id134](#), V.S. Martoiu [id28b](#),
A. Martone [id89](#), A.C. Martyniuk [id96](#), A. Marzin [id37](#), D. Mascione [id77a,77b](#), L. Masetti [id100](#),
J. Masik [id101](#), A.L. Maslennikov [id38](#), S.L. Mason [id41](#), P. Massarotti [id71a,71b](#), P. Mastrandrea [id73a,73b](#),
A. Mastroberardino [id43b,43a](#), T. Masubuchi [id125](#), T.T. Mathew [id124](#), J. Matousek [id134](#), D.M. Mattern [id48](#),
K. Mauer [id47](#), J. Maurer [id28b](#), T. Maurin [id58](#), A.J. Maury [id65](#), B. Maček [id93](#), C. Mavungu Tsava [id102](#),
A.E. May [id101](#), E. Mayer [id40](#), R. Mazini [id34j](#), S.M. Mazza [id137](#), E. Mazzeo [id37](#), J.P. Mc Gowan [id167](#),
S.P. Mc Kee [id106](#), C.C. McCracken [id166](#), E.F. McDonald [id105](#), L.F. Mcelhinney [id91](#),
J.A. Mcfayden [id149](#), R.P. McGovern [id129](#), R.P. McKenzie [id34j](#), D.J. McLaughlin [id96](#), S.J. McMahon [id135](#),
C.M. Mcpartland [id92](#), R.A. McPherson [id167,ab](#), S. Mehlhase [id109](#), A. Mehta [id92](#), D. Melini [id165](#),
B.R. Mellado Garcia [id14,ah](#), A.H. Melo [id54](#), F. Meloni [id47](#), A.M. Mendes Jacques Da Costa [id101](#),
L. Meng [id91](#), S. Menke [id110](#), M. Mentink [id37](#), E. Meoni [id43b,43a](#), G. Mercado [id117](#), S. Merianos [id155](#),
C. Merlassino [id68a,68c](#), C. Meroni [id70a,70b](#), J. Metcalfe [id6](#), A.S. Mete [id6](#), E. Meuser [id100](#), C. Meyer [id67](#),
J-P. Meyer [id136](#), Y. Miao [id112a](#), R.P. Middleton [id135](#), M. Mihovilovic [id65](#), L. Mijović [id51](#),
G. Mikenberg [id171](#), M. Migestikova [id132](#), M. Mikuž [id93](#), H. Mildner [id100](#), A. Milic [id37](#),
D.W. Miller [id39](#), E.H. Miller [id146](#), A. Milov [id171](#), D.A. Milstead [id46a,46b](#), T. Min [id112a](#), I.A. Minashvili [id152b](#),
A.I. Mincer [id118](#), B. Mindur [id85a](#), M. Mineev [id38](#), Y. Mino [id87](#), L.M. Mir [id13](#), M. Miralles Lopez [id58](#),
M. Mironova [id18a](#), M. Missio [id40](#), A. Mitra [id169](#), V.A. Mitsou [id165](#), Y. Mitsumori [id111](#),
P.S. Miyagawa [id94](#), R. Mizuhiki [id84](#), T. Mkrtchyan [id37](#), M. Mlinarevic [id96](#), T. Mlinarevic [id96](#),
M. Mlynarikova [id134](#), L. Mlynarska [id85a](#), C. Mo [id141a](#), S. Mobius [id20](#), M.H. Mohamed Farook [id114](#),
S. Mohapatra [id41](#), M.F. Mohd Soberi [id51](#), S. Mohiuddin [id122](#), G. Mokgatitswane [id34j](#), R. Mole [id21](#),
L. Moleri [id171](#), U. Molinatti [id127](#), L.G. Mollier [id20](#), B. Mondal [id132](#), S. Mondal [id134](#), K. Mönig [id47](#),
E. Monnier [id102](#), L. Monsonis Romero [id165](#), A. Montella [id46a,46b](#), M. Montella [id120](#),
F. Montekali [id76a,76b](#), F. Monticelli [id90](#), S. Monzani [id68a,68c](#), M.E.E. Moors [id25](#),
A. Morancho Tarda [id42](#), N. Morange [id65](#), M. Moreno Llácer [id165](#), C. Moreno Martinez [id55](#),
J.M. Moreno Perez [id23b](#), P. Morettini [id56b](#), S. Morgenstern [id62a](#), M. Morii [id60](#), M. Morinaga [id156](#),
F. Morodei [id74a,74b](#), P. Moschovakos [id37](#), B. Moser [id53](#), M. Mosidze [id152b](#), T. Moskalets [id44](#),
P. Moskvitina [id115](#), C.J. Mosomane [id34b](#), J. Moss [id32](#), T. Motta Quirino [id81d](#), A. Moussa [id36d](#),
Y. Moyal [id171,k](#), H. Moyano Gomez [id13](#), E.J.W. Moyses [id103](#), T.G. Mroz [id86](#), S. Muanza [id102](#),
M. Mucha [id25](#), J. Mueller [id130](#), D. Muller [id144](#), G.A. Mullier [id163](#), A.J. Mullin [id33](#), J.J. Mullin [id50](#),
A.C. Mullins [id44](#), A.E. Mulski [id60](#), D.P. Mungo [id158](#), D. Munoz Perez [id122](#), F.J. Munoz Sanchez [id101](#),
W.J. Murray [id169,135](#), E. Musajan [id61](#), M. Muškinja [id93](#), C. Mwewa [id47](#), A.J. Myers [id8](#), G. Myers [id106](#),
M. Myska [id133](#), B.P. Nachman [id146](#), K. Nagai [id127](#), K. Nagano [id82](#), R. Nagasaka [id156](#), J.L. Nagle [id30,ao](#),
E. Nagy [id102](#), A.M. Nairz [id37](#), T. Nakagawa [id87](#), Y. Nakahama [id82](#), K. Nakamura [id82](#), K. Nakkalil [id5](#),

A. Nandi ^{62b}, H. Nanjo ¹²⁵, E.A. Narayanan ⁴⁴, Y. Narukawa ¹⁵⁶, L. Nasella ^{70a,70b}, S. Nasri ^{83c},
 C. Nass ²⁵, G. Navarro ^{23a}, A. Nayaz ¹⁹, S. Nechaeva ^{24b,24a}, F. Nechansky ¹³², L. Nedic ¹²⁷,
 A. Negri ^{72a,72b}, M. Negrini ^{24b}, C. Nellist ¹¹⁶, C. Nelson ¹⁰⁴, K. Nelson ¹⁰⁶, S. Nemecek ¹³²,
 M. Nessi ^{37,g}, M.S. Neubauer ¹⁶⁴, J. Newell ⁹², P.R. Newman ²¹, Y.W.Y. Ng ¹⁶⁴, B. Ngair ^{83b},
 H.D.N. Nguyen ¹⁰⁸, J.D. Nichols ¹²¹, R. Nicolaidou ¹³⁶, J. Nielsen ¹³⁷, M. Niemeyer ⁵⁴,
 J. Niermann ³⁷, N. Nikiforou ³⁷, I. Nikolic-Audit ¹²⁸, P. Nilsson ³⁰, G. Ninio ¹⁵⁴, A. Nisati ^{74a},
 D. Nishimura ¹⁵⁶, R. Nisius ¹¹⁰, N. Nitika ¹⁷¹, E.K. Nkadimeng ^{34b}, T. Nobe ¹⁵⁶, D. Noll ¹⁴⁶,
 T. Nommensen ¹⁵⁰, M.B. Norfolk ¹⁴², B.J. Norman ³⁵, L.C. Nosler ^{18a}, M. Noury ^{36a}, J. Novak ⁹³,
 T. Novak ⁹³, P. Novotny ¹⁷¹, R. Novotny ¹³³, L. Nozka ¹²³, K. Ntekas ³⁷, D. Ntonis ¹⁴⁶,
 N.M.J. Nunes De Moura Junior ^{81b}, J. Ocariz ¹²⁸, I. Ochoa ^{131a}, A. Odella Rodriguez ¹³,
 S. Oerdek ⁴⁷, J.T. Offermann ³⁹, A. Ogrodnik ⁸⁶, A. Oh ¹⁰¹, C.C. Ohm ¹⁴⁷, H. Oide ⁸²,
 M.L. Ojeda ³⁷, Y. Okumura ¹⁵⁶, L.F. Oleiro Seabra ^{131a}, I. Oleksiyuk ⁵⁵, G. Oliveira Correa ¹³,
 D. Oliveira Damazio ³⁰, J.L. Oliver ¹, R. Omar ⁶⁷, A.P. O'Neill ²⁰, Y. Onoda ¹³⁹,
 A. Onofre ^{131a,131e,e}, P.U.E. Onyisi ¹¹, M.J. Oreglia ³⁹, D. Orestano ^{76a,76b}, R. Orlandini ^{76a,76b},
 R.S. Orr ¹⁵⁸, L.M. Osojnak ⁴¹, Y. Osumi ¹¹¹, G. Otero y Garzón ³¹, H. Otono ⁸⁸,
 M. Ouchrif ^{36d}, F. Ould-Saada ¹²⁶, T. Ovsiannikova ¹⁴⁰, M. Owen ⁵⁸, R.E. Owen ¹³⁵,
 S.A. Oyeniran ¹¹⁴, V.E. Ozcan ^{22a}, F. Ozturk ⁸⁶, N. Ozturk ⁸, S. Ozturk ⁸⁰, H.A. Pacey ¹²⁷,
 K. Pachal ^{159a}, A. Pacheco Pages ¹³, C. Padilla Aranda ¹³, G. Padovano ^{74a,74b},
 S. Pagan Griso ^{18a}, L. Pagani ^{75a,75b}, J. Pampel ²⁵, D.K. Panchal ¹¹, C.E. Pandini ⁵⁹,
 J.G. Panduro Vazquez ¹³⁵, H.D. Pandya ¹, H. Pang ¹³⁶, P. Pani ⁴⁷, G. Panizzo ^{68a,68c},
 L. Panwar ^{128,w}, L. Paolozzi ²¹, S. Parajuli ¹⁶⁴, A. Paramonov ⁶, C. Paraskevopoulos ⁵²,
 D. Paredes Hernandez ^{63b}, S.R. Paredes Saenz ⁵¹, A. Pareti ^{72a,72b}, K.R. Park ⁴¹, T.H. Park ¹¹⁰,
 F. Parodi ^{56b,56a}, J.A. Parsons ⁴¹, U. Parzefall ⁵³, B.A. Paschen ^{18a}, B. Pascual Dias ⁴⁰,
 L. Pascual Dominguez ⁹⁹, E. Pasqualucci ^{74a}, S. Passaggio ^{56b}, F. Pastore ⁹⁵, P. Patel ⁸⁶,
 U.M. Patel ⁵⁰, J.R. Pater ¹⁰¹, T. Pauly ³⁷, A. Paunovic ¹⁶, F. Pauwels ¹³⁴, C.I. Pazos ¹⁶¹,
 M. Pedersen ¹²⁶, R. Pedro ^{131a}, O. Penc ¹³², C.C. Penelaud ¹²⁸, S. Peng ¹⁵, G.D. Penn ¹⁷⁴,
 B.S. Peralva ^{81d}, A.P. Pereira Peixoto ¹⁴⁰, L. Pereira Sanchez ¹⁴⁶, D.V. Perepelitsa ^{30,ao},
 G. Perera ¹⁰³, E. Perez Codina ³⁷, M. Perganti ¹⁰, H. Pernegger ³⁷, S. Perrella ^{74a,74b},
 K. Peters ⁴⁷, R.F.Y. Peters ¹⁰¹, B.A. Petersen ³⁷, T.C. Petersen ⁴², E. Petit ¹⁰², V. Petousis ¹³³,
 A.R. Petri ^{70a,70b}, T. Petru ¹³⁴, M. Pettee ^{18a}, A. Petukhov ⁸⁰, K. Petukhova ³⁷, R. Pezoa ^{138g},
 L. Pezzotti ^{24b,24a}, G. Pezzullo ¹⁷⁴, L. Pfaffenbichler ³⁷, A.J. Pflieger ⁷⁸, T.M. Pham ¹⁷²,
 T. Pham ¹⁰⁵, P.W. Phillips ¹³⁵, G. Piacquadio ¹⁴⁸, E. Pianori ^{18a}, F. Piazza ¹²⁴, R. Piegai ³¹,
 D. Pietreanu ^{28b}, A.D. Pilkington ¹⁰¹, M. Pinamonti ^{68a,68c}, J.L. Pinfeld ², G. Pinheiro Matos ⁴¹,
 B.C. Pinheiro Pereira ^{131a}, J. Pinol Bel ¹³, A.E. Pinto Pinoargote ¹²⁸, L. Pintucci ^{68a,68c},
 K.M. Piper ¹⁴⁹, A. Pirttikoski ⁵⁵, D.A. Pizzi ³⁵, L. Pizzimento ^{63b}, A. Plebani ³³,
 M.-A. Pleier ³⁰, V. Pleskot ¹³⁴, E. Plotnikova ³⁸, G. Poddar ⁹⁴, R. Poettgen ⁹⁸, L. Poggioli ¹²⁸,
 S. Polacek ¹³⁴, G. Polesello ^{72a}, A. Poley ¹⁴⁵, A. Polini ^{24b}, C.S. Pollard ¹⁶⁹, Z.B. Pollock ¹²⁰,
 E. Pompa Pacchi ¹²¹, N.I. Pond ⁹⁶, D. Ponomarenko ⁶⁷, L. Pontecorvo ³⁷, S. Popa ^{28a},
 G.A. Popeneciu ^{28d}, A. Poreba ^{62a}, D.M. Portillo Quintero ^{159a}, S. Pospisil ¹³³, M.A. Postill ¹⁴²,
 P. Postolache ^{28c}, K. Potamianos ¹⁶⁹, P.A. Potepa ^{85a}, I.N. Potrap ³⁸, C.J. Potter ³³, H. Potti ¹⁵⁰,
 J. Poveda ¹⁶⁵, M.E. Pozo Astigarraga ³⁷, R. Pozzi ³⁷, A. Prades Ibanez ^{75a,75b}, S.R. Pradhan ¹⁴²,
 J. Pretel ¹⁶⁷, D. Price ¹⁰¹, M. Primavera ^{69a}, L. Primomo ^{68a,68c}, M.A. Principe Martin ⁹⁹,
 R. Privara ¹²³, T. Procter ^{85b}, M.L. Proffitt ¹⁴⁰, N. Proklova ¹²⁹, K. Prokofiev ^{63c}, G. Proto ¹¹⁰,
 J. Proudfoot ⁶, M. Przybycien ^{85a}, W.W. Przygoda ^{85b}, A. Psallidas ⁴⁵, D. Pudzha ⁵², P. Puhl ⁵⁷,
 H.I. Purnell ¹, D. Pyatizbyantseva ¹¹⁵, J. Qian ¹⁰⁶, R. Qian ¹⁰⁷, D. Qichen ¹²⁷, Y. Qin ¹³,
 T. Qiu ⁵¹, A. Quadt ⁵⁴, M. Queitsch-Maitland ¹⁰¹, G. Quetant ⁵⁵, R.P. Quinn ¹⁶⁶,
 D. Rafanoharana ¹¹⁰, J.L. Rainbolt ³⁹, S. Rajagopalan ³⁰, E. Ramakoti ³⁸, L. Rambelli ^{56b,56a},

I.A. Ramirez-Berend ³⁵, K. Ran ^{106,112c}, S.D. Randles ⁹², D.S. Rankin ¹²⁹, N.P. Rapheeha ^{34j},
 H. Rasheed ^{28b}, A. Rastogi ^{18a}, S. Rave ¹⁰⁰, S. Ravera ^{56b,56a}, B. Ravina ³⁷, I. Ravinovich ¹⁷¹,
 M. Raymond ³⁷, A.L. Read ¹²⁶, N.P. Readioff ¹⁴², D.M. Rebuzzi ^{72a,72b}, A.S. Reed ⁵⁸,
 K. Reeves ²⁷, D. Reikher ³⁷, A. Rej ⁴⁸, C. Rembser ³⁷, H. Ren ⁶¹, M. Renda ^{28b}, F. Renner ⁴⁷,
 A.G. Rennie ⁵⁸, M. Repik ⁵⁵, A.L. Rescia ^{56b,56a}, S. Resconi ^{70a}, M. Ressegotti ^{56b},
 S. Rettie ¹¹⁶, W.F. Rettie ³⁵, M.M. Revering ³³, O.L. Rezanova ³⁸, P. Reznicek ¹³⁴, H. Riani ^{36d},
 N. Ribaric ⁵⁰, B. Ricci ^{68a,68c}, E. Ricci ^{77a,77b}, R. Richter ¹¹⁰, E. Richter-Was ^{85b}, M. Ridel ¹²⁸,
 S. Ridouani ^{36d}, P. Riedler ³⁷, E.M. Riefel ^{46a,46b}, J.O. Rieger ¹¹⁶, M. Rimoldi ^{34c},
 L. Rinaldi ^{24b,24a}, P. Rincke ^{163,54}, G. Ripellino ¹⁶³, I. Riu ¹³, J.C. Rivera Vergara ¹⁶⁷,
 F. Rizatdinova ¹²², E. Rizvi ⁹⁴, B.R. Roberts ³⁹, S.S. Roberts ¹³⁷, D. Robinson ³³, A. Robson ⁵⁸,
 A. Rocchi ^{75a,75b}, C. Roda ^{73a,73b}, F.A. Rodriguez ¹¹⁷, S. Rodriguez Bosca ³⁷,
 Y. Rodriguez Garcia ^{23a}, A.M. Rodríguez Vera ¹¹⁷, S. Roe ³⁷, J.T. Roemer ³⁷, O. Røhne ¹²⁶,
 R.A. Rojas ³⁷, Z. Rokavec ⁹³, C.P.A. Roland ¹²⁸, A. Romaniouk ⁷⁸, E. Romano ^{72a,72b},
 M. Romano ^{24b}, N. Rompotis ⁹², L. Roos ¹²⁸, S. Rosati ^{74a}, L. Roscher ⁴⁷, B.J. Rosser ³⁹,
 E. Rossi ¹²⁷, E. Rossi ^{71a,71b}, L.P. Rossi ⁶⁰, L. Rossini ⁵³, R. Rosten ¹²⁰, M. Rotaru ^{28b},
 R. Roth ³⁷, D. Rousseau ⁶⁵, D. Rousso ⁴⁷, S. Roy-Garand ¹⁵⁸, A. Rozanov ¹⁰²,
 Z.M.A. Rozario ⁵⁸, Y. Rozen ¹⁵³, A. Rubio Jimenez ¹⁶⁵, V.H. Ruelas Rivera ¹⁹, T.A. Ruggeri ¹,
 A. Ruggiero ¹²⁷, A. Ruiz-Martinez ¹⁶⁵, A. Rummler ³⁷, G.B. Rupnik Boero ³⁷,
 N.A. Rusakovich ³⁸, S. Ruscelli ⁴⁸, H.L. Russell ¹⁶⁷, G. Russo ¹³⁷, J.P. Rutherford ⁷,
 S. Rutherford Colmenares ¹¹⁸, M. Rybar ¹³⁴, P. Rybczynski ^{85a}, A. Ryzhov ⁴⁴,
 F. Safai Tehrani ^{74a}, S. Saha ¹, B. Sahoo ¹⁷¹, A. Saibel ¹⁶⁵, B.T. Saifuddin ¹²¹, M. Saimpert ¹³⁶,
 I. Sainz Saenz Diez ^{62a}, G.T. Saito ^{81c}, M. Saito ¹⁵⁶, T. Saito ¹⁵⁶, A. Sala ^{70a,70b}, O.T. Salin ⁶⁵,
 A. Salnikov ¹⁴⁶, J. Salt ¹⁶⁵, A. Salvador Salas ¹⁵⁴, F. Salvatore ¹⁴⁹, A. Salzburger ³⁷,
 D. Sammel ⁵³, E. Sampson ⁹¹, D. Sampsonidis ^{155,d}, D. Sampsonidou ¹²⁴, M.A.A. Samy ⁵⁸,
 J. Sánchez ¹⁶⁵, V. Sanchez Sebastian ¹⁶⁵, H. Sandaker ¹²⁶, C.O. Sander ⁴⁷, J.A. Sandesara ¹⁷²,
 M. Sandhoff ¹⁷³, C. Sandoval ^{23b}, L. Sanfilippo ^{62a}, D.P.C. Sankey ¹³⁵, T. Sano ⁸⁷,
 A. Sansar ^{22c}, A. Sansoni ⁵², M. Santana Queiroz ^{18b}, L. Santi ³⁷, C. Santoni ⁴⁰,
 H. Santos ^{131a,131b}, L. Santos Pereira Trigo ⁴⁷, E. Sanzani ^{24b,24a}, K.A. Saoucha ^{83d},
 J.G. Saraiva ^{131a,131d}, J. Sardain ⁷, S. Sarkar ⁵⁰, O. Sasaki ⁸², K. Sato ¹⁶⁰, C. Sauer ³⁷,
 E. Sauvan ⁴, P. Savard ^{158,aj}, R. Sawada ¹⁵⁶, C. Sawyer ¹³⁵, L. Sawyer ⁹⁷, A.M. Sayed ²⁷,
 C. Sbarra ^{24b}, A. Sbrizzi ^{24b,24a}, R. Scaglioni ^{72a,72b}, T. Scanlon ⁹⁶, J. Schaarschmidt ¹⁴⁰,
 U. Schäfer ¹⁰⁰, A.C. Schaffer ^{65,44}, D. Schaile ¹⁰⁹, R.D. Schamberger ¹⁴⁸, C. Scharf ¹⁹,
 M.M. Schefer ²⁰, D. Scheirich ¹³⁴, M. Schernau ^{138f}, C. Scheulen ⁵⁵, C. Schiavi ^{56b,56a},
 M. Schioppa ^{43b,43a}, S. Schlenker ³⁷, T. Schlomer ⁵⁴, J. Schmeing ¹⁷³, C.R. Schmidt ⁴⁹,
 E. Schmidt ¹¹⁰, M.A. Schmidt ¹⁷³, K. Schmieden ²⁵, C. Schmitt ¹⁰⁰, N. Schmitt ¹⁰⁰,
 S. Schmitt ⁴⁷, N.A. Schneider ¹⁰⁹, L. Schoeffel ¹³⁶, A. Schoening ^{62b}, P.G. Scholer ³⁵,
 E. Schopf ¹⁴⁴, M. Schott ²⁵, S. Schramm ⁵⁵, T. Schroer ⁵⁵, H-C. Schultz-Coulon ^{62a},
 M. Schumacher ⁵³, B.A. Schumm ¹³⁷, Ph. Schune ¹³⁶, H.R. Schwartz ⁷, A. Schwartzman ¹⁴⁶,
 T.A. Schwarz ¹⁰⁶, Ph. Schwemling ¹³⁶, R. Schwienhorst ¹⁰⁷, F.G. Sciacca ²⁰, A. Sciandra ³⁰,
 G. Sciolla ²⁷, S.A. Scoville ¹³⁰, F. Scuri ^{73a}, C.D. Sebastiani ³⁷, K. Sedlaczek ¹¹⁷,
 A. Sehrawat ^{138b}, S.C. Seidel ¹¹⁴, B.D. Seidlitz ⁴¹, C. Seitz ⁴⁷, J.M. Seixas ^{81b},
 G. Sekhniaidze ^{71a}, L. Selem ¹²⁸, N. Semprini-Cesari ^{24b,24a}, A. Semushin ¹⁷⁵,
 V. Senthilkumar ¹¹⁶, L. Serin ⁶⁵, M. Sessa ^{71a,71b}, H. Severini ¹²¹, F. Sforza ^{56b,56a}, A. Sfyrla ⁵⁵,
 Q. Sha ¹⁴, H. Shaddix ¹¹⁷, A.H. Shah ³³, R. Shaheen ¹⁴⁷, J.D. Shahinian ¹²⁹, M. Shamim ³⁷,
 L.Y. Shan ¹⁴, M. Shapiro ^{18a}, A. Sharma ³⁷, A.S. Sharma ¹⁶⁶, P. Sharma ³⁰, K. Shaw ¹⁴⁹,
 S.M. Shaw ¹⁰¹, D. Shemyakin ¹⁷¹, Q. Shen ¹⁴, D.J. Sheppard ¹⁴⁵, P. Sherwood ⁹⁶, L. Shi ^{112b},
 X. Shi ¹⁴, S. Shimizu ⁸², S. Shirabe ⁸⁸, M. Shiyakova ^{38,z}, M.J. Shochet ³⁹, D.R. Shope ¹²⁶,

B. Shrestha [ID121](#), S. Shrestha [ID120,aq](#), I. Shreyber [ID38](#), M.J. Shroff [ID104](#), P. Sicho [ID132](#), A.M. Sickles [ID164](#),
 E. Sideras Haddad [ID34j](#), A.C. Sidley [ID116](#), A. Sidoti [ID24b](#), F. Siegert [ID49](#), Dj. Sijacki [ID16](#), F. Sili [ID61](#),
 J.M. Silva [ID51](#), I. Silva Ferreira [ID81b](#), M.V. Silva Oliveira [ID30](#), S.B. Silverstein [ID46a](#), S. Simion [ID65](#),
 R. Simoniello [ID37](#), E.L. Simpson [ID101](#), H. Simpson [ID149](#), L.R. Simpson [ID6](#), S. Simsek [ID80](#),
 S. Sindhu [ID54](#), S.N. Singh [ID27](#), S. Singh [ID30](#), S. Sinha [ID47](#), S. Sinha [ID101](#), M. Sioli [ID24b,24a](#),
 K. Sioulas [ID9](#), I. Siral [ID37](#), E. Sitnikova [ID47](#), J. Sjölin [ID46a,46b](#), A. Skaf [ID54](#), E. Skorda [ID21](#),
 P. Skubic [ID121](#), M. Slawinska [ID86](#), I. Slazyk [ID17](#), I. Sliusar [ID126](#), V. Smakhtin [ID171](#), B.H. Smart [ID135](#),
 S.Yu. Smirnov [ID138b](#), Y. Smirnov [ID34c](#), O. Smirnova [ID98](#), A.C. Smith [ID41](#), J.L. Smith [ID101](#),
 M.B. Smith [ID35](#), R. Smith [ID146](#), H. Smitmanns [ID100](#), M. Smizanska [ID91](#), K. Smolek [ID133](#),
 P. Smolyanskiy [ID133](#), A.A. Snesarev [ID38](#), H.L. Snoek [ID116](#), R.M. Snyder [ID50](#), S. Snyder [ID30](#),
 R. Sobie [ID167,ab](#), A. Soffer [ID154](#), C.A. Solans Sanchez [ID37](#), E.Yu. Soldatov [ID38](#), U. Soldevila [ID165](#),
 A.A. Solodkov [ID34j](#), S. Solomon [ID27](#), A. Soloshenko [ID38](#), O.V. Solovyanov [ID40](#), P. Sommer [ID49](#),
 A. Sopczak [ID133](#), A.L. Soppio [ID51](#), F. Sopkova [ID29b](#), J.D. Sorenson [ID114](#), I.R. Sotarriva Alvarez [ID139](#),
 V. Sothilingam [ID62a](#), O.J. Soto Sandoval [ID138c,138b](#), S. Sottocornola [ID67](#), R. Soualah [ID83a](#), D. South [ID47](#),
 N. Soybelman [ID171](#), S. Spagnolo [ID69a,69b](#), A.S. Spellman [ID124](#), D. Sperlich [ID53](#), B. Spisso [ID71a,71b](#),
 L. Splendori [ID102](#), M. Spousta [ID134](#), E.J. Staats [ID35](#), R. Stamen [ID62a](#), E. Stanecka [ID86](#),
 W. Stanek-Maslouska [ID47](#), M.V. Stange [ID49](#), B. Stanislaus [ID18a](#), M.M. Stanitzki [ID47](#), G.H. Stark [ID137](#),
 J. Stark [ID89](#), P. Staroba [ID132](#), P. Starovoitov [ID83d](#), R. Staszewski [ID86](#), C. Stauch [ID109](#),
 G. Stavropoulos [ID45](#), A. Stefl [ID37](#), A. Stein [ID100](#), P. Steinberg [ID30](#), B. Stelzer [ID145,159a](#), H.J. Stelzer [ID130](#),
 O. Stelzer [ID159a](#), H. Stenzel [ID57](#), T.J. Stevenson [ID149](#), G.A. Stewart [ID47](#), G. Stoicea [ID28b](#),
 M. Stolarski [ID131a](#), S. Stonjek [ID110](#), A. Straessner [ID49](#), J. Strandberg [ID147](#), S. Strandberg [ID46a,46b](#),
 M. Stratmann [ID173](#), M. Strauss [ID121](#), T. Strebler [ID102](#), P. Strizenec [ID29b](#), R. Ströhmer [ID168](#),
 D.M. Strom [ID124](#), R. Stroynowski [ID44](#), A. Strubig [ID46a,46b](#), S.A. Stucci [ID30](#), B. Stugu [ID17](#), J. Stupak [ID121](#),
 N.A. Styles [ID47](#), D. Su [ID146](#), S. Su [ID61](#), X. Su [ID61](#), D. Suchy [ID29a](#), A.D. Sudhakar Ponnuru [ID54](#),
 L. Sudit [ID171](#), Y. Sue [ID82](#), K. Sugizaki [ID129](#), D.M.S. Sultan [ID127](#), L. Sultanaliyeva [ID25](#), S. Sultansoy [ID3b](#),
 S. Sun [ID172](#), W. Sun [ID14](#), S. Sundar Raman [ID166](#), N. Sur [ID98](#), J.P. Surdutovich [ID120](#), N. Suri Jr [ID174](#),
 M.R. Sutton [ID149](#), M. Svatos [ID132](#), P.N. Swallow [ID33](#), S.N. Swatman [ID37](#), M. Swiatlowski [ID159a](#),
 A. Swoboda [ID37](#), I. Sykora [ID29a](#), M. Sykora [ID134](#), T. Sykora [ID134](#), D. Ta [ID100](#), K. Tackmann [ID47,y](#),
 A. Taffard [ID162](#), R. Tafirout [ID159a](#), Y. Takubo [ID82](#), M. Talby [ID102](#), N.M. Tamir [ID154](#), A. Tanaka [ID156](#),
 J. Tanaka [ID156](#), R. Tanaka [ID65](#), M. Tanasini [ID148](#), Z. Tao [ID166](#), S. Tapia Araya [ID138g](#), S. Tapprogge [ID100](#),
 A. Tarek Abouelfadl Mohamed [ID37](#), S. Tarem [ID153](#), K. Tariq [ID14](#), G. Tarna [ID37](#), G.F. Tartarelli [ID70a](#),
 M.J. Tartarin [ID141b](#), P. Tas [ID134](#), M. Tasevsky [ID132](#), E. Tassi [ID43b,43a](#), A.C. Tate [ID164](#), Y. Tayalati [ID36e,aa](#),
 G.N. Taylor [ID105](#), W. Taylor [ID159b](#), R.J. Taylor Vara [ID165](#), A.S. Tegetmeier [ID89](#), P. Teixeira-Dias [ID95](#),
 J.J. Teoh [ID158](#), K. Terashi [ID156](#), J. Terron [ID99](#), S. Terzo [ID13](#), M. Testa [ID52](#), R.J. Teuscher [ID158,ab](#),
 A. Thaler [ID78](#), T. Theveneaux-Pelzer [ID102](#), J.P. Thomas [ID21](#), E.A. Thompson [ID18a](#), P.D. Thompson [ID21](#),
 E. Thomson [ID129](#), R.E. Thornberry [ID30](#), T.M. Thory-Rao [ID21](#), C. Tian [ID61](#), Y. Tian [ID55](#),
 V. Tikhomirov [ID80](#), Yu.A. Tikhonov [ID38](#), D. Timoshyn [ID134](#), E.X.L. Ting [ID1](#), P. Tipton [ID174](#),
 A. Tishelman-Charny [ID30](#), K. Todome [ID139](#), S. Todorova-Nova [ID134](#), L. Toffolin [ID68a,68c](#), M. Togawa [ID82](#),
 J. Tojo [ID88](#), S. Tokár [ID29a](#), O. Toldaiev [ID67](#), G. Tolkachev [ID102](#), M. Tomoto [ID82](#), L. Tompkins [ID146](#),
 E. Torrence [ID124](#), H. Torres [ID89](#), D.I. Torres Arza [ID138g](#), E. Torres Reoyo [ID165](#), E. Torró Pastor [ID165](#),
 M. Toscani [ID31](#), C. Toscirci [ID39](#), M. Tost [ID11](#), D.R. Tovey [ID142](#), T. Trefzger [ID168](#), P.M. Tricarico [ID13](#),
 A. Tricoli [ID30](#), I.M. Trigger [ID159a](#), S. Trincaz-Duvoid [ID128](#), D.A. Trischuk [ID167](#), A. Tropina [ID38](#),
 D. Truncali [ID75a,75b](#), L. Truong [ID34c](#), M. Trzebinski [ID86](#), A. Trzupek [ID86](#), F. Tsai [ID148](#), A. Tsiamis [ID155](#),
 P.V. Tsiarehka [ID38](#), S. Tsigaridas [ID159a](#), A. Tsirigotis [ID155,t](#), V. Tsiskaridze [ID152a](#), E.G. Tskhadadze [ID152a](#),
 H.F. Tsoi [ID129](#), Y. Tsujikawa [ID87](#), V. Tsulaia [ID18a](#), K. Tsurii [ID119](#), D. Tsybychev [ID148](#), Y. Tu [ID63b](#),
 A. Tudorache [ID28b](#), V. Tudorache [ID28b](#), S.B. Tuncay [ID127](#), S. Turchikhin [ID56b,56a](#), I. Turk Cakir [ID3a](#),
 R. Turra [ID70a](#), T. Turtuvshin [ID38,ac](#), P.M. Tuts [ID41](#), Y. Uematsu [ID82](#), F. Ukegawa [ID160](#),

P.A. Ulloa Poblete [ID138c,138b](#), G. Unal [ID37](#), A. Undrus [ID30](#), J. Urban [ID29b](#), P. Urrejola [ID138e](#), G. Usai [ID8](#),
 R. Ushioda [ID157](#), M. Usman [ID108](#), F. Ustuner [ID51](#), Z. Uysal [ID80](#), V. Vacek [ID133](#), B. Vachon [ID104](#),
 T. Vafeiadis [ID37](#), A. Vaitkus [ID96](#), C. Valderanis [ID109](#), E. Valdes Santurio [ID46a,46b](#), M. Valente [ID37](#),
 S. Valentinetti [ID24b,24a](#), A. Valero [ID165](#), E. Valiente Moreno [ID165](#), A. Vallier [ID89](#), J.A. Valls Ferrer [ID165](#),
 D.R. Van Arneman [ID116](#), R. Van Den Broucke [ID128](#), A. Van Der Graaf [ID48](#), H.Z. Van Der Schyf [ID34j](#),
 P. Van Gemmeren [ID6](#), M. Van Rijnbach [ID37](#), S. Van Stroud [ID96](#), I. Van Vulpen [ID116](#), P. Vana [ID134](#),
 M. Vanadia [ID75a,75b](#), U.M. Vande Voorde [ID147](#), W. Vandelli [ID37](#), E.R. Vandewall [ID146](#), D. Vannicola [ID154](#),
 R. Vari [ID74a](#), M. Varma [ID174](#), E.W. Varnes [ID7](#), C. Varni [ID85a](#), D. Varouchas [ID65](#), L. Varriale [ID165](#),
 K.E. Varvell [ID150](#), M.E. Vasile [ID28b](#), A. Vasileiadou⁹, L. Vaslin⁸², M.D. Vassilev [ID146](#), A. Vasyukov [ID38](#),
 L.M. Vaughan [ID122](#), R. Vavricka¹³⁴, T. Vazquez Schroeder [ID13](#), J. Veatch [ID32](#), V. Vecchio [ID101](#),
 M.J. Veen [ID103](#), I. Veliscek [ID30](#), I. Velkovska [ID93](#), L.M. Veloce [ID158](#), F. Veloso [ID131a,131c](#),
 A.G. Veltman [ID51](#), S.H. Venetianer [ID161](#), S. Veneziano [ID74a](#), A. Ventura [ID69a,69b](#), A. Verbitskiy [ID110](#),
 M. Verducci [ID73a,73b](#), C. Vergis [ID94](#), M. Verissimo De Araujo [ID81b](#), W. Verkerke [ID116](#),
 J.C. Vermeulen [ID116](#), C. Vernieri [ID146](#), M. Vessella [ID162](#), M.C. Vetterli [ID145,aj](#), A. Vgenopoulos [ID100](#),
 N. Viaux Maira [ID138g,af](#), L. Vicenik [ID133](#), T. Vickey [ID142](#), O.E. Vickey Boeriu [ID142](#),
 G.H.A. Viehhauser [ID127](#), L. Vigani [ID62b](#), M. Vigl [ID110](#), M. Villa [ID24b,24a](#), M. Villaplana Perez [ID165](#),
 E.M. Villhauer³⁹, E. Vilucchi [ID52](#), M. Vincent [ID165](#), M.G. Vincter [ID35](#), A. Visibile [ID116](#), A. Visive [ID116](#),
 C. Vittori [ID161](#), I. Vivarelli [ID24b,24a](#), M.I. Vivas Albornoz [ID47](#), E. Voevodina [ID110](#), F. Vogel [ID109](#),
 J.C. Voigt [ID49](#), P. Vokac [ID133](#), Yu. Volkotrub [ID85b](#), L. Vomberg [ID25](#), E. Von Toerne [ID25](#),
 B. Vormwald [ID37](#), K. Vorobev [ID50](#), M. Vos [ID165](#), K. Voss [ID144](#), M. Vozak [ID37](#), L. Vozdecky [ID121](#),
 N. Vranjes [ID16](#), M. Vranjes Milosavljevic [ID16](#), M. Vreeswijk [ID116](#), N.K. Vu [ID112a](#), R. Vuillermet [ID37](#),
 O. Vujinovic [ID100](#), I. Vukotic [ID39](#), I.K. Vyas [ID35](#), J.F. Wack [ID33](#), A. Wada [ID111](#), S. Wada [ID160](#),
 C. Wagner¹⁴⁶, J.M. Wagner [ID18a](#), W. Wagner [ID173](#), S. Wahdan [ID173](#), H. Wahlberg [ID90](#), C.H. Waits [ID121](#),
 J. Walder [ID135](#), R. Walker [ID109](#), K. Walkingshaw Pass [ID58](#), W. Walkowiak [ID144](#), A. Wall [ID129](#),
 E.J. Wallin [ID98](#), T. Wamorkar [ID146](#), K. Wandall-Christensen [ID165](#), A. Wang [ID61](#), A.Z. Wang [ID137](#),
 C. Wang [ID47](#), C. Wang [ID11](#), H. Wang [ID18a](#), J. Wang [ID63c](#), P. Wang [ID101](#), P. Wang [ID96](#), R. Wang [ID60](#),
 R. Wang [ID106](#), R. Wang [ID6](#), S.M. Wang [ID151](#), S. Wang [ID14](#), T. Wang [ID115](#), T. Wang [ID61](#),
 W.T. Wang [ID127](#), X. Wang [ID164](#), X. Wang [ID141a](#), X. Wang [ID47](#), Y. Wang [ID148](#), Y. Wang [ID114](#),
 Z. Wang [ID106](#), Z. Wang [ID14](#), Z. Wang [ID63b](#), C. Wanotayaroj [ID82](#), A. Warburton [ID104](#),
 A.L. Warnerbring [ID144](#), S. Waterhouse [ID96](#), A.T. Watson [ID21](#), H. Watson [ID51](#), M.F. Watson [ID21](#),
 E. Watton [ID37](#), G. Watts [ID140](#), B.M. Waugh [ID96](#), J.M. Webb [ID53](#), C. Weber [ID30](#), M.S. Weber [ID20](#),
 C. Wei [ID61](#), Y. Wei [ID53](#), A.R. Weidberg [ID127](#), E.J. Weik [ID118](#), J. Weingarten [ID48](#), C. Weiser [ID53](#),
 C.J. Wells [ID47](#), P.S. Wells [ID37](#), T. Wenaus [ID30](#), T. Wengler [ID37](#), N.S. Wenke¹¹⁰, N. Wermes [ID25](#),
 M. Wessels [ID62a](#), A.M. Wharton [ID91](#), A.S. White [ID37](#), A. White [ID8](#), M.J. White [ID1](#), D. Whiteson [ID162](#),
 L. Wickremasinghe [ID125](#), W. Wiedenmann [ID172](#), M. Wielers [ID135](#), R. Wierda [ID147](#), C. Wiglesworth [ID42](#),
 H.G. Wilkens [ID37](#), J.J.H. Wilkinson [ID33](#), S. Williams [ID33](#), S. Willocq [ID103](#), D.J. Wilson [ID101](#),
 P.J. Windischhofer [ID39](#), F.I. Winkel [ID31](#), F. Winklmeier [ID124](#), B.T. Winter [ID53](#), M. Wittgen¹⁴⁶,
 M. Wobisch [ID97](#), T. Wojtkowski⁵⁹, Z. Wolffs [ID116](#), J. Wollrath³⁷, M.W. Wolter [ID86](#), H. Wolters [ID131a,131c](#),
 M.C. Wong¹³⁷, E.L. Woodward [ID41](#), S.D. Worm [ID47](#), B.K. Wosiek [ID86](#), K.A. Wozniak [ID55](#),
 K.W. Wozniak [ID86](#), S. Wozniewski [ID54](#), K. Wraight [ID58](#), C. Wu [ID158](#), C. Wu [ID21](#), J. Wu [ID156](#),
 M. Wu [ID112b](#), M. Wu [ID115](#), S.L. Wu [ID172](#), S. Wu [ID14,an](#), X. Wu [ID61](#), Y.Q. Wu [ID158](#), Y. Wu [ID61](#),
 Z. Wu [ID102](#), Z. Wu [ID112a](#), J. Wuerzinger [ID110](#), T.R. Wyatt [ID101](#), B.M. Wynne [ID51](#), S. Xella [ID42](#),
 L. Xia [ID112a](#), M. Xie [ID61](#), A. Xiong [ID124](#), I. Xiotidis [ID37](#), D. Xu [ID14](#), H. Xu [ID61](#), L. Xu [ID61](#), R. Xu [ID129](#),
 T. Xu [ID106](#), W. Xu^{112a}, Y. Xu [ID140](#), Z. Xu [ID51](#), R. Xue [ID130](#), B. Yabsley [ID150](#), S. Yacoob [ID11](#),
 Y. Yamaguchi [ID82](#), E. Yamashita [ID156](#), H. Yamauchi [ID160](#), T. Yamazaki [ID18a](#), Y. Yamazaki [ID84](#),
 S. Yan [ID58](#), Z. Yan [ID103](#), C. Yang [ID18a](#), H.J. Yang [ID141a](#), H.T. Yang [ID61](#), S. Yang [ID61](#), X. Yang [ID37](#),
 X. Yang [ID14](#), Y. Yang [ID156](#), Y. Yang⁶¹, W-M. Yao [ID18a](#), C.L. Yardley [ID149](#), J. Ye [ID14](#), S. Ye [ID30](#),

X. Ye ⁶¹, I. Yeletsikh ³⁸, B. Yeo ^{18b}, M.R. Yexley ⁹⁶, T.P. Yildirim ¹²⁷, K. Yorita ¹⁷⁰, C.J.S. Young ³⁷, C. Young ¹⁴⁶, I.N.L. Young ⁵⁸, N.D. Young ¹²⁴, Y. Yu ⁶¹, J. Yuan ^{14,112c,an}, M. Yuan ¹⁰⁶, R. Yuan ^{141b}, L. Yue ⁹⁶, M. Zaazoua ⁶¹, B. Zabinski ⁸⁶, I. Zahir ^{36a}, Q.U.A. Zahoor ⁵¹, A. Zaio ^{56b,56a}, Z.K. Zak ⁸⁶, T. Zakareishvili ¹⁶⁵, S. Zambito ⁵⁵, J. Zang ¹⁵⁶, R. Zanzottera ^{70a,70b}, O. Zaplatilek ¹³³, E. Zaya ¹⁴⁷, C. Zeitnitz ¹⁷³, H. Zeng ¹⁴, D.T. Zenger Jr ²⁷, T. Ženiš ^{29a}, S. Zenz ⁹⁴, D. Zerwas ⁶⁵, B. Zhang ¹⁶⁹, D.F. Zhang ¹⁴², G. Zhang ^{14,an}, J. Zhang ^{113b}, J. Zhang ⁶, L. Zhang ⁶¹, L. Zhang ^{112a}, P. Zhang ^{14,112c}, R. Zhang ^{112a}, S. Zhang ^{36e}, Y. Zhang ¹⁴⁰, Y. Zhang ⁹⁶, Y. Zhang ⁶¹, Y. Zhang ^{112a}, Z. Zhang ^{18a}, Z. Zhang ^{113b}, Z. Zhang ⁶⁵, H. Zhao ¹⁴⁰, T. Zhao ^{113b}, Y. Zhao ³⁵, Z. Zhao ⁶¹, Z. Zhao ⁶¹, A. Zhemchugov ³⁸, J. Zheng ^{112a}, K. Zheng ¹⁶⁴, L. Zheng ^{113b}, X. Zheng ⁶¹, Z. Zheng ¹⁴⁶, D. Zhong ¹⁶⁴, B. Zhou ¹⁰⁶, B. Zhou ^{141b,141a}, N. Zhou ^{141a}, Y. Zhou ¹⁵, Y. Zhou ^{112a}, Y. Zhou ⁷, Z. Zhou ⁶¹, J. Zhu ¹⁰⁶, X. Zhu ^{141b}, Y. Zhu ^{141a}, X. Zhuang ¹⁴, K. Zhukov ⁶⁷, P. Ziakas ⁴, N.I. Zimine ³⁸, J. Zinsser ^{62b}, M. Ziolkowski ¹⁴⁴, L. Živković ¹⁶, A. Zoccoli ^{24b,24a}, K. Zoch ³⁷, A. Zografos ³⁷, T.G. Zorbas ¹⁴², L. Zwalinski ³⁷.

¹Department of Physics, University of Adelaide, Adelaide; Australia.

²Department of Physics, University of Alberta, Edmonton AB; Canada.

³(^a)Department of Physics, Ankara University, Ankara; (^b)Division of Physics, TOBB University of Economics and Technology, Ankara; Türkiye.

⁴LAPP, Université Savoie Mont Blanc, CNRS/IN2P3, Annecy; France.

⁵APC, Université Paris Cité, CNRS/IN2P3, Paris; France.

⁶High Energy Physics Division, Argonne National Laboratory, Argonne IL; United States of America.

⁷Department of Physics, University of Arizona, Tucson AZ; United States of America.

⁸Department of Physics, University of Texas at Arlington, Arlington TX; United States of America.

⁹Physics Department, National and Kapodistrian University of Athens, Athens; Greece.

¹⁰Physics Department, National Technical University of Athens, Zografou; Greece.

¹¹Department of Physics, University of Texas at Austin, Austin TX; United States of America.

¹²Institute of Physics, Azerbaijan Academy of Sciences, Baku; Azerbaijan.

¹³Institut de Física d'Altes Energies (IFAE), Barcelona Institute of Science and Technology, Barcelona; Spain.

¹⁴Institute of High Energy Physics, Chinese Academy of Sciences, Beijing; China.

¹⁵Physics Department, Tsinghua University, Beijing; China.

¹⁶Institute of Physics, University of Belgrade, Belgrade; Serbia.

¹⁷Department for Physics and Technology, University of Bergen, Bergen; Norway.

¹⁸(^a)Physics Division, Lawrence Berkeley National Laboratory, Berkeley CA; (^b)University of California, Berkeley CA; United States of America.

¹⁹Institut für Physik, Humboldt Universität zu Berlin, Berlin; Germany.

²⁰Albert Einstein Center for Fundamental Physics and Laboratory for High Energy Physics, University of Bern, Bern; Switzerland.

²¹School of Physics and Astronomy, University of Birmingham, Birmingham; United Kingdom.

²²(^a)Department of Physics, Bogazici University, Istanbul; (^b)Department of Physics Engineering, Gaziantep University, Gaziantep; (^c)Department of Physics, Istanbul University, Istanbul; Türkiye.

²³(^a)Facultad de Ciencias y Centro de Investigaciones, Universidad Antonio Nariño,

Bogotá; (^b)Departamento de Física, Universidad Nacional de Colombia, Bogotá; Colombia.

²⁴(^a)Dipartimento di Fisica e Astronomia A. Righi, Università di Bologna, Bologna; (^b)INFN Sezione di Bologna; Italy.

²⁵Physikalisches Institut, Universität Bonn, Bonn; Germany.

- ²⁶Department of Physics, Boston University, Boston MA; United States of America.
- ²⁷Department of Physics, Brandeis University, Waltham MA; United States of America.
- ²⁸(^a) Transilvania University of Brasov, Brasov; (^b) Horia Hulubei National Institute of Physics and Nuclear Engineering, Bucharest; (^c) Department of Physics, Alexandru Ioan Cuza University of Iasi, Iasi; (^d) National Institute for Research and Development of Isotopic and Molecular Technologies, Physics Department, Cluj-Napoca; (^e) National University of Science and Technology Politehnica, Bucharest; (^f) West University in Timisoara, Timisoara; (^g) Faculty of Physics, University of Bucharest, Bucharest; Romania.
- ²⁹(^a) Faculty of Mathematics, Physics and Informatics, Comenius University, Bratislava; (^b) Department of Subnuclear Physics, Institute of Experimental Physics of the Slovak Academy of Sciences, Kosice; Slovak Republic.
- ³⁰Physics Department, Brookhaven National Laboratory, Upton NY; United States of America.
- ³¹Universidad de Buenos Aires, Facultad de Ciencias Exactas y Naturales, Departamento de Física, y CONICET, Instituto de Física de Buenos Aires (IFIBA), Buenos Aires; Argentina.
- ³²California State University, CA; United States of America.
- ³³Cavendish Laboratory, University of Cambridge, Cambridge; United Kingdom.
- ³⁴(^a) Department of Physics, University of Cape Town, Cape Town; (^b) iThemba Labs, Western Cape; (^c) Department of Mechanical Engineering Science, University of Johannesburg, Johannesburg; (^d) National Institute of Physics, University of the Philippines Diliman (Philippines); (^e) Department of Physics, Stellenbosch University, Matieland; (^f) University of KwaZulu-Natal, School of Agriculture and Science, Mathematics, Westville; (^g) University of South Africa, Department of Physics, Pretoria; (^h) University of Pretoria, Department of Mechanical and Aeronautical Engineering, Pretoria; (ⁱ) University of Zululand, KwaDlangezwa; (^j) School of Physics, University of the Witwatersrand, Johannesburg; South Africa.
- ³⁵Department of Physics, Carleton University, Ottawa ON; Canada.
- ³⁶(^a) Faculté des Sciences Ain Chock, Université Hassan II de Casablanca; (^b) Faculté des Sciences, Université Ibn-Tofail, Kénitra; (^c) Faculté des Sciences Semlalia, Université Cadi Ayyad, LPHEA-Marrakech; (^d) LPMR, Faculté des Sciences, Université Mohamed Premier, Oujda; (^e) Faculté des sciences, Université Mohammed V, Rabat; (^f) Institute of Applied Physics, Mohammed VI Polytechnic University, Ben Guerir; Morocco.
- ³⁷CERN, Geneva; Switzerland.
- ³⁸Affiliated with an international laboratory covered by a cooperation agreement with CERN.
- ³⁹Enrico Fermi Institute, University of Chicago, Chicago IL; United States of America.
- ⁴⁰LPC, Université Clermont Auvergne, CNRS/IN2P3, Clermont-Ferrand; France.
- ⁴¹Nevis Laboratory, Columbia University, Irvington NY; United States of America.
- ⁴²Niels Bohr Institute, University of Copenhagen, Copenhagen; Denmark.
- ⁴³(^a) Dipartimento di Fisica, Università della Calabria, Rende; (^b) INFN Gruppo Collegato di Cosenza, Laboratori Nazionali di Frascati; Italy.
- ⁴⁴Physics Department, Southern Methodist University, Dallas TX; United States of America.
- ⁴⁵National Centre for Scientific Research "Demokritos", Agia Paraskevi; Greece.
- ⁴⁶(^a) Department of Physics, Stockholm University; (^b) Oskar Klein Centre, Stockholm; Sweden.
- ⁴⁷Deutsches Elektronen-Synchrotron DESY, Hamburg and Zeuthen; Germany.
- ⁴⁸Fakultät Physik, Technische Universität Dortmund, Dortmund; Germany.
- ⁴⁹Institut für Kern- und Teilchenphysik, Technische Universität Dresden, Dresden; Germany.
- ⁵⁰Department of Physics, Duke University, Durham NC; United States of America.
- ⁵¹SUPA - School of Physics and Astronomy, University of Edinburgh, Edinburgh; United Kingdom.
- ⁵²INFN e Laboratori Nazionali di Frascati, Frascati; Italy.
- ⁵³Physikalisches Institut, Albert-Ludwigs-Universität Freiburg, Freiburg; Germany.

- ⁵⁴II. Physikalisches Institut, Georg-August-Universität Göttingen, Göttingen; Germany.
- ⁵⁵Département de Physique Nucléaire et Corpusculaire, Université de Genève, Genève; Switzerland.
- ⁵⁶(^a) Dipartimento di Fisica, Università di Genova, Genova; (^b) INFN Sezione di Genova; Italy.
- ⁵⁷II. Physikalisches Institut, Justus-Liebig-Universität Giessen, Giessen; Germany.
- ⁵⁸SUPA - School of Physics and Astronomy, University of Glasgow, Glasgow; United Kingdom.
- ⁵⁹LPSC, Université Grenoble Alpes, CNRS/IN2P3, Grenoble INP, Grenoble; France.
- ⁶⁰Laboratory for Particle Physics and Cosmology, Harvard University, Cambridge MA; United States of America.
- ⁶¹Department of Modern Physics and State Key Laboratory of Particle Detection and Electronics, University of Science and Technology of China, Hefei; China.
- ⁶²(^a) Kirchhoff-Institut für Physik, Ruprecht-Karls-Universität Heidelberg, Heidelberg; (^b) Physikalisches Institut, Ruprecht-Karls-Universität Heidelberg, Heidelberg; Germany.
- ⁶³(^a) Department of Physics, Chinese University of Hong Kong, Shatin, N.T., Hong Kong; (^b) Department of Physics, University of Hong Kong, Hong Kong; (^c) Department of Physics and Institute for Advanced Study, Hong Kong University of Science and Technology, Clear Water Bay, Kowloon, Hong Kong; China.
- ⁶⁴Department of Physics, National Tsing Hua University, Hsinchu; Taiwan.
- ⁶⁵IJCLab, Université Paris-Saclay, CNRS/IN2P3, 91405, Orsay; France.
- ⁶⁶Centro Nacional de Microelectrónica (IMB-CNM-CSIC), Barcelona; Spain.
- ⁶⁷Department of Physics, Indiana University, Bloomington IN; United States of America.
- ⁶⁸(^a) INFN Gruppo Collegato di Udine, Sezione di Trieste, Udine; (^b) ICTP, Trieste; (^c) Dipartimento Politecnico di Ingegneria e Architettura, Università di Udine, Udine; Italy.
- ⁶⁹(^a) INFN Sezione di Lecce; (^b) Dipartimento di Matematica e Fisica, Università del Salento, Lecce; Italy.
- ⁷⁰(^a) INFN Sezione di Milano; (^b) Dipartimento di Fisica, Università di Milano, Milano; Italy.
- ⁷¹(^a) INFN Sezione di Napoli; (^b) Dipartimento di Fisica, Università di Napoli, Napoli; Italy.
- ⁷²(^a) INFN Sezione di Pavia; (^b) Dipartimento di Fisica, Università di Pavia, Pavia; Italy.
- ⁷³(^a) INFN Sezione di Pisa; (^b) Dipartimento di Fisica E. Fermi, Università di Pisa, Pisa; Italy.
- ⁷⁴(^a) INFN Sezione di Roma; (^b) Dipartimento di Fisica, Sapienza Università di Roma, Roma; Italy.
- ⁷⁵(^a) INFN Sezione di Roma Tor Vergata; (^b) Dipartimento di Fisica, Università di Roma Tor Vergata, Roma; Italy.
- ⁷⁶(^a) INFN Sezione di Roma Tre; (^b) Dipartimento di Matematica e Fisica, Università Roma Tre, Roma; Italy.
- ⁷⁷(^a) INFN-TIFPA; (^b) Università degli Studi di Trento, Trento; Italy.
- ⁷⁸Universität Innsbruck, Department of Astro and Particle Physics, Innsbruck; Austria.
- ⁷⁹Department of Physics and Astronomy, Iowa State University, Ames IA; United States of America.
- ⁸⁰Istinye University, Sariyer, Istanbul; Türkiye.
- ⁸¹(^a) Departamento de Engenharia Elétrica, Universidade Federal de Juiz de Fora (UFJF), Juiz de Fora; (^b) Universidade Federal do Rio De Janeiro COPPE/EE/IF, Rio de Janeiro; (^c) Instituto de Física, Universidade de São Paulo, São Paulo; (^d) Rio de Janeiro State University, Rio de Janeiro; (^e) Federal University of Bahia, Bahia; Brazil.
- ⁸²KEK, High Energy Accelerator Research Organization, Tsukuba; Japan.
- ⁸³(^a) Khalifa University of Science and Technology, Abu Dhabi; (^b) New York University Abu Dhabi, Abu Dhabi; (^c) United Arab Emirates University, Al Ain; (^d) University of Sharjah, Sharjah; United Arab Emirates.
- ⁸⁴Graduate School of Science, Kobe University, Kobe; Japan.
- ⁸⁵(^a) AGH University of Krakow, Faculty of Physics and Applied Computer Science, Krakow; (^b) Marian Smoluchowski Institute of Physics, Jagiellonian University, Krakow; Poland.
- ⁸⁶Institute of Nuclear Physics Polish Academy of Sciences, Krakow; Poland.

- ⁸⁷Faculty of Science, Kyoto University, Kyoto; Japan.
- ⁸⁸Research Center for Advanced Particle Physics and Department of Physics, Kyushu University, Fukuoka ; Japan.
- ⁸⁹L2IT, Université de Toulouse, CNRS/IN2P3, UPS, Toulouse; France.
- ⁹⁰Instituto de Física La Plata, Universidad Nacional de La Plata and CONICET, La Plata; Argentina.
- ⁹¹Physics Department, Lancaster University, Lancaster; United Kingdom.
- ⁹²Oliver Lodge Laboratory, University of Liverpool, Liverpool; United Kingdom.
- ⁹³Department of Experimental Particle Physics, Jožef Stefan Institute and Department of Physics, University of Ljubljana, Ljubljana; Slovenia.
- ⁹⁴Department of Physics and Astronomy, Queen Mary University of London, London; United Kingdom.
- ⁹⁵Department of Physics, Royal Holloway University of London, Egham; United Kingdom.
- ⁹⁶Department of Physics and Astronomy, University College London, London; United Kingdom.
- ⁹⁷Louisiana Tech University, Ruston LA; United States of America.
- ⁹⁸Fysiska institutionen, Lunds universitet, Lund; Sweden.
- ⁹⁹Departamento de Física Teórica C-15 and CIAFF, Universidad Autónoma de Madrid, Madrid; Spain.
- ¹⁰⁰Institut für Physik, Universität Mainz, Mainz; Germany.
- ¹⁰¹School of Physics and Astronomy, University of Manchester, Manchester; United Kingdom.
- ¹⁰²CPPM, Aix-Marseille Université, CNRS/IN2P3, Marseille; France.
- ¹⁰³Department of Physics, University of Massachusetts, Amherst MA; United States of America.
- ¹⁰⁴Department of Physics, McGill University, Montreal QC; Canada.
- ¹⁰⁵School of Physics, University of Melbourne, Victoria; Australia.
- ¹⁰⁶Department of Physics, University of Michigan, Ann Arbor MI; United States of America.
- ¹⁰⁷Department of Physics and Astronomy, Michigan State University, East Lansing MI; United States of America.
- ¹⁰⁸Group of Particle Physics, University of Montreal, Montreal QC; Canada.
- ¹⁰⁹Fakultät für Physik, Ludwig-Maximilians-Universität München, München; Germany.
- ¹¹⁰Max-Planck-Institut für Physik (Werner-Heisenberg-Institut), München; Germany.
- ¹¹¹Graduate School of Science and Kobayashi-Maskawa Institute, Nagoya University, Nagoya; Japan.
- ¹¹²(^a)Department of Physics, Nanjing University, Nanjing; (^b)School of Science, Shenzhen Campus of Sun Yat-sen University; (^c)University of Chinese Academy of Science (UCAS), Beijing; China.
- ¹¹³(^a)School of Physics, Nankai University, Tianjin; (^b)Institute of Frontier and Interdisciplinary Science and Key Laboratory of Particle Physics and Particle Irradiation (MOE), Shandong University, Qingdao; (^c)School of Physics, Zhengzhou University; China.
- ¹¹⁴Department of Physics and Astronomy, University of New Mexico, Albuquerque NM; United States of America.
- ¹¹⁵Institute for Mathematics, Astrophysics and Particle Physics, Radboud University/Nikhef, Nijmegen; Netherlands.
- ¹¹⁶Nikhef National Institute for Subatomic Physics and University of Amsterdam, Amsterdam; Netherlands.
- ¹¹⁷Department of Physics, Northern Illinois University, DeKalb IL; United States of America.
- ¹¹⁸Department of Physics, New York University, New York NY; United States of America.
- ¹¹⁹Ochanomizu University, Otsuka, Bunkyo-ku, Tokyo; Japan.
- ¹²⁰Ohio State University, Columbus OH; United States of America.
- ¹²¹Homer L. Dodge Department of Physics and Astronomy, University of Oklahoma, Norman OK; United States of America.
- ¹²²Department of Physics, Oklahoma State University, Stillwater OK; United States of America.
- ¹²³Palacký University, Joint Laboratory of Optics, Olomouc; Czech Republic.

- ¹²⁴Institute for Fundamental Science, University of Oregon, Eugene, OR; United States of America.
- ¹²⁵Graduate School of Science, University of Osaka, Osaka; Japan.
- ¹²⁶Department of Physics, University of Oslo, Oslo; Norway.
- ¹²⁷Department of Physics, Oxford University, Oxford; United Kingdom.
- ¹²⁸LPNHE, Sorbonne Université, Université Paris Cité, CNRS/IN2P3, Paris; France.
- ¹²⁹Department of Physics, University of Pennsylvania, Philadelphia PA; United States of America.
- ¹³⁰Department of Physics and Astronomy, University of Pittsburgh, Pittsburgh PA; United States of America.
- ¹³¹(^a)Laboratório de Instrumentação e Física Experimental de Partículas - LIP, Lisboa;(^b)Departamento de Física, Faculdade de Ciências, Universidade de Lisboa, Lisboa;(^c)Departamento de Física, Universidade de Coimbra, Coimbra;(^d)Centro de Física Nuclear da Universidade de Lisboa, Lisboa;(^e)Departamento de Física, Escola de Ciências, Universidade do Minho, Braga;(^f)Departamento de Física Teórica y del Cosmos, Universidad de Granada, Granada (Spain);(^g)Departamento de Física, Instituto Superior Técnico, Universidade de Lisboa, Lisboa; Portugal.
- ¹³²Institute of Physics of the Czech Academy of Sciences, Prague; Czech Republic.
- ¹³³Czech Technical University in Prague, Prague; Czech Republic.
- ¹³⁴Charles University, Faculty of Mathematics and Physics, Prague; Czech Republic.
- ¹³⁵Particle Physics Department, Rutherford Appleton Laboratory, Didcot; United Kingdom.
- ¹³⁶IRFU, CEA, Université Paris-Saclay, Gif-sur-Yvette; France.
- ¹³⁷Santa Cruz Institute for Particle Physics, University of California Santa Cruz, Santa Cruz CA; United States of America.
- ¹³⁸(^a)Departamento de Física, Pontificia Universidad Católica de Chile, Santiago;(^b)Millennium Institute for Subatomic physics at high energy frontier (SAPHIR), Santiago;(^c)Instituto de Investigación Multidisciplinario en Ciencia y Tecnología, y Departamento de Física, Universidad de La Serena;(^d)Universidad Andres Bello, Department of Physics, Santiago;(^e)Universidad San Sebastian, Recoleta;(^f)Instituto de Alta Investigación, Universidad de Tarapacá, Arica;(^g)Departamento de Física, Universidad Técnica Federico Santa María, Valparaíso; Chile.
- ¹³⁹Department of Physics, Institute of Science, Tokyo; Japan.
- ¹⁴⁰Department of Physics, University of Washington, Seattle WA; United States of America.
- ¹⁴¹(^a)State Key Laboratory of Dark Matter Physics, School of Physics and Astronomy, Shanghai Jiao Tong University, Key Laboratory for Particle Astrophysics and Cosmology (MOE), SKLPPC, Shanghai;(^b)State Key Laboratory of Dark Matter Physics, Tsung-Dao Lee Institute, Shanghai Jiao Tong University, Shanghai; China.
- ¹⁴²Department of Physics and Astronomy, University of Sheffield, Sheffield; United Kingdom.
- ¹⁴³Department of Physics, Shinshu University, Nagano; Japan.
- ¹⁴⁴Department Physik, Universität Siegen, Siegen; Germany.
- ¹⁴⁵Department of Physics, Simon Fraser University, Burnaby BC; Canada.
- ¹⁴⁶SLAC National Accelerator Laboratory, Stanford CA; United States of America.
- ¹⁴⁷Department of Physics, Royal Institute of Technology, Stockholm; Sweden.
- ¹⁴⁸Departments of Physics and Astronomy, Stony Brook University, Stony Brook NY; United States of America.
- ¹⁴⁹Department of Physics and Astronomy, University of Sussex, Brighton; United Kingdom.
- ¹⁵⁰School of Physics, University of Sydney, Sydney; Australia.
- ¹⁵¹Institute of Physics, Academia Sinica, Taipei; Taiwan.
- ¹⁵²(^a)E. Andronikashvili Institute of Physics, Iv. Javakhishvili Tbilisi State University, Tbilisi;(^b)High Energy Physics Institute, Tbilisi State University, Tbilisi;(^c)University of Georgia, Tbilisi; Georgia.
- ¹⁵³Department of Physics, Technion, Israel Institute of Technology, Haifa; Israel.

- ¹⁵⁴Raymond and Beverly Sackler School of Physics and Astronomy, Tel Aviv University, Tel Aviv; Israel.
- ¹⁵⁵Department of Physics, Aristotle University of Thessaloniki, Thessaloniki; Greece.
- ¹⁵⁶International Center for Elementary Particle Physics and Department of Physics, University of Tokyo, Tokyo; Japan.
- ¹⁵⁷Graduate School of Science and Technology, Tokyo Metropolitan University, Tokyo; Japan.
- ¹⁵⁸Department of Physics, University of Toronto, Toronto ON; Canada.
- ¹⁵⁹^(a)TRIUMF, Vancouver BC; ^(b)Department of Physics and Astronomy, York University, Toronto ON; Canada.
- ¹⁶⁰Division of Physics and Tomonaga Center for the History of the Universe, Faculty of Pure and Applied Sciences, University of Tsukuba, Tsukuba; Japan.
- ¹⁶¹Department of Physics and Astronomy, Tufts University, Medford MA; United States of America.
- ¹⁶²Department of Physics and Astronomy, University of California Irvine, Irvine CA; United States of America.
- ¹⁶³Department of Physics and Astronomy, University of Uppsala, Uppsala; Sweden.
- ¹⁶⁴Department of Physics, University of Illinois, Urbana IL; United States of America.
- ¹⁶⁵Instituto de Física Corpuscular (IFIC), Centro Mixto Universidad de Valencia - CSIC, Valencia; Spain.
- ¹⁶⁶Department of Physics, University of British Columbia, Vancouver BC; Canada.
- ¹⁶⁷Department of Physics and Astronomy, University of Victoria, Victoria BC; Canada.
- ¹⁶⁸Fakultät für Physik und Astronomie, Julius-Maximilians-Universität Würzburg, Würzburg; Germany.
- ¹⁶⁹Department of Physics, University of Warwick, Coventry; United Kingdom.
- ¹⁷⁰Waseda University, Tokyo; Japan.
- ¹⁷¹Department of Particle Physics and Astrophysics, Weizmann Institute of Science, Rehovot; Israel.
- ¹⁷²Department of Physics, University of Wisconsin, Madison WI; United States of America.
- ¹⁷³Fakultät für Mathematik und Naturwissenschaften, Fachgruppe Physik, Bergische Universität Wuppertal, Wuppertal; Germany.
- ¹⁷⁴Department of Physics, Yale University, New Haven CT; United States of America.
- ¹⁷⁵Yerevan Physics Institute, Yerevan; Armenia.
- ^a Also at Affiliated with an institute formerly covered by a cooperation agreement with CERN.
- ^b Also at An-Najah National University, Nablus; Palestine.
- ^c Also at Borough of Manhattan Community College, City University of New York, New York NY; United States of America.
- ^d Also at Center for Interdisciplinary Research and Innovation (CIRI-AUTH), Thessaloniki; Greece.
- ^e Also at Centre of Physics of the Universities of Minho and Porto (CF-UM-UP); Portugal.
- ^f Also at CERN, Geneva; Switzerland.
- ^g Also at Département de Physique Nucléaire et Corpusculaire, Université de Genève, Genève; Switzerland.
- ^h Also at Departament de Física de la Universitat Autònoma de Barcelona, Barcelona; Spain.
- ⁱ Also at Department of Financial and Management Engineering, University of the Aegean, Chios; Greece.
- ^j Also at Department of Modern Physics and State Key Laboratory of Particle Detection and Electronics, University of Science and Technology of China, Hefei; China.
- ^k Also at Department of Physics, Ben Gurion University of the Negev, Beer Sheva; Israel.
- ^l Also at Department of Physics, Bolu Abant İzzet Baysal University, Bolu; Türkiye.
- ^m Also at Department of Physics, King's College London, London; United Kingdom.
- ⁿ Also at Department of Physics, Stellenbosch University; South Africa.
- ^o Also at Department of Physics, University of Fribourg, Fribourg; Switzerland.
- ^p Also at Department of Physics, University of Thessaly; Greece.
- ^q Also at Department of Physics, Westmont College, Santa Barbara; United States of America.

- r* Also at Faculty of Physics, Sofia University, 'St. Kliment Ohridski', Sofia; Bulgaria.
- s* Also at Faculty of Physics, University of Bucharest; Romania.
- t* Also at Hellenic Open University, Patras; Greece.
- u* Also at Henan University; China.
- v* Also at Imam Mohammad Ibn Saud Islamic University; Saudi Arabia.
- w* Also at Indian Institute of Technology (IIT), Jodhpur; India.
- x* Also at Institutio Catalana de Recerca i Estudis Avancats, ICREA, Barcelona; Spain.
- y* Also at Institut für Experimentalphysik, Universität Hamburg, Hamburg; Germany.
- z* Also at Institute for Nuclear Research and Nuclear Energy (INRNE) of the Bulgarian Academy of Sciences, Sofia; Bulgaria.
- aa* Also at Institute of Applied Physics, Mohammed VI Polytechnic University, Ben Guerir; Morocco.
- ab* Also at Institute of Particle Physics (IPP); Canada.
- ac* Also at Institute of Physics and Technology, Mongolian Academy of Sciences, Ulaanbaatar; Mongolia.
- ad* Also at Institute of Physics, Azerbaijan Academy of Sciences, Baku; Azerbaijan.
- ae* Also at Institute of Theoretical Physics, Iliia State University, Tbilisi; Georgia.
- af* Also at Millennium Institute for Subatomic physics at high energy frontier (SAPHIR), Santiago; Chile.
- ag* Also at National Institute of Physics, University of the Philippines Diliman (Philippines); Philippines.
- ah* Also at School of Physics, University of the Witwatersrand, Johannesburg; South Africa.
- ai* Also at The Collaborative Innovation Center of Quantum Matter (CICQM), Beijing; China.
- aj* Also at TRIUMF, Vancouver BC; Canada.
- ak* Also at Università di Napoli Parthenope, Napoli; Italy.
- al* Also at Università degli Studi Link; Italy.
- am* Also at University and INFN Torino, Torino; Italy.
- an* Also at University of Chinese Academy of Sciences (UCAS), Beijing; China.
- ao* Also at University of Colorado Boulder, Department of Physics, Colorado; United States of America.
- ap* Also at University of Siena; Italy.
- aq* Also at Washington College, Chestertown, MD; United States of America.
- ar* Also at Yeditepe University, Physics Department, Istanbul; Türkiye.
- * Deceased